Friction measurement and compensation on a laparoscopic instrument of a medical robot

Briaire, E.

Award date:
2006

Eindhoven University of Technology
Department of Electrical Engineering
Control Systems

TU/e technische universiteit eindhoven

Friction Measurement and Compensation on a Laparoscopic Instrument of a Medical Robot

by
Emile Briaire

Master of Science thesis

Project period:	Oct 2004 / May 2006
Report Number:	06A/06
Commissioned by:	Prof. dr. ir. P.P.J. van den Bosch
Supervisor:	Prof. dr. ir. M. Steinbuch

Additional Commission member:
Dr. ir. A. Veltman (TU/e)

Preface

Quite a while ago, I started my study at the University of Eindhoven. I experienced that most of the time a study and a full-time job can be combined well. Okay, spending almost every vacation behind books does test your relationship with your partner, but if it survives, and I'm lucky it did, you have a serious clue that there must be something worthwhile... Irma, thanks!

I enjoyed my graduation project: first because the subject of medical robots is a most interesting one. I am convinced that great developments are coming up soon. Second because the project gave me the opportunity to play with theoretical issues in a way they come to life, using the awesome playgrounds of Matlab, Simulink, State Flow and XPC. Third, as an electro student with a strong affection for mechanical engineering I saw it as a challenge to design the mechanical hardware for the project myself, using 3D design software Autodesk Inventor. It gave me insight in several practical and design issues that mechanical engineers cope with in their every day work.

I say a word of thanks to my colleagues Hans Sluiters and Richard Paliwoda, for their showing interest in the progress of my study and for their support whenever that was possible (even if it was only because they were waiting for a party).
I thank Maarten Steinbuch for his motivating enthusiasm and coaching throughout this project.

And what now?
Beer brewing, building a Darius wind turbine, start a search for my guitar, pimp up our farmhouse together with Irma... and who knows, maybe some haptics too!

Someren-Heide, 24 May 2006

Emile

Abstract

Robotic laparoscopic surgery is used in a growing number of hospitals in the world. Approximately two hundred and fifty systems are installed worldwide. In the Netherlands there are three hospitals using a surgery robot in the OR. The surgeon controlling the robot can manipulate the robot in a natural intuitive way while trembling is filtered out and the magnitude of his moves may be scaled up or down. During the operation the surgeon sits comfortably behind the control console where a 3D vision system provides an excellent view on the operation scene inside the body of the patient.
What the surgeon is missing is the feeling of the patient's tissue, since the only robotic laparoscopic surgery system that is commercially available at the moment (robot system Da Vinci of Intuitive Surgical) does not provide haptic feedback.

A haptic feedback system in a surgery robot requires information on the forces the robot is applying on the patient's tissue. Force sensors can be integrated in the robotic laparoscopic instruments in order to provide this force information. In stead of this, an alternative approach is investigated in this work that tries to avoid the addition of force sensors in the instrument. One of the important reasons to do this is to avoid higher costs of the disposable instruments. In this work the forces applied on the tissue by the instrument inside the patient's body are derived from the currents of the motors that drive the instrument from outside the body.

The first chapters in this work will give an introduction to haptic feedback, minimally invasive surgery, medical tele-robots in general and the Da Vinci system in specific. Hereafter the design of a mechanical test setup that is capable of driving all four axis of the Da Vinci instrument is discussed including the disturbances it introduces with respect to force measurement. Compensation methods used to compensate these disturbances are discussed. Besides model based feed forward, Iterative Learning Control (ILC) is used to suppress instrument friction and other disturbances that are function of motor position and speed.

Table of Contents

Table of Figures

Table of Tables

1 Introduction to haptics

Haptic feedback is under investigation at many institutes, companies and universities for a few decades already. It is used in a variety of different applications for research, gaming professional simulators and manipulators. Also in the consumers product haptic feedback is introduced such as the iDrive system of BMW [34]. Even an experimental haptic radio has been reported that helps the user find the optimum position of a tuner knob [35].

In this chapter a short introduction is given on what haptic feedback is, followed by an overview of several applications in which haptic feedback is implemented.

1.1 Haptic-, force- tactile- and rumble-feedback

In literature about haptics, often words as force feedback, tactile feedback and sometimes rumble feedback are used. In this section these terms are explained shortly.

Rumble feedback is a simple sort of feedback that is used in computer gaming. In rumble feedback applications low fidelity shakes or rumbles are produced in the joystick or steering wheel that is used for the game. These effects are generally turned on during high action events in a game. This type of feedback will not be discussed further.

Tactile sensing is created by excitation of the skin. It gives us information about the texture of the surface of an object. Is it rough, smooth, slippery, etcetera? It does not give information on the mechanical compliance, weight, or inertia of the object.
By means of tactile displays the sensation of touch is reproduced. Different techniques have been used to develop tactile displays e.g.: vibrotactile arrays, thermal displays, electro-rheological devices [7], and many more.

Force feedback devices apply forces to the human body, in most cases to the hands of the user. The forces that are reproduced by a force feedback device can result from solid boundaries, weight, inertia and mechanical compliance of an object.

Haptic feedback is tactile feedback plus force feedback. This kind of feedback comprises techniques to reproduce all object information that is required to produce a high-fidelity feedback environment.
In literature the term haptic feedback is often used when actually only a high-fidelity force feedback is meant. Also in this report the term haptic feedback will be used in this way.

1.2 Haptic feedback applications

One of the leading companies in commercial haptic products is Immersion Corporation [34]. The wide range of haptic products of Immersion is not limited to game related devices as joy-sticks, racing steers, etcetera but they also developed haptic devices for automotive, medical training, industrial control and many more areas. Partners using Immersion products are for instance companies as Philips Medical Systems, Medtronic, Integrated Surgical Systems, BMW, and Siemens. This indicates that haptic feedback is getting embedded in more and more professional and consumer products.

In this section a few areas that use haptic feedback are described. Because haptic feedback is used in such a variety of applications this chapter is far from complete.

There are many ways to group different types of haptic feedback systems (on basis of their application area, the number of degrees of freedom of the system, etcetera). In this section haptic feedback systems are divided in two groups. The first group consists of systems that provide haptic feedback in virtual environments. Most of these systems can be titled as simulators. The second group consists of systems that measure forces in the real world and simultaneously reproduce the measured environment real-time. Most of these systems may be titled as tele-presence manipulators.
The important difference between these two groups is the fact that the first group is using models to simulate the environment and in the second group there is a bi-directional information flow between the operator and the real-world object.

1.2.1 Haptic feedback Simulators

All computer games with haptic feedback are part of this group. But there are also many professional simulators available with high-fidelity visual (2D or 3D) and audio feedback. High-risk professions such as aviation industry, military maritime and nuclear energy are using simulators for training.
But also in other fields with low risks, professional simulators are used. In those cases often financial aspects are the motivation to use simulations. For instance for training purposes, in [8] a welding simulator is presented that uses FCS's Haptic Master [9].

Medical operation simulators with force-feedback allow medical professionals to practice and prepare difficult procedures in a risk-free, virtual environment. A few vendors of simulators for procedures as bronchoscopy, colonoscopy, placing pacemakers, catheter placement are [10]:

- AccuTouch Endoscopy Simulator (Immersion Medical),
- AccuTouch Endovascular Simulator (Immersion Medical),
- ENT Surgical Simulator (Lockheed Martin Tactical Defense Systems),
- EYESI (VRMagic),
- GI Mentor (Simbionix),
- Key Surgical Activities (Mentice Medical),
- PERC Mentor (Simbionix),

- Procedicus MIST (Mentice Medical),
- Procedicus Virtual Arthroscopy (VA) (Mentice Medical),
- Uro Mentor (Simbionix),
- Vascular Intervention System Training (Mentice Medical).

For training purposes several vendors developed laparoscopic simulators (see Chapter 2). In a simulator, trainees can be guided through a series of exercises of progressive complexity, enabling them to develop the skills essential for good clinical practice. During the tasks, realistic models are used of sutures, needles and instruments interacting with simulations of (soft) tissue. The interface and the tools interact with the simulations through software that also initiates the forces that are reflected in the tools (for haptic feedback).
Several simulators with haptic feedback for laparoscopic procedures are listed below [10]:

- Lap Mentor (Simbionix),
- MIST (Mentice),
- LapSim (Immersion Medical and Surgical Science).

Figure 1. Xitact LS500.

The simulators above use the Xitact LS500 open platform. According to [11] the simulator is an important and useful tool in laparoscopic teaching. The quality of the haptic feedback of this system needs further development since it was found not very realistic.

1.2.2 Haptic feedback manipulator systems

In contrast to simulators, haptic feedback manipulator systems measure forces in the real world and simultaneously reproduce the measured environmental parameters to the operator.
In most cases the operator provides the system with position setpoints for the end-effector of the manipulator. In return the system reproduces forces on the hands of the operator proportional to the forces working on the end-effector of the manipulator. So there is a bi-directional information flow between the operator and the real-world object that is manipulated. The perfect haptic feedback manipulator system would be totally transparent and therefore unnoticeable for the operator. In that case the operator would have the impression to be directly in contact with the object.

In several haptic feedback applications the 'object' that is manipulated comprises a whole system. For instance in case of the automotive application "steer by wire". In this case the mechanical link between the steering wheel and the front wheels of the car is replaced by electronics. Here, the haptic feedback system should not only reproduce the steering forces working on the wheels (effects of a slippery road or a wheel hitting the sidewalk during parking) but it should also reproduce the end-stop positions of the steering system as a whole.

Several robotic telemanipulators are developed for hazardous environments such as deep-sea [17, 18] and space [12, 13]. Especially in space applications tele-presence suffers from communication time delay between the master (controlled by the operator) and the slave (the manipulator in space) since there is a time difference between the actions of the operator and the feedback. This time delay does not only affect transparency, but more important, also stability.

For manipulation of objects with sizes of micro or even nanometers several micro- and nanomanipulators have been developed. For biological cell manipulation at the University of Oldenburg a micromanipulator has been designed with a haptic feedback interface [14, 15]. In micro assembly and nanohandling force and tactile feedback is indispensable for a reliable and non-destructive manipulation of fragile micro objects. Only visual feedback is not good enough for nanomanipulation because when handling parts with dimensions less than 100 μm, adhesive forces such as electrostatic force, Van der Waals force and surface tension become dominant with respect to inertial forces. Contact forces in a range of 0.1 μN up to 200 μN must be sensed, therefore force scaling must be applied [16].

For medical applications many telemanipulators have been developed. Chapter 3 is dedicated to this type of telemanipulators. Since most of the manipulators described in Chapter 3 are designed for laparoscopic surgery, first, in Chapter 2 an introduction is given on this type of surgery.

2 Minimally Invasive Surgery

Laparoscopic surgery is a relative new surgical technique. It is a Minimally Invasive Surgery (MIS) technique. This means that surgery is performed through small incisions of about 10 mm (or smaller) rather than by making a large incision to expose the operating site. Pumping carbon dioxide inside the abdominal cavity expands it and creates a workspace. Trocars are placed in the incisions to avoid gas leakage. Through the trocars instruments and a laparoscope are inserted into the patient's body. The laparoscope is composed of a chain of lens optics to transmit the image of the operation site to the CCD camera connected to its outer end, and optical fibers to illuminate inside [19].

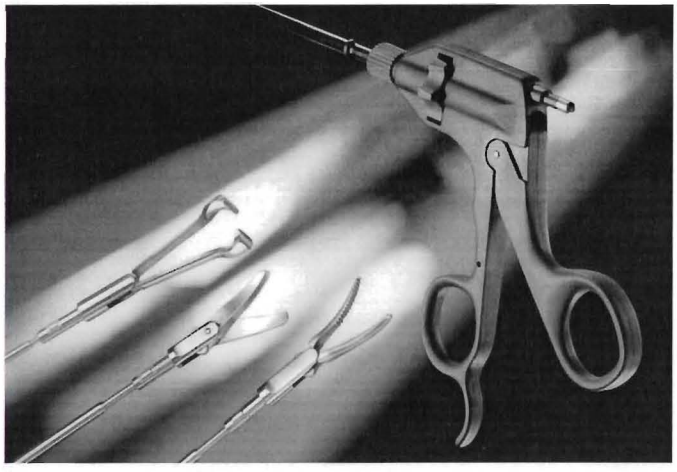

Figure 2. Laparoscopic instruments

Laparoscopic instruments as depicted in Figure 2 are long and thin with trigger-like handles. They are available in many types such as scissors, forceps, scalpel, needle driver, etc.

Minimally Invasive Surgery includes: laparoscopy (abdominal cavity), thoracoscopy (chest cavity), arthroscopy (joints), pelviscopy (pelvis) and angioscopy (blood vessels). Though, in this report the terms laparoscopic surgery and minimally invasive surgery will be used as synonyms as is done frequently in literature.
Minimally invasive surgery has many advantages over open surgery. For instance, it reduces the risk of infections. Also blood loss is reduced which may avoid blood transfusions. In [37] a case is reported where this was crucial since blood transfusion was not an option for a Jehovah's Witness patient. Further the surgeon is not in direct contact with the patient as in open surgery and this may reduce the risks for the medical staff when the patient is HIV-contaminated. One of the greatest advantages of laparoscopic surgery is that this technique reduces trauma to healthy tissue. For the patient this means he will have less post-operative pain. The patient also has an esthetical advantage since the operation leaves only a few minor scars instead of a big scar of several inches.

Hospital stay costs are lower because the patient recovers faster. This also means the patient can go back to work sooner and this saves money too.

However laparoscopic surgery has some major disadvantages [20, 21, 22]:

- Dexterity is reduced significantly because of the loss of DOF's (Degrees of freedom). The motion of the instrument is restricted to 4 DOF since the instrument enters the body at one point. As a result the surgeon cannot approach the workspace from an arbitrary angle.
- Reversed motion: the trocar (also called cannula) forms a pivoting point for the surgical instrument.
- Amplification of tremor due to the long instruments.
- Surgeon's lack of direct view on the operation scene resulting in disturbed hand-eye coordination. The camera has another point of view that is not related to the position of the surgeon with respect to the patient. Second, the monitor on which the surgeon is watching his actions is located somewhere else than where his hands are moving the instruments. Third, the monitor lacks stereovision so there is no depth perception.
- Reduced haptic feedback: the surgeon cannot palpate the tissue, as there is no direct access possible. Haptic feedback through the instrument is minimal, because of the friction of the instrument and the friction between the instrument and the trocar. Haptic feedback information is crucial for examination (localizing arteries or a tumor hidden in tissue) or treatment of delicate tissues or when tying sutures. The surgeon must compensate the lack of haptic feedback with visual feedback, doing so he must interpret the deformation of the tissue as a measure of force. This leads to longer operation times and can make the operation extremely exhausting for the surgeon.
- Training (costs): Surgeons need intensive training to get familiar with the handling of the instrument and the interpretation of the available visual information.

Figure 3. Awkward grasp and arm positions in laparoscopic surgery.

In Chapter 3 several research results and applications are presented that reduce or take away one or more of the disadvantages listed above.

3 Introduction to medical tele- robots and manipulators

In section 1.2.2 haptic feedback telemanipulator systems were introduced. In this Chapter haptic feedback telemanipulator systems for medical applications are examined further.

3.1 Medical haptic feedback systems

There are many medical robots and manipulators such as endoscope (camera) positioning robots (AESOP of Computer Motion, or the Endoscope manipulator of Hitachi), instrument holding and navigation robots (PathFinder of Armstrong Healthcare), autonomous medical robots (ROBODOC of Integrated Surgical Systems Inc. [55]), pure mechanic 7-DOF laparoscopic manipulator (AMC, [29]), pure mechanic (low friction) laparoscopic palpation (hand) tools, needle puncturing/insertion manipulators [64], steady-hand robots [62, 63], etc., etc.
In Table 1 this kind of tools, robots and manipulators are excluded. The list contains only those mechatronic telesurgery systems that are able to control a forceps for laparoscopic, colonoscopic or microsurgical operations. This selection is made in order to create an overview of systems for which haptic feedback has been developed (or in the future may be developed) for one or more DOF's of a forceps such as used by the DaVinci system of Intuitive Surgical that will be discussed in section 3.2.
The presented list is not a complete list of all projects in the world in this category. For instance in Japan several more laparoscopic master slave systems can be found.

	System	Institution	Country	# manip / # DOF's	Commercial available / FDA-approved	Haptic feedback	Comments (actuation and force measurements)	Ref.
1	ZEUS	Computer Motion	USA	2 / 7	Not anymore / Yes	No	Merged with Intuitive Surgical	[54]
2	DaVinci	Intuitive Surgical (IS)	USA	2 / 7	Yes / Yes	No	-	[54]
3	Laprotek	Broc rogers Surgical						
4	No name	Univ. of Western Ontario, London	Canada	1 / 5	No / No	Yes	Force measurement with a loadcell (outside the body) and strain gauges.	[46]
5	UC Berkeley/Endorobotic/UCSF Telesurgical workstation	Univ. of Berkeley Univ. Of San Francisco	USA	2 / 6	No / No	Yes	Force feedback in only 4 axes. Driven by leadscrews connected to motors, the gripper and roll actuated by hydraulic actuators (limiting factors w.r.t. bandwidth), jaw by tendon to motor outside the body.	[47] [59]
6	No name	Johns Hopkins Univ.	USA	1 / 4	No / No	Yes	Two 3-dof Phantom systems. Added a gripping mechanism: 4-th dof.	[48]
7	MCM	Toshiba Corporation, Keio Univ.	Japan	1 / 3	No / No	No	Master and slave in one Master-slave Combined Manipulator.	[49]
8	Endo platform	Univ. of Berkeley	USA	1 / 7(?)	No / No	Yes	Slave: Endo-platform manipulator (tendon driven). Master: glove-like dextrous master with a tactile display for the first finger. Installed the manipulator and glove on a robotic platform.	[50]
9	Active Trocar & Active Forceps	Univ. of Tokyo	Japan	1 / 7	No / No	No	-	[51]
10	PUMA -> SARP -> Urobot -> SPUD	First at Imperial College in London (UK) then at NTU in Singapore.	UK -> Singapore	1 / 6(?)	? / ?	?	?	[52]
11	RAMS (Robot Assisted MicroSurgery)	NASA -> Jet Propulsion Laboratory and MicroDexterity Systems Inc,	USA	1,2 / 7	? / ?	No (to come)	Tendon driven (low geared) system for eye, ear, nose, throat, face, hand and cranial (brain) surgery.	[53] [56] [63]
12	FREG (Force Feedback Endoscopic Grasper)	Univ. of Washington Haptic Technology Inc.	USA	1 / 1	No / No	Yes	Master and slave each consist of an actuator and a position sensor (position error based force feedback). Also automatic palpation to measure material properties.	[57] [58]
13	Silver Falcon -> Black Falcon	Massachusetts Institute of Technology	USA	1 / 8	No / No	Yes	Save: Cable driven. Master: modified Phantom. With motion and force scaling. Several people that developed the Black Falcon also were involved in the development of the Da Vinci system (e.g. Niemeyer, Salisbury).	[60]
14	No Name	Deutsches Zentrum fur Luft- und raumfahrt	Germany	1 / 7	No / No	Yes	Tendon driven. Tendon forces and positions are measured (outside the human body). Master: modified Phantom.	[65]
15	No Name	Drexel Univ., Philadelphia	USA	1 / 3	No / No	Yes	Incorporated force sensors in a tendon driven laparoscopic tool (slave). Direct drive	[66] [69]

							motors. Force measurement by motor current measurement. Master: Phantom.	**[70]**
16	No Name	Dep. Of Mechanical Engineering, KAIST.	Korea	1 / 7	No / No	Yes	6-DOF Micromanipulator attached to a 6-DOF industrial robot. Force and motion scaling.	[67]
17	No Name	Johns Hopkins Univ.	USA	1 / 2	No / No	Yes	Developed a stainless steel sleeve around an existing lap. instrument shaft. Strain gauges incorporated in the sleeve. Haptic feedback using sensor substitution (audio).	[68]
18	No Name	TU Eindhoven	Holland	1 / 1	No / No	Yes	Smart Memory Alloy driven slave forceps.	[61]
19	No Name	Univ. of Tokyo	Japan	?	?	?	Tele Micro Surgical System (TMSS). Master slave system with three arms for MIS.	[33]
20	No Name	TU Delft	Holland	1 / 1	No / No	Yes	Laparoscopic hand tool (forceps). 1-Dof	[24]

Table 1. Medical telemanipulators with forceps control

3.2 Medical Robot Da Vinci

In previous sections different types of medical telemanipulators are discussed. In this section only one medical telesurgery robot will be discussed, the Da Vinci system developed by Intuitive Surgical in Sunnyvale, California.
The Da Vinci system is a very expensive system of about 1 million euros. The service costs are approximately 100.000 euros a year. Seen from the point of view that a Da Vinci system basically only consists of three (or four) robot arms and a control console this price is extremely high. Though, the price of a surgery robot is not determined just by the mechanical and electrical development and material costs. The vast part of the costs of a medical robot is determined by the cost made to make it FDA (Food and Drug Administration) approved. The Da Vinci received European Community clearance for abdominal and thoracic surgery in 1998 and FDA approval for general surgery in 2001. At this moment approximately 250 systems have been sold. Most systems are installed in the US. In Europe the most, about 40 systems, are sold in Italy. In the Netherlands there are only three Da Vinci's: in the academic hospitals of Utrecht, Maastricht and Amsterdam. The Da Vinci in Maastricht is the only one with four arms in the Netherlands.

The original goal for the development of the Da Vinci was to allow surgeons to operate from remote locations on patients in hazardous environments such as a battlefield or in space. Also it would allow surgeons to operate on patients with dangerous infections without endangering the surgeons themselves.
As a part of the Star Wars program, the US government supported research at the Stanford Research Institute that was developing a telesurgery robot. In 1994 the patents of the development were licensed to Intuitive Surgical. Within three years Intuitive Surgical venture capital based company developed the first seven-DOF robotic minimally invasive surgery system for operations on humans. Intuitive Surgical formed relationships with IBM, Massachusetts Institute of Technology (MIT) and Heartport. The first laparoscopic operation with this system was performed in March 1997 in Brussels (Belgium) [27].

Today the Da Vinci system is the state-of-the-art robotic minimally invasive surgery system. Until recently it's only competitor was ZEUS (Computer Motion). After a merge of Intuitive Surgical and Computer Motion in 2003, Intuitive Surgical acquired the rights for both machines. ZEUS is being phased out since commercial sale has been stopped.

The main competition for Da Vinci may come from two directions: other telesurgical robots that have been developed such as EndoVia. This system did not yet receive its FDA approval. A big advantage of the EndoVia is that it has haptic feedback integrated already [28].
The second competition may come from the mechanical manipulators as developed at AMC in Amsterdam [29]. This group of manipulators has a price related advantage since it will be much cheaper than Da Vinci [30]. A disadvantage of mechanical manipulators is that no adjustable (force- and) motion scaling is possible.

3.2.1 System overview

The Da Vinci system consists of two modules: a robot with three or four arms on a base frame on wheels (Figure 8.A). The second module is the console (Figure 8.B). During an operation the arms of the robot are covered with sterile bags. One arm of the robot holds the camera (endoscope); the other two or three arms hold medical instruments to operate with. The degrees of freedom of the robot plus the four degrees of freedom of the forceps (discussed in detail in section 3.2.2) give a total of 7 DOF. This includes the open-close move of the forceps. This number of DOF's gives the surgeon almost all the dexterity he was used to during open surgery.

Figure 4. a) Da Vinci robot with three arms. b) Surgeon-wannabe at the console.

The surgeon can operate comfortably sitting at the console a few feet away from the patient. He can rest his forehead while viewing a 'stereo' image of the surgical field and rest his underarms on a support table. The Endowrist® instruments are controlled by means of two tweezers-like joysticks that are naturally positioned relative to his eyes. This gives the surgeon back the eye-hand coordination he is used to in open surgery. The stereo view (for each eye a camera and a display) gives him back a sense of depth. The instruments in the patient exactly follow the movements of the surgeon's fingers in real-time (Figure 5). So the surgeon's motions aren't mirrored anymore as they were in conventional laparoscopy. And the tremor that was amplified due to the long shaft of the conventional instrument is no longer an issue since tremor is filtered out.

For very precise work the surgeon can downscale his movements in such a way that big movements of his hands result in small moves of the instruments. For safety reasons the instruments are disabled immediately when the surgeon moves away from the display.

When the surgeon wants to bring the joysticks in a more comfortable position he can disable the instruments with a footswitch, bring the joysticks there where he wants them while the instruments remain in a frozen position and then enable them again and continue with his task.

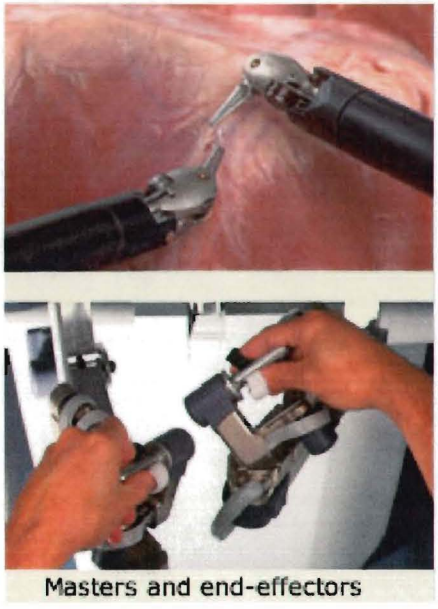

Figure 5. Da Vinci's instruments controlled by joysticks.

The surgeon can move the two-channel endoscope using another footswitch that disables the instruments and simultaneously enables the robot arm that holds the endoscope. Now the endoscope can be controlled with one of the joysticks.

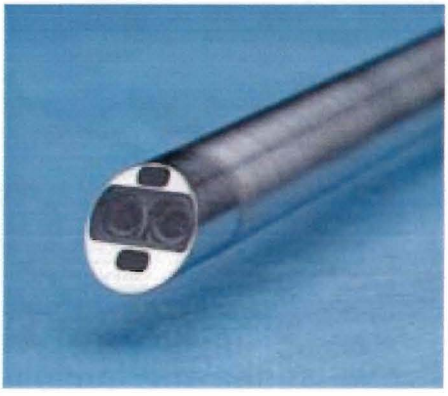

Figure 6. A.) Two-channel endoscope. **B.) Stereo binoculars above the joysticks.**

Controlling the robot and camera is very intuitive. Even an inexperienced user is able to perform several tasks such as pick and place tasks and even make a knot with suturing needle and wire after a few minutes already [31]. With conventional laparoscopic instruments the learning curve would be much worse. This means that using the Da Vinci system may reduce training costs.

So all disadvantages of laparoscopic surgery mentioned in Chapter 2 are reduced or solved by Da Vinci except for one. The surgeon still does not feel anything of the forces the instruments apply on the tissue. The Da Vinci system does not provide any haptic feedback. What the surgeon does feel via the joysticks is a vague pillow like feeling of force feedback when one of the DOF's of a robot arm is blocked. Blocking any of the DOF's of the instrument cannot be felt via the joysticks.

The electronic controller [32] that is mounted in the console is a custom designed control computer capable of controlling forty-eight motors at update rates exceeding one thousand cycles per second. It can read up to 48 encoders and 96 analog input channels and drive up to 48 DAC's. Surrounding the floating point DSP is a network of 24 micro-controllers and integer DSP's. Redundant sensors, hardware watchdogs and real-time error detection ensure fail-safe operation.

3.2.2 The Da Vinci's Forceps

For the Da Vinci robot many different types of operation Endowrist® instruments are available such as scissors, needle drivers, forceps's, etcetera. In this report only one type of the available forceps's will be discussed.
Figure 7 shows this forceps of the Da Vinci robot of Intuitive Surgical.

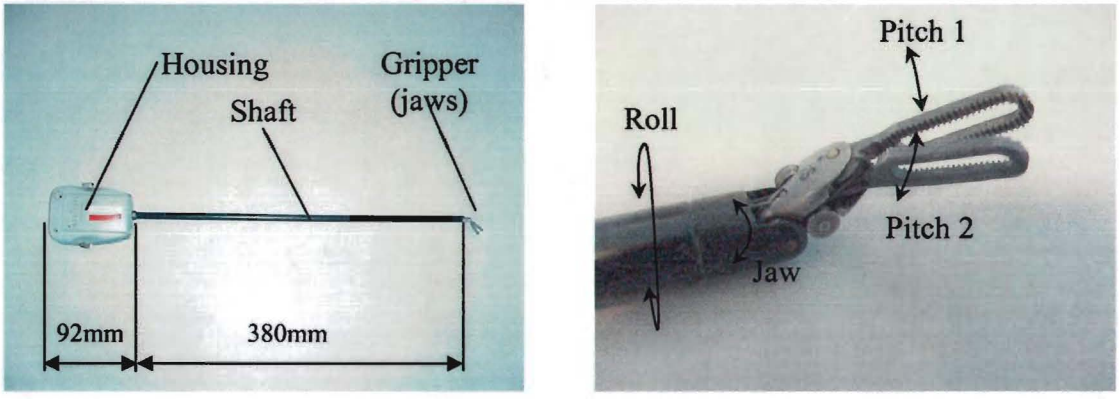

Figure 7. Da Vinci forceps

The degrees of freedom of the forceps are: jaw, pitch and roll. The two jaws of the forceps are controlled individually. All degrees of freedom are rotational moves and are driven by steel tendons. The arrows in Figure 7 clarify terms used to describe the degrees of freedom of the forceps.

The mechanical interface of the forceps with the Da Vinci robot consists of a mounting mechanism and four wheels shown in Figure 8. These wheels conduct the forces between the instrument and the robot with respect to the rotational moves described before. The rotation range of each instrument wheel is less than one revolution. The mechanical dimensions of the interface are given in appendix A.

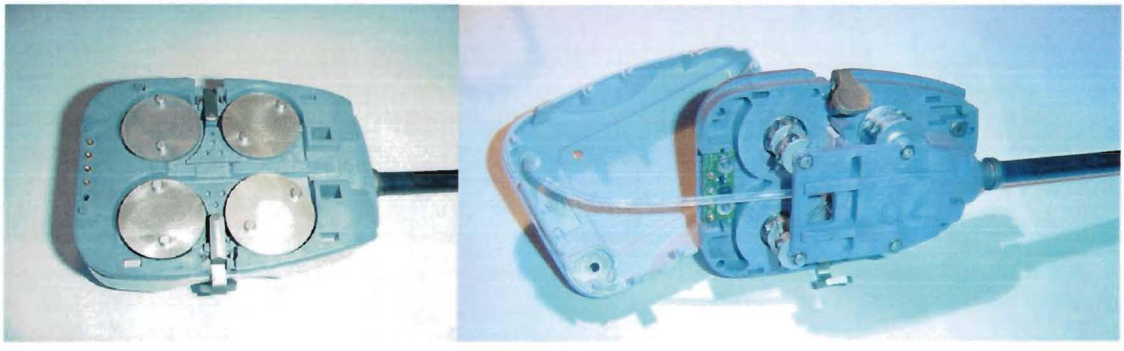

Figure 8. Driving wheels of the Da Vinci instrument.

Inside the housing of the instrument pulleys are mounted on the axis of the wheels. These pulleys drive the tendons that run via a pulley through the shaft of the instrument. Within

the shaft a metal tube is fixed around every tendon shown in Figure 9. The ends of the tendons are fixed to the forceps. The pre-tension in the tendons avoid backlash. Besides the metal tubes (tendons) also a plastic tube runs through the shaft. Close to the forceps this tube has an open end. The other end is connected to an opening in the housing of the instrument as shown in Figure 8. This plastic tube is used for sterilization purposes.

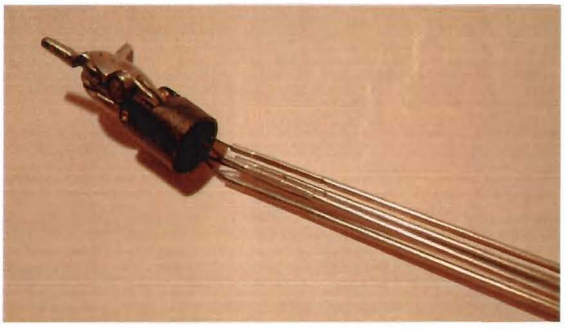

Figure 9. Metal tubes fixed around every tendon.

3.2.3 Shortcomings of the Da Vinci system

As stated before the Da Vinci system solves almost all disadvantages of conventional laparoscopic surgery as mentioned in Chapter 2. Besides these enormous advantageous properties of the system there are still some aspects that can be improved [21, 27, 31]:

- solving the lack of haptic feedback would be the most important improvement for the next generation Da Vinci. The current lack of haptic feedback is largely compensated for by the excellent stereo visual system,
- the time loss caused by system preparation and setup should be reduced. The size and the weight of the system are contributing to this problem. Attachment of the robot to the ceiling could be an improvement,
- a practical issue that needs improvement is the mechanical interface between the robot and the instrument. Frequently it dysfunctions when an instrument is exchanged during an operation, this takes too much time,
- the price of the system is still very high. Probably it will go down when Da Vinci gets accepted more in the medical world and more systems are sold [36].

3.2.4 Recent (and future) research on the Da Vinci system

This section gives an overview of the institutes and universities that are doing research with or on the Da Vinci surgical system with respect to force measurement or haptic feedback.
Many universities and other institutes use the Da Vinci robot or parts of it for many different kinds of researches or they research different aspects of the Da Vinci robot itself e.g.:

- learning curves of laparoscopic procedures: conventional versus Da Vinci,
- advantages, disadvantages and safety of telesurgery,
- analysis and evaluations of medical procedures executed with the Da Vinci,
- move-analyses of the surgeon's hands and instruments during surgical procedures,
- force analysis during knotting and suturing by hand, instrument and robot,
- time efficiency and (other) cost analyses for standard laparoscopy vs. Da Vinci,
- influence on suture forces with / without haptic / force feedback,
- influence on suture forces with visual and / or audio force feedback.

In this report only research with respect to force measurement and haptic feedback is described briefly.

First the backgrounds of Da Vinci, the involved parties and a few persons that played and still play a roll in the development of Da Vinci will be described.

As mentioned before several institutes contributed in the development of the Da Vinci surgical system. First it was the Stanford research Institute; then, when the patents were licensed to Intuitive Surgical, more companies, institutions and universities were involved such as MIT. Now Intuitive Surgical also works closely together with: IBM Corporation, AFX, Ethicon Endo-Surgery, Heartport Inc. (a Johnson & Johnson company), Medtronic Inc., Olympus Optical, Storz, Stryker Communications and Ventrica.

Gary Guthart was part of the core team developing technology for computer enhanced-surgery at Stanford research Institute. In 1996 he joint Intuitive Surgical where he now is Sr. Vice President Product Operations.
Kenneth Salisbury received his PhD from Stanford in Mechanical Engineering in 1982. After that, he worked at MIT until 1999. He is one of the developers of the Black Falcon Surgical Robot [60]. Intuitive Surgical has licensed aspects of the technology used in the Black Falcon for their Da Vinci system. Salisbury is the founder of SensAble Technologies Inc. producer of the Phantom haptic interface. In 1997 Salisbury joined the staff at Intuitive Surgical. In 1999 he joined the faculty at Stanford in the Departments of Computer Science and Surgery. In spring 2004 Salisbury said in an interview [39] about the Da Vinci system that: *"he would like to develop a method to translate the tactile sensations experienced by the instruments inside the patient to the control handles held by the surgeon"*.
Gunter Niemeyer received his B.S in Aachen (Germany). He received his M.S and PhD at MIT in 1990 and 1999 resp. Niemeyer came to Stanford University from Intuitive Surgical where he helped develop the Da Vinci system. Niemeyer worked on the Black

Falcon and on the THUMP [3] that is a haptic console for surgical simulation and training. *It incorporates two Da Vinci master mechanisms (joysticks) provided by Intuitive surgical and is capable of providing force and torque feedback to the operator.* In September 2004 Niemeyer said in [38] *he is working to add force feedback to Intuitive Surgical Inc.'s Da Vinci system. He states: "This will necessitate adding contact sensors to the system, but there is strong evidence that force feedback will be useful. My guess is it will be at least four to five years before this will appear in production systems.*

On the website of the University of Nebraska Medical Center the following text can be found:
"Research with the Da Vinci Surgical System. Researchers at the UNMC are currently working on advancement in the technology regarding the Da Vinci system. Areas of investigation include incorporation of feedback mechanisms for given forces used by the system (i.e. haptic feedback)".
In [41] is stated that the research on haptic feedback is in a very early stage and no details are available yet.

Allison Okamura is the lab director of the Haptic Exploration Laboratory of the Johns Hopkins University. She is focused on developing robotic sensory feedback capabilities. In [2] Okamura studied the difference between applied suture forces in three knot tying exercises: hand ties, instrument ties (using needle drivers), and robot ties (using the Da Vinci). The results of this research indicate that force feedback would improve robot-assisted performance during complex surgical tasks such as knot tying with fine suture.

In [42] a short description can be found on a project of Okamura in which *strain gauges were added to the shaft of a Da Vinci instrument in order to measure forces working on the tip of the instrument.* The force information could be presented to the surgeon in two different ways:

1. as an audio signal that grows louder as the force increases. Some surgeons objected because the operating room already is cluttered with the sounds of spoken commands and medical equipment,
2. as a visual signal. A bar graph was implemented in the corner of the video screen of the Da Vinci console. The bar graph rises and changes color as the force increases. The surgeon also sees a dotted line that indicates the appropriate level of force for the procedure. The experimental setup was added to a Da Vinci being used for training and research at the Johns Hopkins Hospital.

A paper describing more details about the strain gauges in the instrument could not be found. In [43] Okamura said a paper about this setup will be ready shortly.

In [1] Okamura proved that substituting direct haptic feedback with visual and auditory cues to provide the surgeon with a representation of forces he is applying with the Da Vinci, results in quantifiable advantage in applied force accuracy and consistency during the performance of surgical tasks. The surgeon's performance, in terms of the accuracy and consistency of applied forces, of robotic ties with force sensory substitution was at least comparable with performances during hand ties if not better.

Sensory substitution (providing force feedback through a visual display and auditory tones) is an interim alternative to haptic feedback directly to the surgeon's joysticks. *Okamura laboratory's next technical goal is to equip robotic surgical instrumentation with force feedback mechanisms that would enable direct haptic feedback to the operating surgeon.*

During the experiments of both [1] and [2] the forces that were applied were measured with a 'Suture Tension Measurement Device" (TMD). This device consists of two 1-DOF load cells tied to the sutures. The resolution of the TMD is 0.09 N.

At the University of München Hermann Mayer developed a robotic system to evaluate force feedback in minimally invasive surgery [4, 5]. The system consists of two industrial Kuka KR6/2 6-DOF robots. On each robot a Da Vinci surgery instrument is mounted provided by Intuitive Surgical.

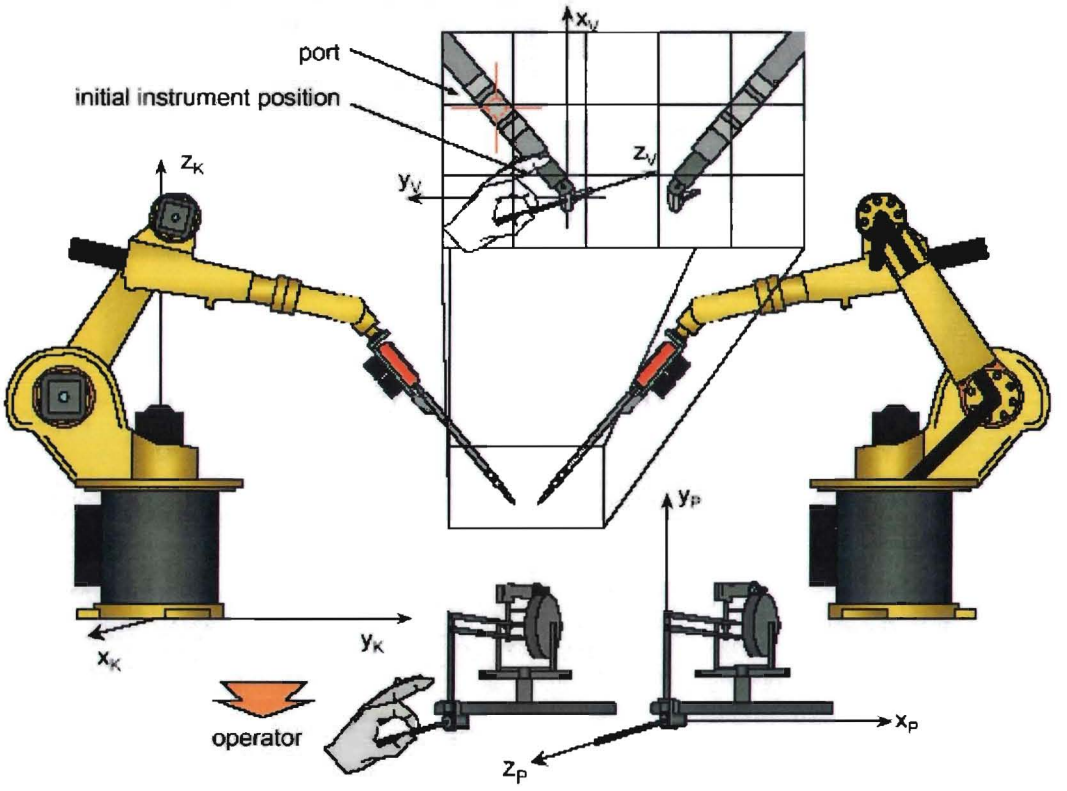

Figure 10. System at München with Da Vinci instruments, Phantoms and Kuka robots.

Four servomotors directly drive the wheels of each instrument via an Oldham coupling. The operator controls the instruments via two SensAble Phantoms (with 3-DOF force feedback). There are plans to develop an own input instrument to replace the Phantom. A switch is used to open and close the micro grippers of the instrument.

The strain gauges are applied directly on the shaft of the instrument near the gripper as shown in Figure 11.

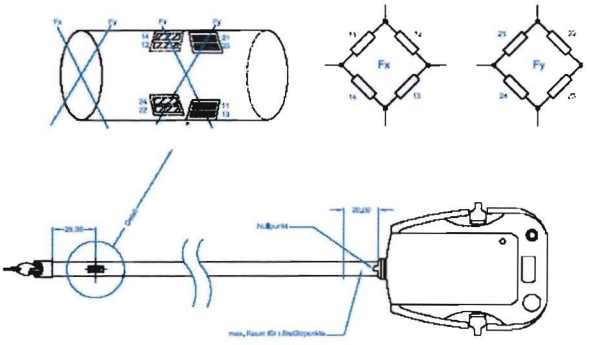

Figure 11. Da Vinci instrument with strain gauges (University of München).

Forces are acquired only in the XY-plane perpendicular to the instrument shaft.
The system's software interface and mechanical set-up descriptions are freely available to enable other research groups to participate in the development.

4 Problem definition

Adding force sensors to the instrument inevitably means it becomes more expensive. Since the Da Vinci robot instruments are disposables that are used only 10 times and cost about 2000 euros, costs should not get much higher according to the users [21]. Implementing sensors in, or close to the tip of the forceps may also introduce problems associated with electrical interference when (electric) ablation techniques are used during an operation. Ablation techniques will also cause temperature variations that may disturb the force measurements, either when force is measured with electrical or (fiber-) "optical" strain gauges.

It is our goal to provide force measurement in a laparoscopic instrument of the DaVinci robot of Intuitive Surgical without adding sensors to the instrument. In this way not only the disadvantages as described above are avoided but also extra complications with respect to sterilization at temperatures of over 130 degrees Celsius are avoided. An extra important advantage is that no extra hardware costs (strain gauges and amplifiers) are involved. For our research we use the laparoscopic forceps instrument of the Da Vinci surgical system as depicted in Figure 7.

Our goal is to derive the magnitudes of the forces working on the tip of the instrument from the currents of the actuators that drive the forceps, outside the patient's body. It is obvious that the price we will have to pay for this approach is a lower accuracy level of force measurement than the level that can be achieved with force measurement directly at the tip of the instrument. This lower accuracy is caused by instrument characteristics as friction and limited mechanical stiffness etc. In this work we will try to compensate for the instrument friction in such a way that force measurements will provide sufficient information for proper haptic feedback.

We will investigate whether the described approach can result in a haptic feedback setup that provides sufficient force/torque information for an intuitive laparoscopic haptic feedback system with a limited amount of degrees of freedom for laparoscopic surgery.

Problem description:

Forces working on the environment applied by the tip of the instrument in motion, are derived from the current setpoints of the actuators that drive the instrument. Instrument friction and the friction and disturbances introduced by the current amplifiers and actuators make the force measurement less accurate if they are not compensated for. In order to limit this loss of accuracy the mentioned frictions and disturbances are investigated and, it is investigated how they can be compensated for during instrument motion.

For these investigations a test setup will be developed that drives the joints of the Da Vinci laparoscopic instrument. Figure 12 clarifies the measurement setup.

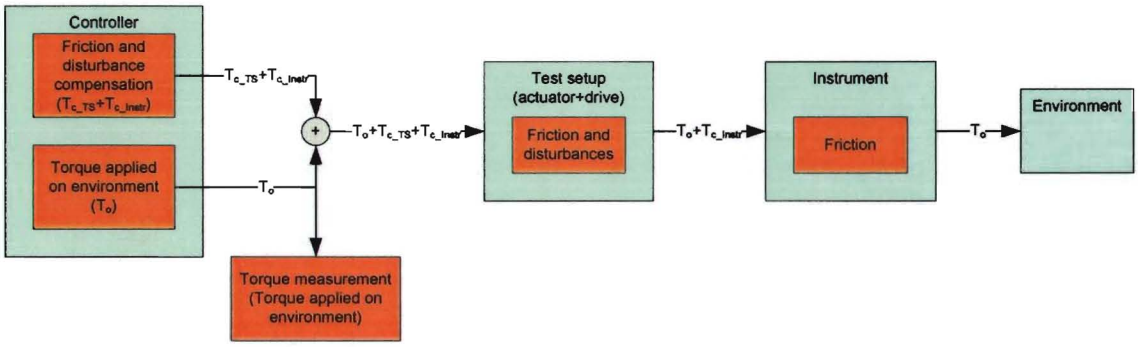

Figure 12. Measurement of torque applied on the environment

In this report we will concentrate on one pitch joint. This joint will be analyzed with respect to (position dependant) friction and other disturbances. In order to qualify the results of the analysis we will compare them with the requirements for a laparoscopic robot with haptic feedback [23].

4.1 Project approach

As described in the previous section, a test setup will be developed that drives the joints of the Da Vinci laparoscopic instrument. Using this setup, measurements are performed on the Da Vinci instrument.

In Chapter 5 a few specifications are generated for the test setup. Chapter 6 gives a description of several design aspects of the test setup and Chapter 7 describes the measurements results performed on the realized test setup with respect to the friction and disturbances the setup introduces. Also the compensation methods for the introduced frictions and disturbances are discussed. In Chapter 8 the Da Vinci instrument is mounted on the test setup and the results of the friction measurements are presented.
In Chapter 9 the conclusions are discussed and a statement is made on the feasibility of accurate force measurement with the Da Vinci instrument using actuator current.

Since we work with a standard Da Vinci instrument there is no position measurement locally at the instrument joints. The instrument is considered as a black box. The joint positions are derived from the actuator positions that drive the joints so the actual joint position remains invisible for the controller.
Since only instrument friction and not instrument stiffness is investigated in this report, measurements will be performed with low frequent motion only.

5 Forces on the operation instrument

5.1 Torques and forceps dimensions

For the Da Vinci robot many different instruments are available in different sizes. In order to standardize the way torque's working on the forceps are measured we will assume that all forces working on the forceps take action 20 mm from the rotation axis of the grippers (pitch 1 and pitch 2).

5.2 Human sensing

Before defining system specifications it is necessary to know something about properties of human sensing.
Kinesthetic sensing is a form of sensing that comprises large-scale details such as basic mechanical properties e.g. the stiffness of a pencil. In this report only two main properties of kinesthetic sensing will be mentioned that are important for the specifications of a haptic feedback system [23]: frequencies can be detected up to 10 Hz [43] and force resolution is 0.06 Newton [45].

5.3 Forces and bandwidth of instrument moves

The forces that instruments exert on tissue or other materials like needles, strongly depend on the operation task that is being executed. During microsurgical tasks the forces are smaller than during knot tying or suturing. In Table 2 the forces that a forceps exerts on tissue during microsurgery are shown [44].

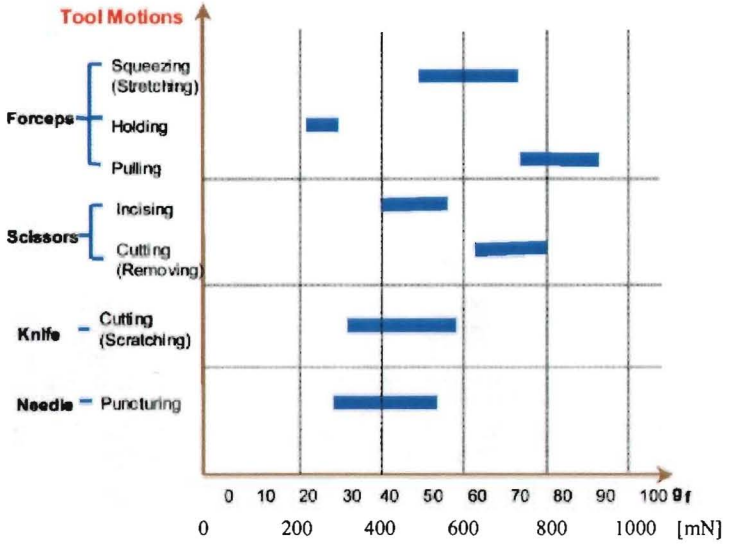

Table 2. Forces exerted by instruments during micro-surgery

During tying suturing knots with a needle driver much larger forces are required. Among other parameters the forces and bandwidth of these motions are given in Table 3.

Parameter	Value
Force: at the point of needle for driving the needle through tissue	> 1.5 N
Torque: about grasper axis, for driving needle (assumes curved needle, 15 mm from grasper to needle tip)	> 100 Nmm
Torque: wrist (yaw)	> 300 Nmm
Force: gripping, while driving a needle	> 40 N
Speed: Grasper, full close in	< 0.5 sec
Speed: Wrist roll	> 540 degrees/sec
Speed: Wrist	> 360 degrees/sec
Bandwidth	> 5 Hz

Table 3. Instrument forces required for suture knot tying

5.4 Pre-investigation of the Da Vinci instrument

In order to have an indication of the properties of the Da Vinci instrument before designing a test setup the Coulomb frictions and spring constants of the mechanics between the instrument wheels and the forceps are measured roughly. The spring constants are determined for low torques (5 N) only. This measurement is performed applying a force on one DOF of the forceps while blocking the corresponding wheel. The values are shown in Table 4.

Wheel function	Coulomb friction [Nmm]	Spring constant [Nm/rad]
Roll	2	-
Jaw	7	-
Pitch1	5	50
Pitch2	5	50

Table 4. Da Vinci pre-investigation results

The spring constants for low torques show a low stiffness. It is expected this stiffness is non-linear.

Compared to the forces applied during microsurgery operation tasks described in section 5.3 the Coulomb friction of the instrument is relatively high. For instance, for the gippers of the forceps the forces in the range of 0.2 N till 0.9 N mentioned in section 5.3 correspond with torques in a range of 4 Nmm till 18 Nmm. The force resolution of 0.06 N corresponds to 1.2 Nmm.
The roll axis shows a spring constant because the jaw and pitch tendons are wound up during a positive and negative roll move. The (asymmetric) spring constant derived from the rough measurement is approximately 5 mNm/rad.

The results mentioned above are used to define coarse specifications for the setup design. Further the results indicate that friction is a very important disturbing factor that must be dealt with when the Da Vinci instrument is used in a haptic system where torques are measured at the driving wheels (instead of at the forceps).

6 Design of the test setup

For the design of the test setup no extensive Technical Product Documentation will be generated as is done during development processes at CCM (Centre for Concepts in Mechatronics). This would comprehend documents such as SPS, EPS, EDS, TPS, TAR, etc. Instead of this only the essential requirements/specifications and several concept choices are discussed.

6.1 Requirements

The tests described before sketch a framework for the requirements for the test setup. It would be possible to execute the tests with a setup that drives only one instrument wheel at a time while the other wheels are blocked. Though, for convenience, symmetry and flexibility reasons a test setup must be designed to drive two instrument wheels simultaneously. In this way both grippers can be moved symmetrically. Later the test setup may be expanded with two more motors to drive all instrument wheels.

The setup must be a mounting frame for the Da Vinci instrument and for the motors that drive the wheels of the instrument. Further the setup must provide couplings between each motor and the corresponding instrument wheel. Because the instrument wheels do not have a standard interface, a wheel interface must be designed that can be mounted on the instruments wheels. A block diagram of the functional parts of the setup is shown in Figure 13.

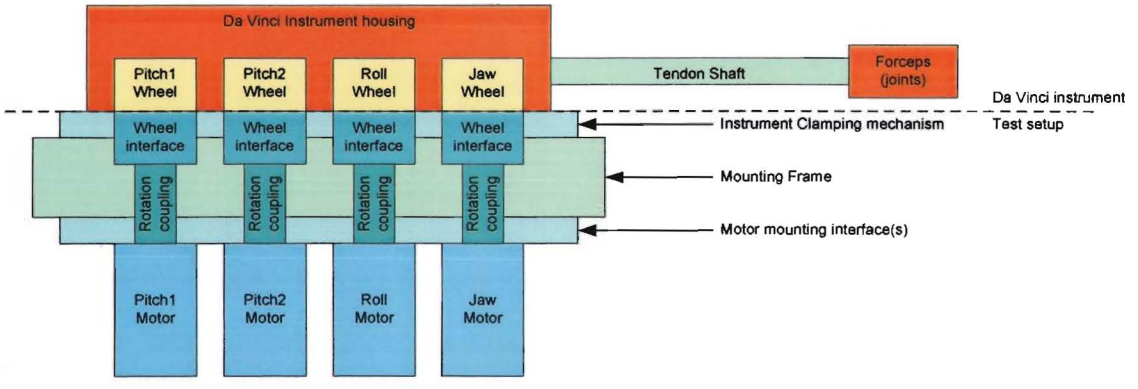

Figure 13. Functional block diagram

Friction and backlash introduced by the setup must be kept as minimal as possible since position measurement will be done by means of the motor encoder and the magnitude of the applied motor torque will be derived from the motor current setpoint.
For future dynamic analysis the inertia of all moving parts of the setup should be as low as possible.
The results of the pre-investigation measurements give an indication of the Coulomb frictions of the instrument. From these values a specification is derived for the maximum

Coulomb friction of the setup. The specification for the maximum Coulomb friction of the setup is set to 1/3 of the instrument Coulomb friction.
The drive/servo- stiffness requirement of the setup is also derived from the results of the pre-investigation measurements. For the setup stiffness specification a minimum value is chosen of 3 times the instrument stiffness.

Setup parameters	Value
Coulomb friction	< 1.7 Nmm
Drive stiffness	> 150 Nm/rad

Table 5. Friction and stiffness specifications for the wheel drive train of the test setup

The specifications described in Chapter 5 are adopted as measure requirements for the setup. A summary of the applicable requirements is listed in Table 6. Notice this is a combination of the requirements for suturing and knotting and the requirements for microsurgical tasks. For minimum force measurement accuracy a value of 5% is used.

Parameter	Value
Torque: about grasper axis	> 100 mN
Torque: wrist jaw	> 300 mN
Force: gripping, while driving a needle	> 40 N (for gripper: corresponds to 0.8 Nm)
Speed: Grasper, full close in	< 0.5 sec
Speed: Wrist roll	> 540 degrees/sec
Speed: Wrist jaw	> 360 degrees/sec
Force sensing resolution	> 60 mN (for gripper: corresponds to 1.2 Nmm)
Bandwidth actuation	> 5 Hz
Bandwidth force measurement	> 10 Hz *
* see section 6.2	

Table 6. Actuator and measurement requirements

6.2 Design

In the previous sections we have defined a set of requirements/specifications for the test setup. In this Chapter a design is described based on these requirements, only the bandwidth of the force measurement is chosen equal to the actuation bandwidth of 5 Hz. For driving the four instrument wheels and for measurement (or determination) of the torques applied by the actuators to the instrument wheels, among several alternatives, four different concepts were considered and compared. Three of these design concepts are discussed in Appendix B *Alternative concepts for the setup*. The selected (fourth) concept is implemented and is described in this chapter.

6.2.1 Mechanical design

Because the diameter of the selected motor (specified later in this report) exceeds 32 mm, direct drive as described above is not possible. The configuration that is chosen is a combination of concept 2 (tendon driven, torque measurement using a load cell) and concept 3 (motor current measurement) as described in Appendix B *Alternative concepts for the setup*. The instrument will be driven by tendons and torque measurement will be based on motor current.

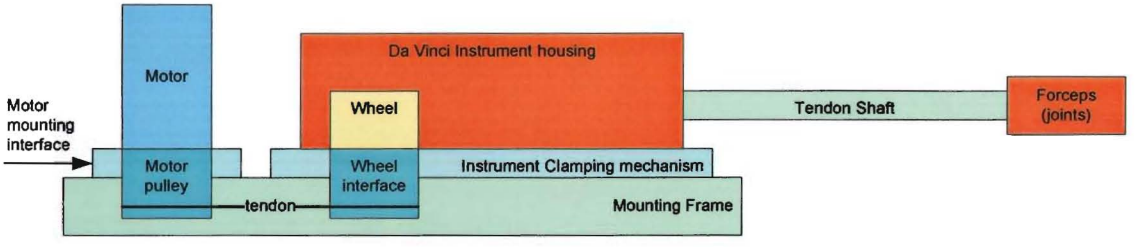

Figure 14. Selected concept

In order to eliminate the disadvantages mentioned in concept 2, no extra pulleys and therefore no extra ball bearings and inertias are introduced. The tendons are kept short so stiffness is high. Disadvantage of the high stiffness is that a disturbance force is introduced by the unroundness and eccentricity of the instrument wheels and motor pulleys. In order to reduce this disturbance force, the motor is mounted on two parallel leaf springs (see Figure 15). Since the disturbance force is linear to the spring constant of the leaf springs, this spring constant must be chosen as low as possible. The lower limit of the spring constant is determined by the required tendon pre-tension that must be applied and physical dimensions of the setup (the dimensions of the springs and the deflection they are allowed to make). The leaf springs are exchangeable, making the motor suspension stiffness selectable. In Appendix E *Spring constant of the motor assembly*, the spring constant of the motor assembly is calculated and also verification measurement results are presented.
The pre-tension in the tendon can be adjusted with the tension screw (see Figure 15).

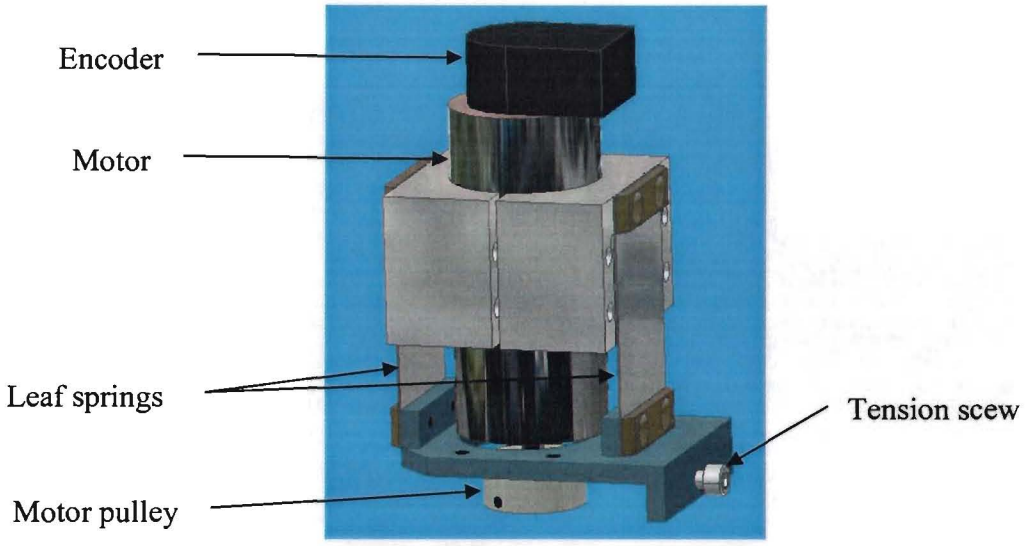

Figure 15. Motor mounted on leaf springs

The purpose of the pre-tension applied by the leaf springs is to maintain tendon straightness between the wheels and consequently to maintain drive stiffness and avoid backlash. For the unloaded instrument the lower limit of the pre-tension is determined empirically and has a magnitude of 5 [N]. This lower limit is referred to as the 'absolute lower limit of the pre-tension'. The magnitude of the applied pre-tension also depends on the torque that must be transferred between the pulleys. In order to keep both wires under a tension that is at least as high as the magnitude of the absolute lower limit of the pre-tension, the pre-tension must have a magnitude that is equal to the sum of the absolute lower limit of the pre-tension and the maximum tension (tensile force) expected due to torque transfer during measurements.

With the availability of several sets of leaf springs and due to the adjustable motor position (using the tension-screw), the spring constant and the pre-tension can be adjusted for each type of measurement.
For friction measurements only low torques are required. Therefore a low pre-tension of only 5 Newton will be applied during those measurements. This low pre-tension allows us to use leaf springs with a low spring constant.
Also when a low spring constant is used, a small portion of the disturbance force remains. Since the disturbance force is a function of the motor position, it is perfectly predictable. Therefore it can be calibrated and compensated for in the controller.

The tendon is not only wrapped around but also fixed to both the motor pulley and the instrument wheel. This is done for two reasons: First, in order to avoid accumulating micro slip. Secondly, in order to avoid the necessity of high pre-tension that would be needed to create enough friction between the tendon and the wheels to conduct the specified torque from the motor to the instrument wheel. This high pre-tension would increase the friction in the ball bearing of the motor and the instrument.

For the mechanical interface with the instrument wheels a clamp mechanism is designed. On the clamp mechanism a wheel is mounted as depicted in Figure 16.

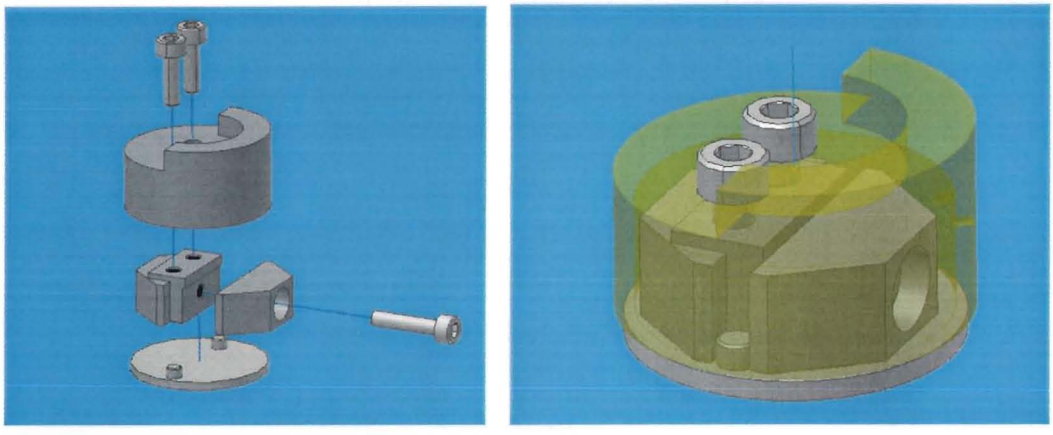

Figure 16. Instrument wheel interface. a) Exploded view. b) Assembled view.

Since the motors of the setup hardly produce mechanical energy due to their limited rotation, they dissipate most of the electrical energy that is supplied. Consequently, if a motor is loaded heavily during tests its temperature rises. In order to reduce motor constant variations due to temperature variations the motor is mounted in a cooling body (see Figure 15). A thermal past between the motor and the body reduces the thermal resistance.

Three 3-D drawings of the total setup, drawn Inventor, are shown in Figure 17. The four motors and the instrument are placed on the same side of the mounting frame with the instrument in the centre. For detailed drawings see Appendix I *Mechanical drawings*.

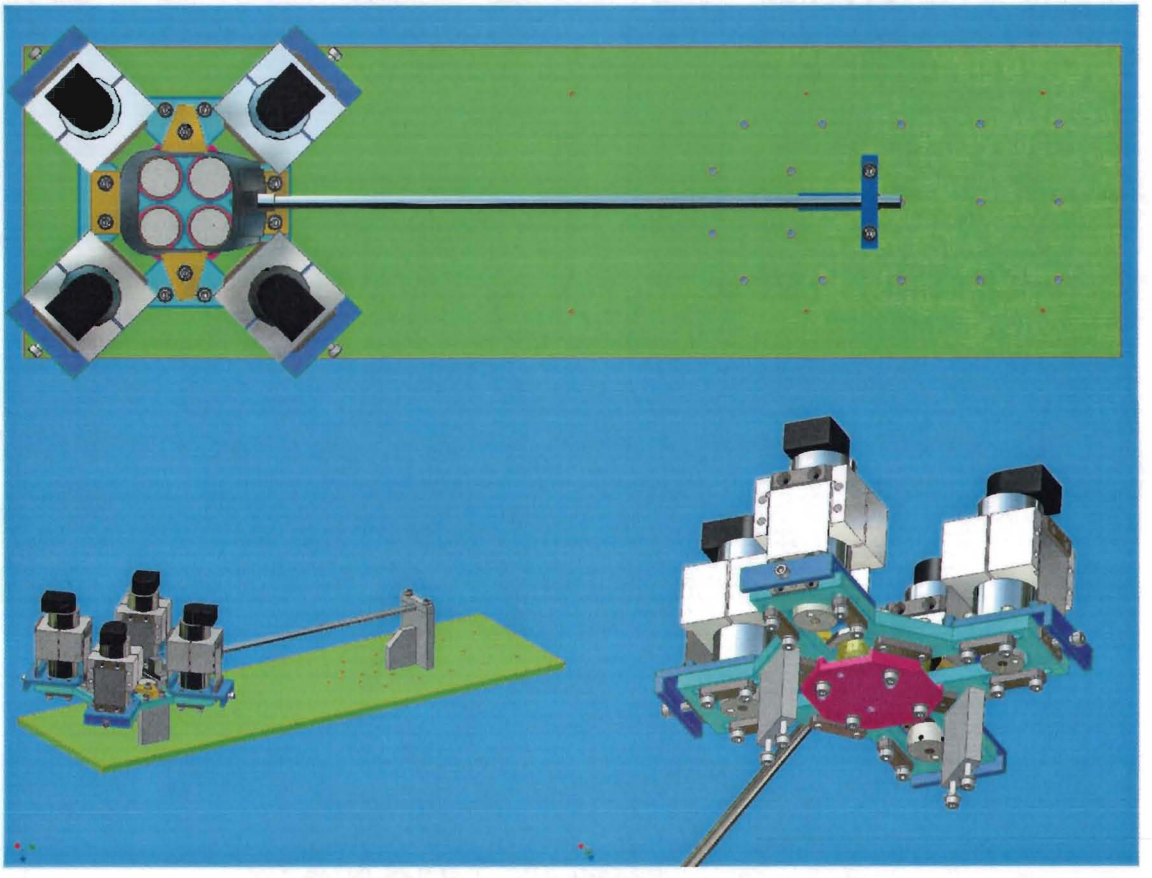

Figure 17. Drawings of the total setup.

6.2.2 Electrical and software design

Matlab Simulink (incl. StateFlow) is used to design and implement the controller. Real Time Workshop and XPC are used to run code that was generated by the host PC on the Target PC that is connected to the hardware.
The Host PC and the Target PC are connected by an Ethernet interface. This interface is used for code upload to the Target PC, setting parameters and reading signal values. For fast data acquisition signal traces and loggings are stored on the Target PC. After the measurement the data is transferred to the Host PC where it is processed and analyzed. During the measurement, signals may be monitored in real time on the Target PC monitor.

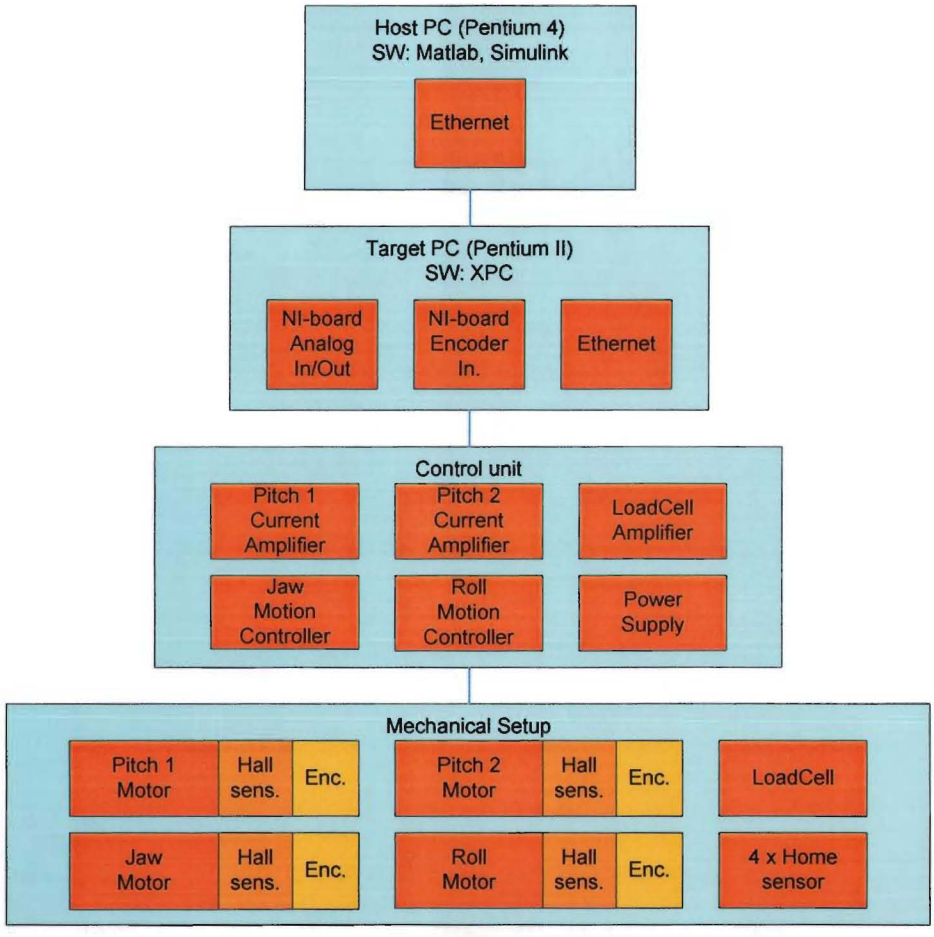

Figure 18. System control Top view

Details about the control unit can be found in Appendix G *Control Unit Details*. Figure 19 shows a picture of the implementation of the total setup.

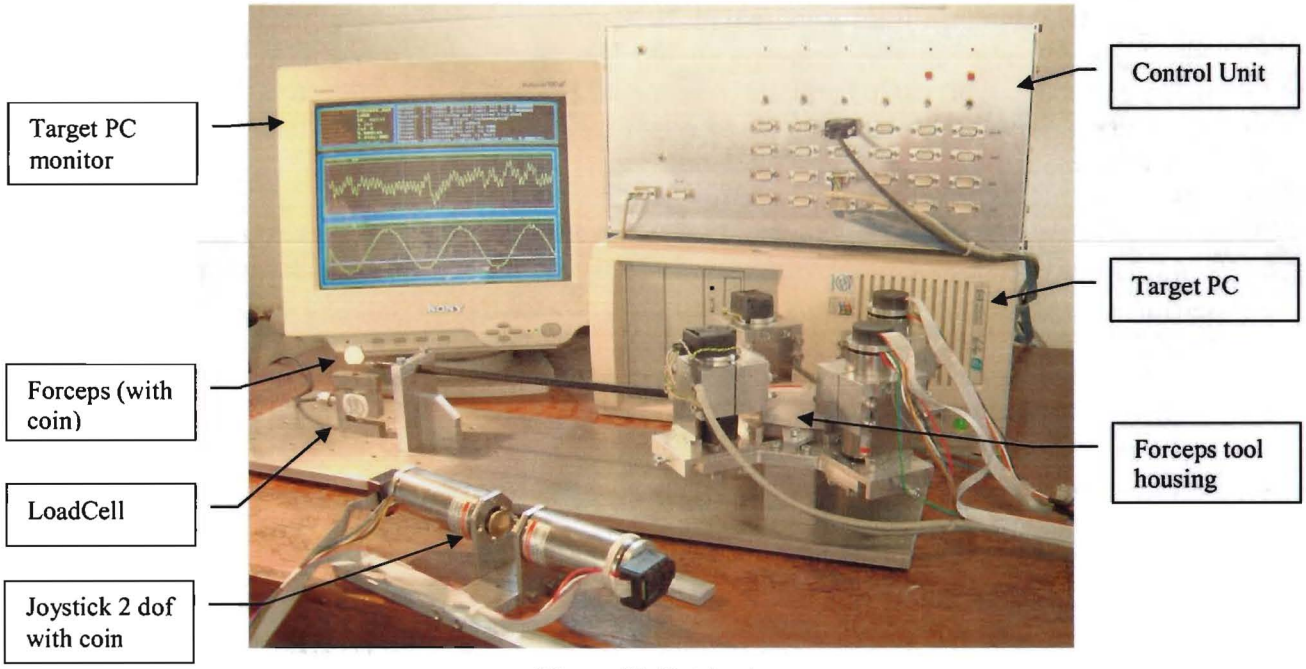

Figure 19. Total setup

Motor selection is based on system specifications of Table 6. The motor selection is limited to the product range of Maxon motors that are reliable high quality electro motors used in high tech applications worldwide (and beyond: e.g. Pathfinder).

Criteria used for motor selection are:

- no reductor (avoidance of backlash and friction),
- low friction (ball bearings),
- sufficient torque (continuous and max. torque),
- low torque ripple (electronic sinusoidal commutation (EC)),
- low rotor inertia (EC inertia is lower than RE inertia),
- preferred diameter < 32 mm (related to motor power / torque),
- encoder resolution (preferred at least 1000 counts/revolution),
- low torque constant (higher resolution current measurement).

The motor/load-ratio will depend strongly on the mechanical load that will be applied on the forceps. Unfortunately, this load is far from constant during operation tasks. Since the first priority of this setup is analyzing the instrument, this issue is not taken into account in this design.

The selected motor is a Maxon EC-motor with ball bearings and without reductor. Since there is no Maxon motor available with the required torque that has a diameter smaller than 32 mm, a motor is selected with a diameter of 40 mm.
Since the delivery time of an encoder with 1000 counts/revolution would have postponed the project with two months, a motor with 500 counts/revolution was selected. Motor and encoder specifications can be found in Appendix D *Maxon motor data sheet.* Many tests could be performed with an identical motor with a 1000 pulses encoder that was provided by Maxon motors for free.

Since an electronic commutated motor is selected for sinusoidal commutation the current amplifier must support this. Further, in order to avoid unnecessary costs the controller selection was based on availability. Motion controllers IDM640 (product of TechnoSoft) and DES 70/10 (Maxon motors) were selected to be used as a current amplifiers. The DES70/10 controllers were donated by Maxon motors.

The IDM640 of Technosoft seemed not to function correctly in current control mode when an unloaded (or low loaded) EC-motor is controlled. This gets very clear when looking at the Stribeck curve of the unloaded motor measured with this controller (see Appendix C *Stribeck curve with MC IDM640*).
Since we are highly interested in measuring low torques, the IDM640 seemed not suitable for the setup and was not used any further.

7 Measurements on the test setup

Section 7.1 will discuss the torque disturbances that are present in the setup. Section 7.2 discusses the compensation methods for the torque disturbances.

7.1 Torque disturbances in the setup

In order to derive the applied torque on the instrument interface wheel accurately from the motor current setpoint, the following disturbances that are present in the setup have been analyzed:

- temperature dependency of the motor constant,
- motor commutation torque ripple,
- motor cogging,
- motor friction (static, Coulomb and viscous),
- motor position dependent motion controller current ripple,
- motor acceleration,
- torque disturbance due to eccentricities in pullies.

The roughness of the tendon is neglected. The roughness of the pullies is better than the roughness of the tendon and therefore also neglected.
The torque disturbances due to eccentricities in pullies are analyzed in Appendix J by calculation and simulation in 20-Sim.

The last part of this section will describe the compensation method that is used to eliminate the vast part of the repetitive disturbances.

7.1.1 Motor constant as function of temperature

In order to derive the applied motor torque accurately from the motor current setpoint, it is necessary to know the motor constant accurately. Since the motor constant is a function of temperature it is determined for a number of temperatures. If required the controller can be corrected for the changing value of the motor constant.

According to the data sheet (Appendix D *Maxon motor data sheet*) the motor constant is 45 mNm/A. The motor constant is measured over a temperature range from 20 until 50 degrees Celsius. Temperature is measured with a Pt-100 sensor mounted on the cooling body of the motor. Motor current measurement is provided by the motion controller and is monitored using a PC connected to it.
An arm with the length of 540 mm is fixed to the motor shaft radially. Motor torque is determined by multiplying the arm length with the force measured by a force gauge at the end of the arm.

Before the motor constant measurement was executed, the DC-linearity of the motion controller that is used as a current amplifier was checked. From the measurement results (not included) it appears legitimate to consider the motion controller perfectly linear (input setpoint voltage vs. output current) for DC-currents in at least the range from 0 to 4 Ampere, in which the motor constant measurement is performed.

As shown in Figure 20 the motor constant slightly decreases when temperature rises. This is mainly caused by the reduction of magnetic field strength of the Neodymium magnets inside the motor when temperature rises. In literature is found that the temperature dependant reduction of strength of a Neodymium magnet is -0.11 %/C.

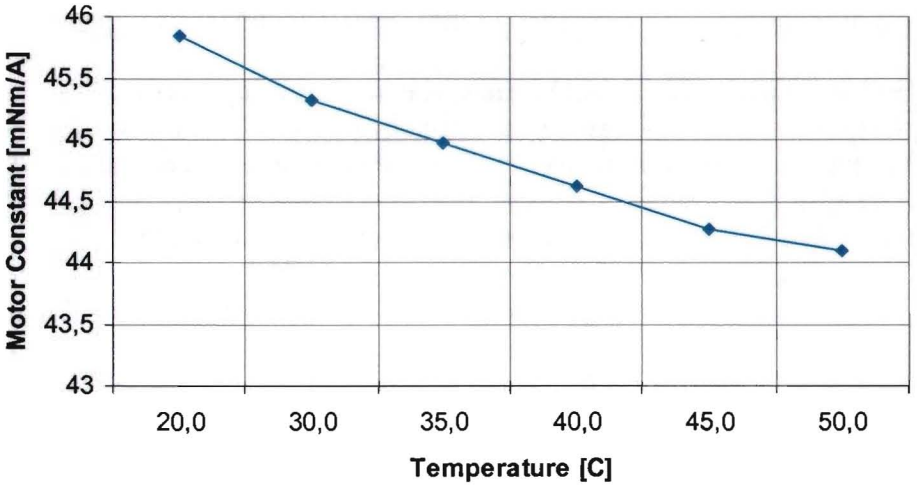

Figure 20. Motor constant as function of motor temperature

From Figure 20 we see that the value of the motor constant is between 45 and 45.8 mNm/A when the motor temperature remains in the range between 20 and 35 degrees Celsius. This is equal to (1 - 45 / 45.8) *100 / 15 = -0.116 %/C which is in the same range as the value found in literature about Neodymium magnets.

The question rises whether it is essential to add temperature measurement systems for every motor. This measurement would make it possible to compensate for the changing motor constant with changing temperatures.
It seems that during tests the motor temperature remains in the range between 20 and 35 degrees. When in this temperature range the motor constant is assumed to have a constant value of 45.4 mNm/A this would introduce an error of about +/- 0.9 %.
Since this error is small, no active temperature measurement system is added to the setup.

7.1.2 Motor commutation, cogging and friction

In the setup the motor torque ripple caused by commutation is neglectable since the motor is commutated sinusoidal electronically in stead of block-shaped commutation triggered by Hall-sensors or mechanical commutator segments. Details about magnetic alignment at motion controller start-up can be found in Appendix F *Magnetic alignment of the MC.*

Some motor properties can cause a torque ripple called 'cogging'. In a servomotor cogging can be caused by e.g. asymmetry or imbalances in magnet positions and magnetization. This torque ripple is a function of the motor current and motor position. When the torque ripple caused by cogging is measured once, it can be compensated for since the motor current and motor position are constantly known during operation.

Motor friction is caused by the ball bearings that are preloaded with an axial force of at least 10 Newton. This friction can be visualized by means of a Stribeck curve that shows the torques that are required to rotate the rotor in a continuous speed range from a high negative speed to a high positive speed.
When rotor velocity is zero, the minimum torque required to make the rotor move is the Static friction. The non-linear part of the curve at low speeds is the Stribeck effect. The slope of the curve at high speeds gives a measure for the viscous friction of the motor. The Coulomb friction is found there where the linear curve would cross the vertical axis of the plot. Figure 21 shows a schematic sketch of a typical Stribeck curve.

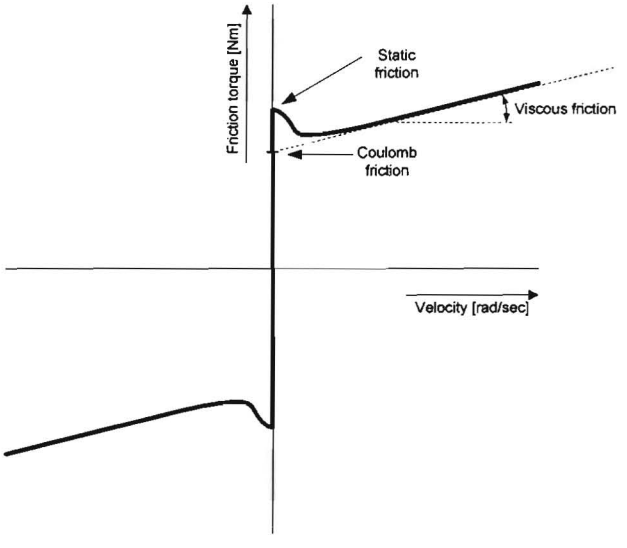

Figure 21. Schematic Stribeck Curve

When the Stribeck effect is not included the friction may be written as:

$$f_t = f_C \cdot \mathrm{sgn}(v) + f_V \cdot v,$$

where f_t is the total friction, v is the velocity of the rotor, f_C is the Coulomb friction and f_V is the coefficient of the viscous friction.
The viscous and Coulomb friction are compensated for in the controller design of the setup. This will be discussed in section 7.2. In sections 7.1.2.1 and 7.1.2.2 measurements are performed to estimate the viscous, Coulomb and static friction of the motor.
Internal motor losses such as speed dependant iron losses have not been investigated. It is assumed that there is a linear relation between motor current and motor torque. This linear relation is given by the motor coefficient.

7.1.2.1 Friction of the radial unloaded motor

The static friction of the unloaded motor is measured by applying a slowly ramping current to the motor. The torque needed to set the rotor in motion is called the break out torque and is equal to the static torque. The static friction is found using:

$$T_S = K_{mc} \cdot I_m$$

where T_S is the magnitude of the static friction, K_{mc} is the motor constant and I_m is the motor current.
Cogging and the rotor position dependant controller disturbance (discussed in section 7.1.3) are of major influence on the measurement results as can be seen in Figure 22. At a torque of 2.4 mNm the rotor starts rotating but it is stopped after half a revolution. At a torque of 5 mNm the rotor starts to ramp up. The value found for the static friction seems to be motor position dependant mainly due to cogging and the rotor position dependant controller current disturbance. The static friction lies in a range between 2.4 and 5 mNm. One instance of multiple measurements is given in Figure 22.

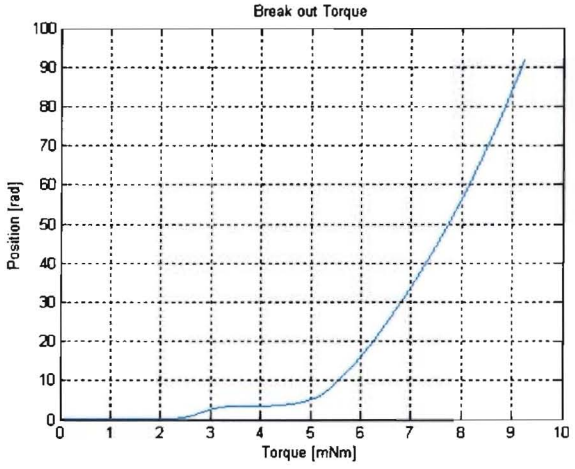

Figure 22. Static friction of unloaded motor

Coulomb- and viscous friction will be read from the measured Stribeck curve later in this chapter.

7.1.2.2 Motor friction of the radial loaded motor

In the setup a radial load is working on the motor shaft because of the pre-tension applied by the leaf-springs (see Figure 15). This load causes extra friction in the motor ball bearings. For practical reasons, only the static friction measurement has been performed for the radial loaded motor.
To measure the static friction of the loaded motor, first the motor pulley is mounted to the shaft. Then the motor is mounted horizontally. The steel wire, which is used in the setup as a tendon, is hung over the pulley and at both ends of the wire a weight of 1.12 kg is attached, hanging down.
The weights represent a pre-tension of 2 * 1.12 kg * 9.8 = 22 Newton.

The automatic static friction measurement is executed as described in the unloaded situation above. Since the acceleration during the static friction measurement is extremely low the inertia of the weights is neglected. Also the friction of the steel wire rolling over the motor pulley is neglected here.

Measurement shows that the static friction of the motor with a radial pre-load of 22 Newton has increased by 1.05 mNm compared to the unloaded measurement results. Assuming the relation between radial ball bearing load and friction is linear, this means that during friction measurements with a pre-tension of only 5 Newton the static friction increases only with (5 / 22) * 1.05 = 0.24 mNm. Friction compensation (feed forward) is discussed in section 7.2.

7.1.3 Cogging and rotor position dependant controller disturbance

In the motion controller a rotor position dependant ripple occurs which is caused by the limited precision of the initial calibration procedure which is executed by the DES 70/10 at startup (info from the development department of Maxon motor in Switzerland). The disturbance is within the motion controller specifications but if required it can be reduced by modifying the driver firmware.
The other disturbance that is a function of the motor position is cogging. These two disturbances have not been measured individually. Since both disturbances are function of the rotor position and motor current they are treated as one repetitive disturbance.

The motion controller ripple reproduces as a function of the motor position but a complicating factor of this disturbance is that the shape and the amplitude of the ripple can change drastically when the power supply of the motion controller is switched off and on again. This can be seen in Figure 23. The Y-axis is expressed in [Nm] and is a representation of the analog signal applied to the analog input of the motion controller in order to maintain a constant speed of 0.2*2*pi [rad/sec]. The X-axis shows the encoder position of one full revolution of the rotor in encoder pulses (4000 quad counts). Every plot is the average of twenty low pass filtered cycles. The DC offset (due to Coulomb and viscous friction) has been removed.

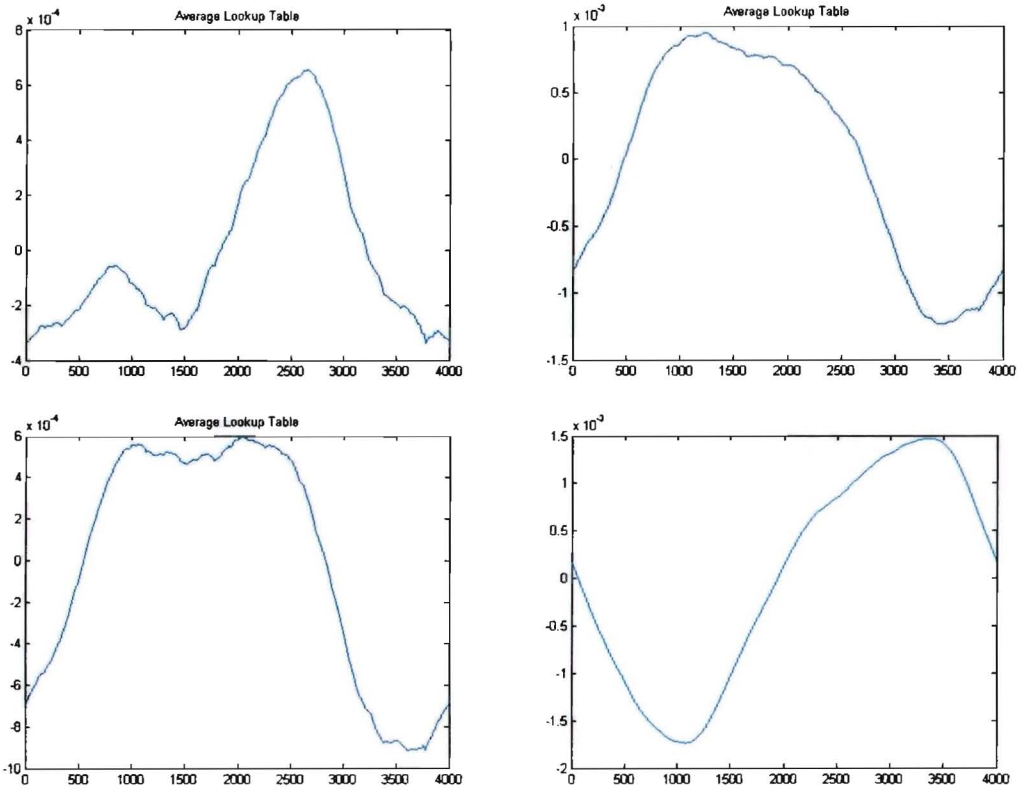

Figure 23. Controller plus motor cogging disturbance after power Off/On

Figure 24 shows that the disturbance reproduces very well. It shows twenty curves, measured during twenty motor revolutions.

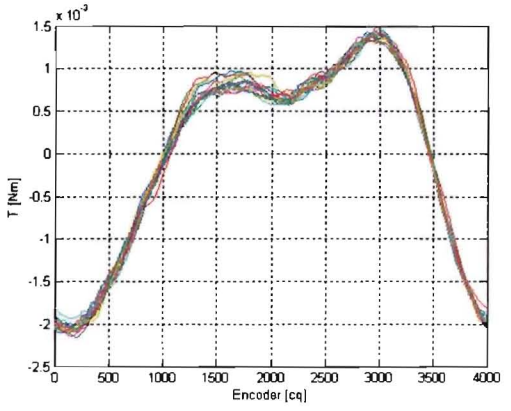

Figure 24. Twenty revolutions

The amplitude of the ripple increases with increasing current as shown in Figure 25.

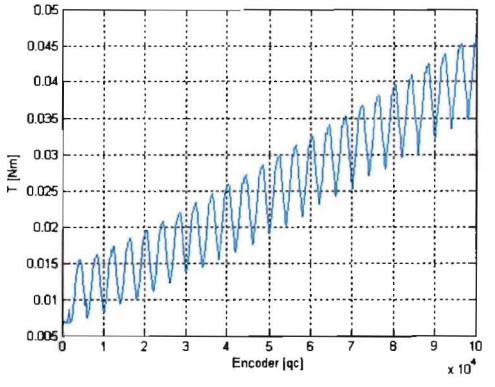

Figure 25. Ripple increases with increasing motor current

Figure 26 shows the motor current of a motor running at a constant speed of 0.2 Hz. The plots show the motor current at three different constant torques, 14 mNm (310 mA), 37 mNm (820 mA) and 160 mNm (3500 mA).

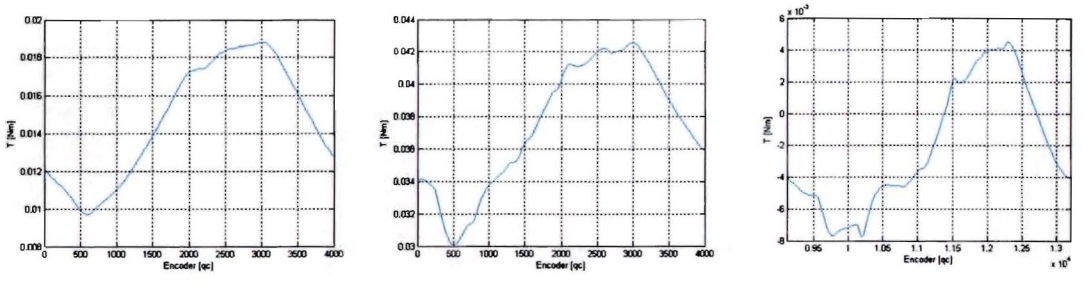

Figure 26. Current dependent frequency content

The shape (frequency content) of the ripple is related to the magnitude of the motor current. This dependency is not discussed any further in this work.
The shape of the motor current ripple is also a function of the motor speed. Figure 27 shows the changing ripple as a function of increasing motor speed.

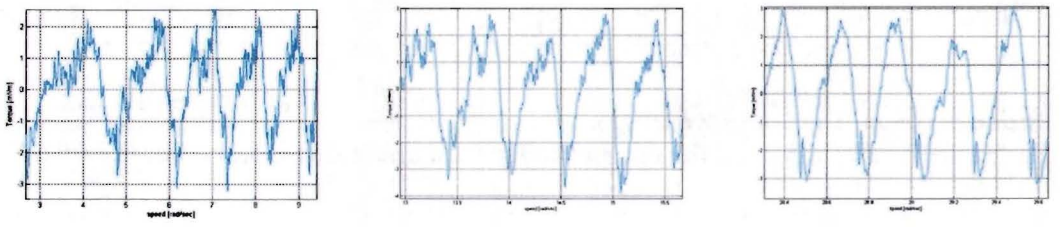

Figure 27. Ripple at motor speeds ranging from 3 up till 30 rad/sec.

The PSD's of the signals of Figure 27 are shown in Figure 28. With increasing motor speed the first harmonic of the motor speed gets more dominant over the second harmonic. At 30 rad/sec (about 5 Hz) the ripple frequency content is almost reduced totally to the first harmonic of the motor rotation frequency.

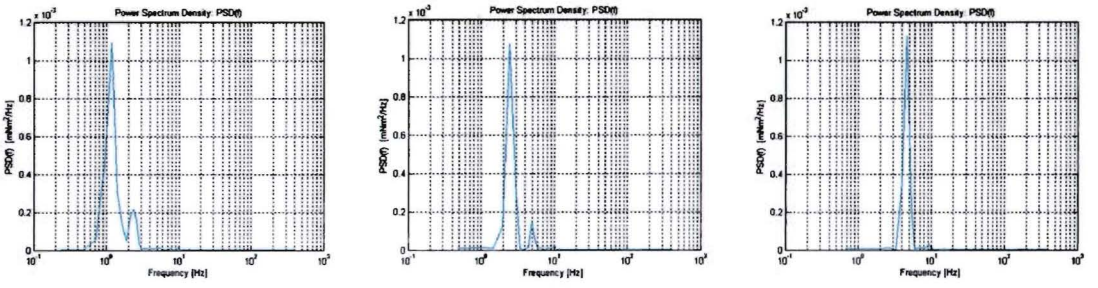

Figure 28. PSD of the ripple in Figure 27

The motor speed dependency of the frequency content of the repetitive disturbance and its compensation will be discussed later.

7.2 Torque disturbance compensation

In this section we will look at methods to compensate for the disturbances mentioned above. The disturbance compensation is divided in two parts:

- model based feed-forward for viscous-, Coulomb- and static friction and for acceleration,
- disturbances that are a function of the motor position.

The Stribeck effect is not compensated for.
The controller design in which the compensations are integrated is shown in Figure 29.

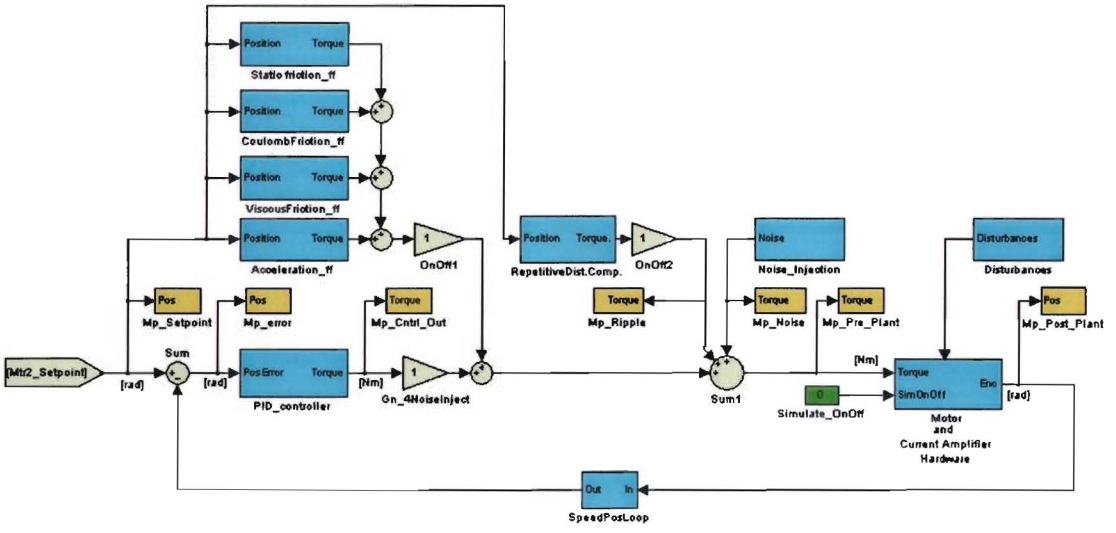

Figure 29. Motor controller

In this section the test setup itself is analyzed. Therefore all measurements and compensations in this section are related to the motor and the motion controller only.

7.2.1 Coulomb friction compensation

The magnitude of the Coulomb friction is read from the torque-speed curve in Figure 30 at 0 rad/sec. A value of 2.3 mNm is found.

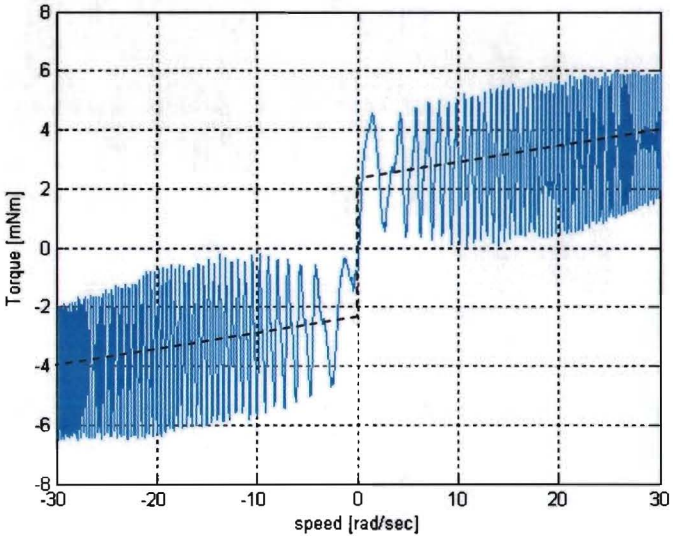

Figure 30. Torque-speed curve without any compensations

Compensating the Coulomb friction by means of a sign-function would introduce a discontinuity resulting in high frequent disturbance. This is avoided by using a tanh-function:

$$f_t = f_C \cdot \tanh(v) + f_V \cdot v$$

The compensation for the Coulomb friction is implemented as shown in Figure 31.

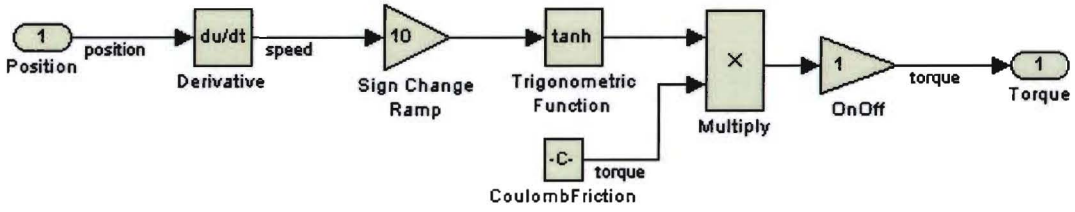

Figure 31. Coulomb friction compensation

The effect of the Coulomb friction compensation is shown by measuring the same torque-speed curve as in Figure 30 but now with Coulomb friction compensation switched on. The result is shown in Figure 32.

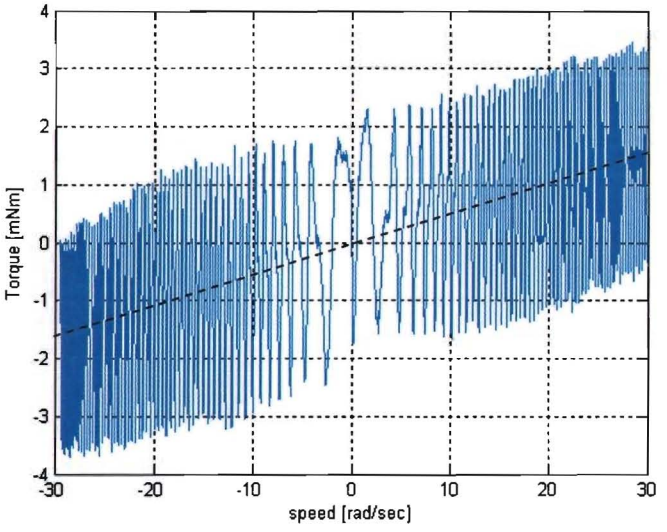

Figure 32. Torque-speed curve with Coulomb friction compensation

7.2.2 Viscous friction compensation

The speed dependant disturbance caused by viscous friction is compensated for by means of speed feed forward. It is implemented as shown in Figure 33.

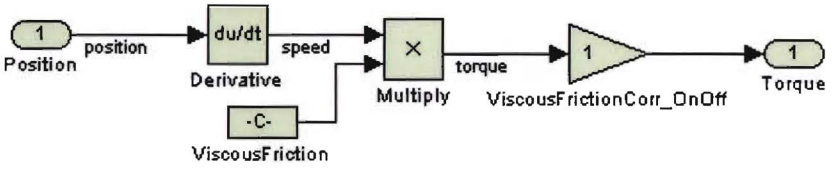

Figure 33. Viscous friction compensation

The dashed line in Figure 32 shows the torque at 30 rad/sec is 1.6 mNm. Since the Coulomb friction is compensated in this figure, the viscous friction is found by division:

$$f_v = \frac{1.6 \cdot 10^{-3}}{30} = 5.33 \cdot 10^{-5} \text{ Nm.s/rad.}$$

Using this value in the viscous friction compensation creates a horizontal torque-speed curve as shown in Figure 34.

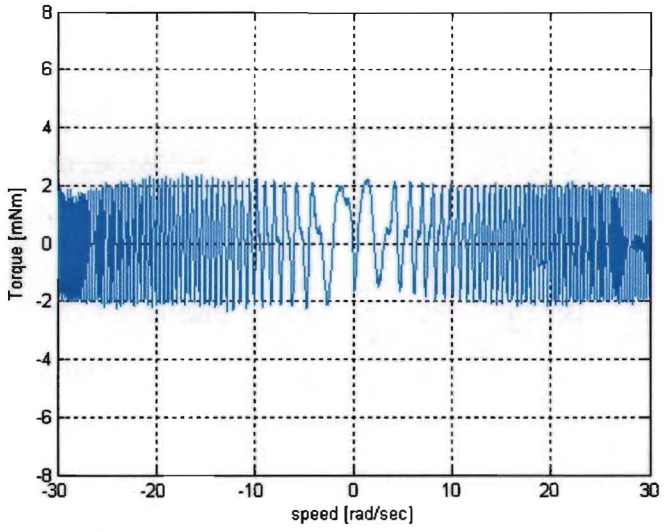

Figure 34. Torque-speed curve with Coulomb- and viscous friction compensation

7.2.3 Motor acceleration

According to the datasheet the inertia of the rotor of the motor is 1.01e-005 [kgm ^{2}].
The inertia of the encoder is 1.7e-007 [kgm ^{2}]).
The inertia of the motor pulley (drive wheel) is computed from parameters:
Pulley_diam = 0.0268 [m]
Pulley_weight = 0.053 [kg]

$$\text{Motor1\_Pulley\_J} = \frac{1}{2} \cdot \text{Pulley\_weight} \cdot \left(\frac{\text{Pulley\_diam}}{2} \right)^2 = 4.758\text{e-}006\,[\text{kgm}^2]$$

The Total_Inertia of the rotor, pulley and encoder is *1.503e-5 [kgm ^{2}]*
This value is checked by measuring the FRF of the Plant which shows a -40 dB mass-line crosses *H(s) = 0 [dB]* at $f = 40$ *Hz*, see Figure 35.
With gain $A = 1$, $w = 2 \cdot \pi \cdot f = 251$ [rad/sec] and f_v = 5.3e-5 [Nm.s/rad] an inertia is found of:

$$|H(s)| = \left| \frac{1}{m \cdot s^2} \right| \Rightarrow A = 1 = \frac{1}{J \cdot w^2 + f_v \cdot w} \Rightarrow J = \frac{1}{w^2} - \frac{f_v}{w} =$$

1.587e-5 – 0.02e-5 = 1.566e-5 [kgm ^{2}]

This verification shows an error of about 4 % which may be caused by measurement errors.

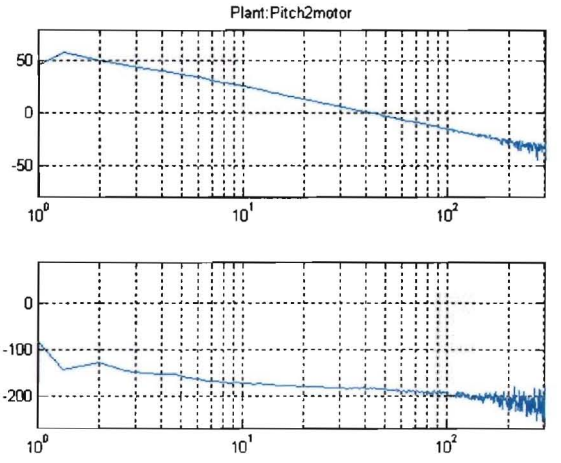

Figure 35. FRF Plant, rotor plus pulley

The rotor and pulley inertias are used in the model for acceleration feed forward implemented as shown in Figure 36.

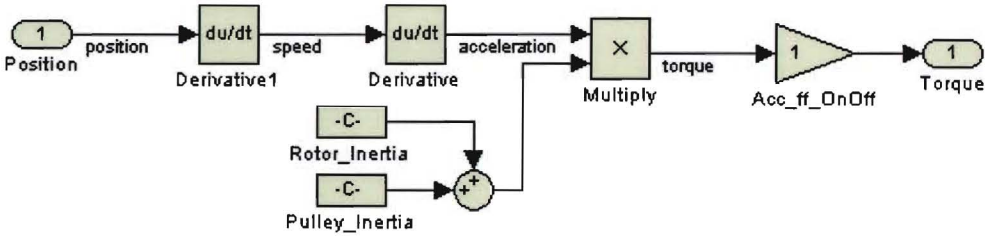

Figure 36. Acceleration feed forward

Later in this work also the inertia of the instrument wheel interface will be added to the feed forward. For motions with low acceleration the effect of acceleration feed forward is neglectable. For the motion trajectory used in Chapter 8 this feed forward will appear useful.

7.2.4 Repetitive disturbance compensation

The disturbances that are a function of motor position and motor current are the motion controller ripple and motor cogging. As mentioned before, these disturbances are treated as one repetitive disturbance. Only motor position dependency is discussed in this work, not motor current dependency. In this section the motor plus pulley are not connected to the Da Vinci instrument and can run free. We will investigate how the predictable disturbance can be reduced using Iterative Learning Control (ILC). In this application ILC is not used to improve system performance but to reduce current disturbances in order to improve the accuracy of the determination of the applied torque by the motor. First a short description is given of the standard ILC method [25].

7.2.4.1 Standard iterative learning control

Iterative learning control (ILC) can be used to reduce repetitive disturbances in systems that perform a specific trajectory over and over again.
The lower part of Figure 37 shows a basic feedback control loop consisting of a controller C and a plant P. As shown the ILC feed-forward loop is added to this loop, consisting of a learning filter L(s), a robustness filter Q(s), a memory table and an add-up point.

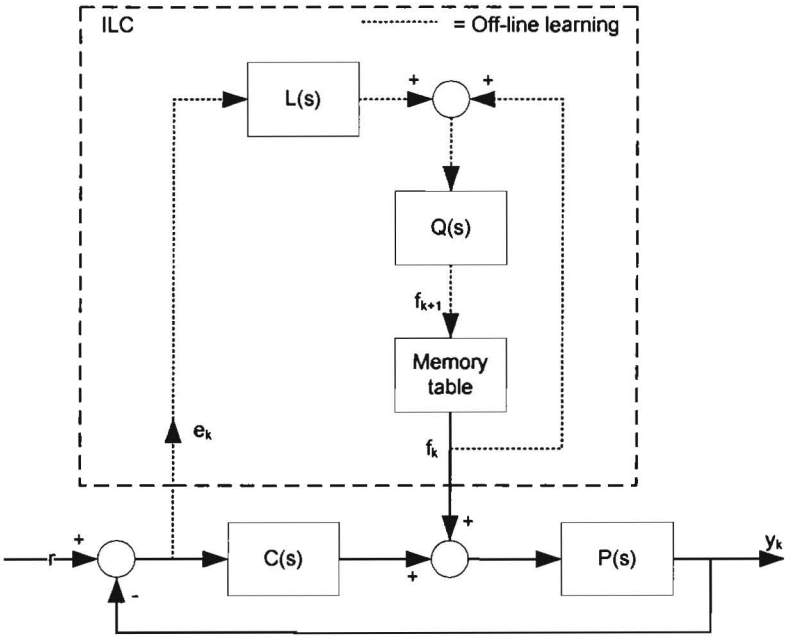

Figure 37. Standard ILC

A basic feedback controller reacts on errors that occur during a trajectory regardless how many times this same trajectory is repeated. The output of this controller is always too late because it is a 'response' to an occurring error and therefore an error remains. When using ILC on the other hand, system and trajectory information is used in order to

generate the correct output at every instance of a specific trajectory. ILC compensates for:

- repetitive disturbances,
- trajectory dependant static-, Coulomb- and viscous friction,
- errors caused by accelerations.

Before ILC improves the performance of the system on a specific trajectory, first a learning phase must be executed. During the first run of the learning phase, the system will follow the specific trajectory without ILC feed-forward. The time dependant (and therefore also position- dependant) error is filtered with filter L and stored in a memory table together with its time-stamps. Next, the stored data is processed off-line (filtered with filter Q) and a memory table containing the required feed-forward data is generated. During the next run of the trajectory the feed-forward data is added up to the control signal (Figure 37) resulting in a reduction of the error. During this run also a new table is stored with the remaining error data. Subsequently this data is processed and a new feed-forward table is generated. This procedure can be repeated several times and after each run the feed-forward data is updated. When the ILC algorithm converges, after each run the remaining reproducing error will be reduced until only random noise and no reproducing disturbance is left. At that moment the learning phase is finished.

The design of the L-filter is derived as using convergence (stability) arguments. In the derivation we assume initial and end conditions to be zero, in order to use a frequency domain description for a finite time problem.

$$Sp = \frac{P}{1 + P \cdot C} = \frac{y_k}{f_k} = -\frac{e_k}{f_k}, \quad (1)$$

where Sp is the Process sensitivity. So:

$$e_k = -Sp \cdot f_k . \qquad (2)$$

The feed-forward update in the next run equals:

$$f_{k+1} = Q(f_k + L \cdot e_k) . \qquad (3)$$

Using (2) and (3) the error of this run equals:

$$e_{k+1} = -Sp \cdot f_{k+1} = -Sp \cdot Q(f_k + L \cdot e_k) . \qquad (4)$$

Using (1) and (4) follows:

$$\begin{aligned} e_{k+1} &= -Sp \cdot Q(f_k + L \cdot (-Sp \cdot f_k)) \Rightarrow \\ e_{k+1} &= -Sp \cdot f_k \cdot Q \cdot (1 - L \cdot Sp) \Rightarrow \\ e_{k+1} &= -(-e_k) \cdot Q \cdot (1 - L \cdot Sp) \Rightarrow \\ e_{k+1} &= Q \cdot (1 - L \cdot Sp) \cdot e_k \qquad (5) \end{aligned}$$

A sufficient condition for convergence is now:

$$\frac{e_{k+1}}{e_k} = |Q(1 - L \cdot Sp)| < 1. \qquad (6)$$

When learning filter L can be chosen equal to the inverse process sensitivity, converence is assured since the result is equal to zero (i.e. only one iteration: deadbeat learning). However computing Sp^{-1} can result in a non-proper model (the power of the numerator is higher than the power of the denumerator). The next section shows this problem can be solved by using Zero Phase Error Tracking Control (ZPETC).

If L is not equal to Sp^{-1} a robustness filter Q is needed in order to guarantee that (6) is satisfied.

7.2.4.2 ILC used in this project

In this section an ILC method will be designed that is not only applicable for one specific trajectory but for any trajectory within the performance specifications of the setup. This type of control is required because during operation, movements of the setup will be random. Experiments show (section 7.1.3) that the amplitude and frequency content of the repetitive disturbance are a function of the motor speed. The ILC method designed in this section will deal with this issue.

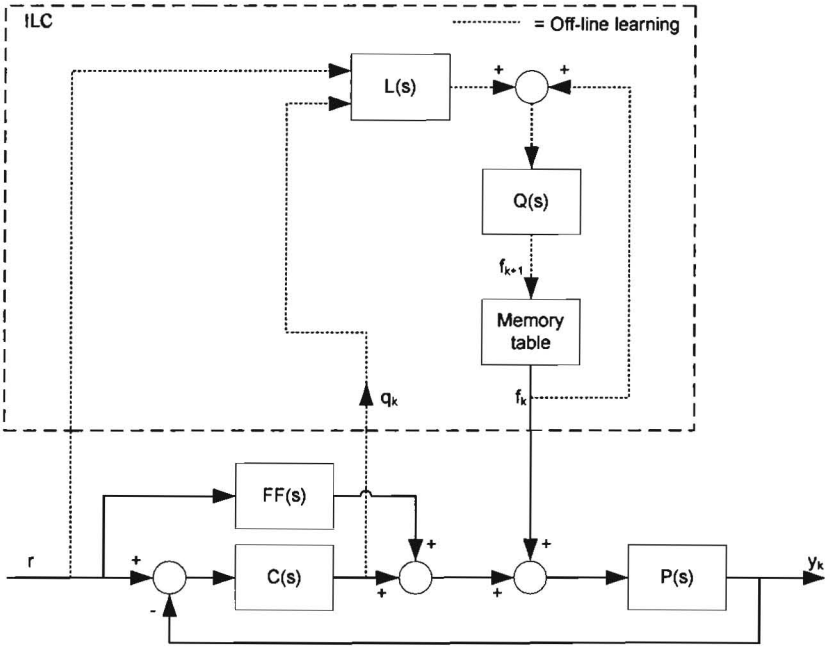

Figure 38. ILC used in this project

The ILC design in Figure 38 differs in the following aspects from standard ILC described above:

- for the input of the ILC method, not error e_k but controller output q_k is used,
- errors caused by acceleration (and static friction) are not compensated by ILC but by model based feed-forward (FF),
- not time but the absolute motor position information is used as a reference.

Now that not error e_k but controller output q_k is used as input for the ILC method, the L and Q filters differ from those in the standard ILC method. The new filters are derived assuming FF(s) = 0. The content of component FF(s) depends on the configurations discussed later.

For the design of the L-filter a correct model is required of the plant P. For the test setup without instrument the plant consists only of the motor and the motor-pulley.

Figure 39 shows that the transfer function of the plant can be approximated well by:

$$P(s) = \frac{1}{J \cdot s^2}$$

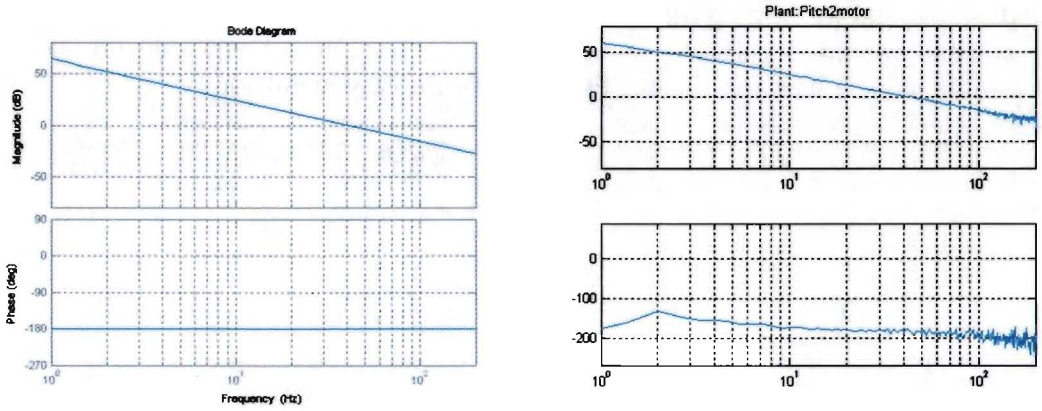

Figure 39. Simulated and measured FRF of the Plant

When we assume normal time based ILC the design of the L-filter is derived as follows:

$$T = \frac{C \cdot P}{1 + P \cdot C} = -\frac{q_k}{f_k}, \quad (7)$$

where T is the complementary sensitivity. So:

$$q_k = -T \cdot f_k . \qquad (8)$$

The feed-forward update in the next run equals:

$$f_{k+1} = Q(f_k + L \cdot q_k) . \qquad (9)$$

Using (8) and (9) the controller output of this run equals:

$$q_{k+1} = -T \cdot f_{k+1} = -T \cdot Q(f_k + L \cdot q_k) . \qquad (10)$$

Using (7) and (10) follows:

$$\begin{aligned} q_{k+1} &= -T \cdot Q(f_k + L \cdot (-T \cdot f_k)) \Rightarrow \\ q_{k+1} &= -T \cdot f_k \cdot Q \cdot (1 - L \cdot T) \Rightarrow \\ q_{k+1} &= -(-q_k) \cdot Q \cdot (1 - L \cdot T) \Rightarrow \\ q_{k+1} &= Q \cdot (1 - L \cdot T) \cdot q_k \qquad (11) \end{aligned}$$

In case of convergence controller output q_{k+1} is reduced with respect to q_k. So:

$$\frac{q_{k+1}}{q_k} = |Q(1 - L \cdot T)| < 1. \qquad (12)$$

A good choice for the learning filter L is to make it equal to the inverse of the complementary sensitivity. However computing T^{-1} can result in a non-proper model (the power of the numerator is higher than the power of the denumerator):

$$T^{-1} = \frac{565.4\,z^5 - 2488\,z^4 + 4356\,z^3 - 3788\,z^2 + 1634\,z - 278.9}{z^4 + 1.408\,z^3 - 5\,z^2 + 1.898\,z + 0.6939}$$

This problem can be solved by using Zero Phase Error Tracking Control (ZPETC) [25]. Without going into detail, this method provides a proper approximation of the inverse of the complementary sensitivity:

$$T^{-1} = \frac{103.3\,z^6 - 421.7\,z^5 + 651.7\,z^4 - 440\,z^3 + 79.36\,z^2 + 43.5\,z - 16.12}{z^6 - 1.751\,z^5 + 0.5312\,z^4 + 0.2196\,z^3}$$

The left plot of Figure 40 shows the complementary sensitivity T and it's non-proper inverse. The right plot T is shown together with a proper approximation of T^{-1} generated by the ZPETC method.

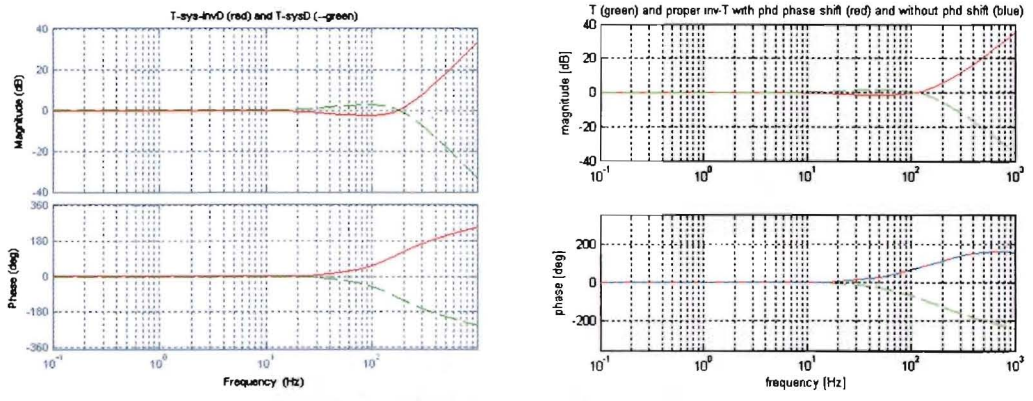

Figure 40. Left: T and non-proper T^{-1}, Right: T and proper T^{-1}

When the proper inverse of T is generated, ZPETC also generates a scalar called *phd*. This number is used to correct the phase of the inverse function as described in [26]:

$$phase(T^{-1}(\omega)) = phase(T^{-1}(\omega)) + (\omega \cdot phd \cdot Ts).$$

In the phase plot of the proper T^{-1} in Figure 40 the blue and the dashed red lines are respectively the T^{-1} (not shifted with *phd*) and the T^{-1} which is shifted with *phd*. The two lines almost totally overlap since *phd* = 2 and *Ts* = 125 µsec.
Since L is not exactly equal to T^{-1} a low-pass filter Q is needed in order to guarantee that (12) is true. For the Q-filter an anti-causal 4^{th} order low pass Butterworth filter is used with a cut-off frequency of 100 Hz. Matlab function filtfilt is used to implement this filter. From a plot of the convergence criterion, shown in Figure 41, can be seen that its magnitude is smaller than one, so the ILC method will converge.

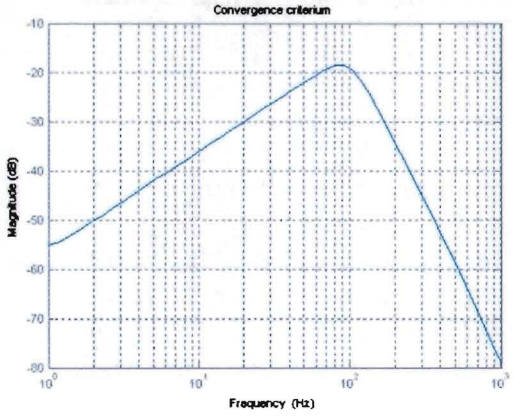

Figure 41. Convergence criterion

As mentioned above, the second difference between the standard ILC of Figure 37 and the ILC method used in this project (Figure 38) is that model based feed-forward (FF) is used for acceleration compensation.
Using model based feed-forward for acceleration compensation is legitimate because the inertia of the setup is not a function of motor position.
Static friction compensation is not implemented in model based feed-forward since we are interested in the forces applied during instrument motion (Chapter 4).

Now ILC compensates only for:

- repetitive disturbances,
- trajectory dependant Coulomb- and viscous friction.

Two ILC implementations have been analyzed, these will be referred to as implementation A and implementation B.
With respect to the position dependent Coulomb and viscous friction, implementation A ignores this dependency and implementation B includes it. Implementation A compensates these frictions in model based FF and implementation B compensates for them in ILC.
With respect to the motor speed dependency of the frequency content of the repetitive disturbance (mentioned in section 7.1.3), implementation A ignores this dependency and implementation B includes it. Both implementations compensate for the speed dependant magnitude and phase of the disturbance.
Table 7 gives an overview of the properties of the two implementations.

Compensates for	Implementation A	Implementation B
Repetitive disturbances	Yes, speed dependent freq. content ignored	Yes, speed dependent freq. content included
Coulomb friction	Yes, no function of position	Yes, function of position
Viscous friction	Yes, no function of position	Yes, function of position
Acceleration	Yes, no function of position	Yes, no function of position
Static friction	No (may be added)	No (may be added)

Table 7. Two ILC implementations

Implementation A

Implementation A performs the learning phase at a low constant speed. The learned feed forward data is related only to the absolute motor position and is not a function of speed. At each absolute position of the encoder (4000 quad counts) a feed-forward value is stored. In Figure 42 the Memory table of Figure 38 is shown with the name Repetitive Disturbance Lookup Table. The input of that table is the position setpoint.
In section 7.1.3 it is shown that the amplitude of the repetitive disturbance is a function of motor speed. When the feed-forward data is used to compensate for repetitive disturbances at a different speed than the learning speed, this means the amplitude must be corrected for this speed. Since trajectories with continuous speed profiles are allowed this would mean that an amplitude correction parameter should be found for an infinite number of speeds. Because this is not feasible, an Amplitude Lookup table is used with a finite number of amplitude correction parameters. At the input of the lookup table the motor speed is connected (see Figure 42). This input is used as the index of the table. At the output of the lookup table the value of the amplitude correction parameter is presented that is selected by the index. When the index (motor speed) points to a table position in between of two parameter values, the output value is computed by interpolation. The output of the Repetitive Disturbance Lookup Table (feed-forward signal) is multiplied by this computed amplitude correction parameter.

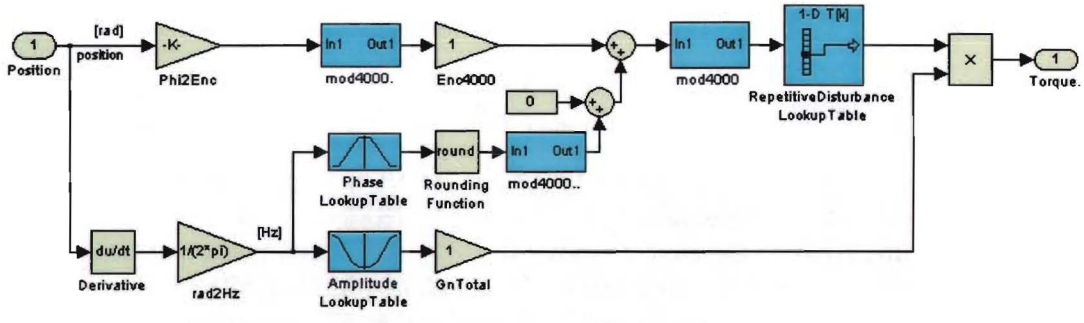

Figure 42. Disturbance compensation with phase and amplitude tables

Because the feed forward table is tuned for one frequency only, phase shifts occur when the motor rotates at different speeds than the learning speed. This speed dependant phase shift can be tuned using the Phase Lookup Table shown in Figure 42. Like the Amplitude

Lookup Table, the Phase Lookup Table outputs a motor speed dependant value. This output is added to the position index of the Repetitive Disturbance Lookup Table, resulting in a phase shift of the feed-forward signal.

The feed-forward data that is stored in the Repetitive Disturbance Lookup Table is generated by an automated procedure. Automating the procedure that is used to determine the content of the Amplitude Lookup Table and the Phase Lookup Table is less trivial. The table content is determined by manual tuning at different rotation frequencies which is time consuming.

The cut-off frequency of filter Q is determined as follows; the complementary sensitivity function T in Figure 40 is reasonably flat up till 100 Hz, which is the bandwidth (BW) of the system. During the learning phase, the motor rotation frequency is $f_l = 1$ Hz. The maximum rotation frequency according to the system specifications is $f_{max} = 5$ Hz. The maximum frequency content of the feed-forward signal is chosen equal to the BW, therefore the learned feed forward signal must be low pass filtered by filter Q at a cut-off frequency f_Q of:

$$f_Q \leq \frac{BW}{f_{\max}} = \frac{100}{5} \Rightarrow$$

$$f_Q \leq 20Hz.$$

For the Q-filter a 4th order low pass Butterworth filter is used with a cut-off frequency of 20 Hz.
Because data processing is performed off-line, anti-causal filtering is possible using Matlab function filtfilt. This avoids a phase shift of the feed-forward memory table data that would occur during causal filtering.

In order to speed up the learning phase, at each iteration not the learned data of just one motor revolution is processed but the average data of 20 motor revolutions (Figure 43).

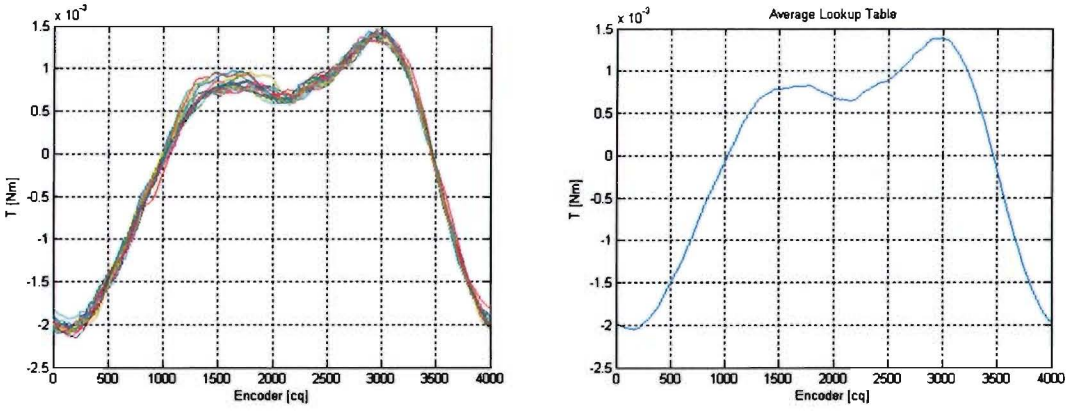

Figure 43. Left: 20 revolutions. Right: average of the 20 revolutions

Figure 44 shows the amplitude of the disturbance for ten iterations during ILC learning. During learning, a new feed forward table f_{k+1} was generated by adding feed forward table f_k and the latest measured data q_k, so the new table contained 50% history and 50% new data:

$$f_{k+1} = Q(f_k + \cdot L \cdot q_k)$$

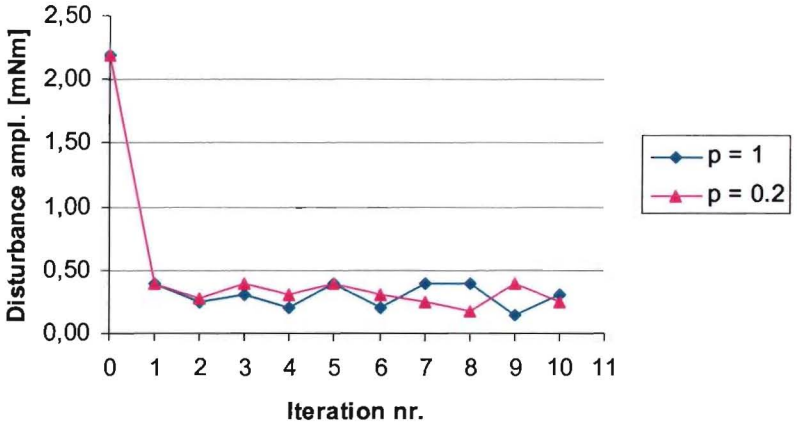

Figure 44. Disturbance amplitude as function of iteration number

In order to make better use of history measurements, the same measurement is performed but now new table f_{k+1} is generated as follows:

$$f_{k+1} = Q(f_k + p \cdot L \cdot q_k),$$

where p is the learning factor. After the first run the repetitive disturbances have been reduced drastically. The runs that follow do not contribute to a disturbance reduction (nor increase). Figure 45 shows the random disturbance of twenty synchronized revolutions that is left after the first ILC learning run.

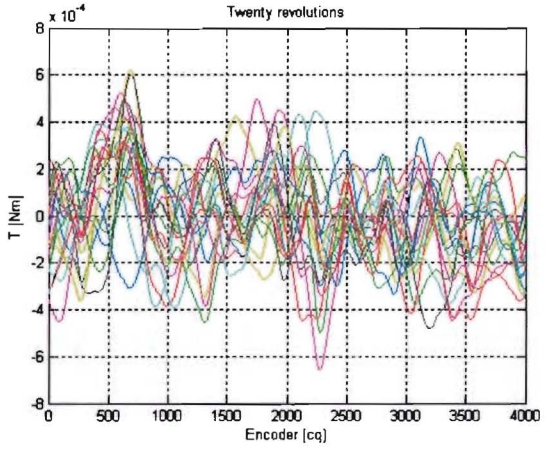

Figure 45. Disturbances left after the first learning run

As discussed earlier, when the motor speed changes after the learning phase has been completed, the disturbance's amplitude, phase and frequency content changes. In order to adjust the feed forward signal for the amplitude and phase changes, both the Phase Lookup Table and the Amplitude Lookup Table (Figure 42) are tuned manually. The frequency content cannot be adjusted in Implementation A. In Figure 45 the torque-speed plot is shown without ILC. Figure 47 shows the torque-speed plot with ILC but with the amplitude- and phase tables inactive. Figure 48 shows the same plot with ILC and with the tables tuned and active.

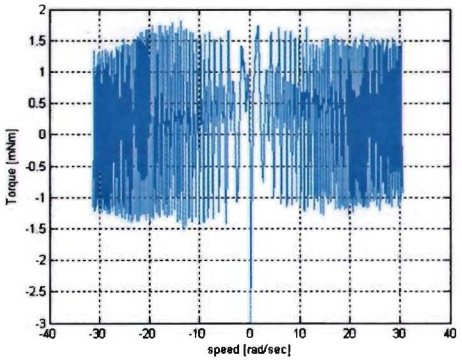

Figure 46. No repetitive disturbance compensation (no ILC)

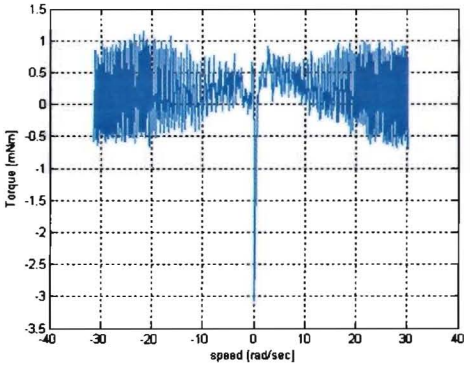

Figure 47. Implementation A, Ampl.- and Phase tables not active

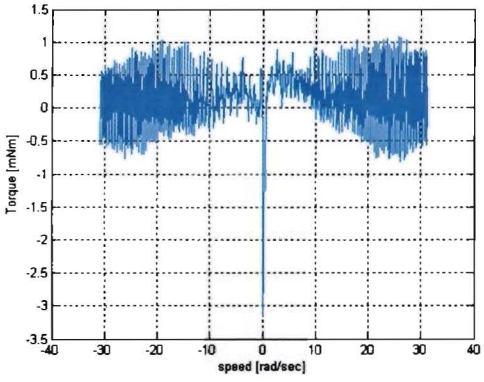

Figure 48. Implementation A, Ampl.- and Phase tables active

In Figure 47 the reduction of the repetitive disturbance due to ILC is clearly visible, especially at low frequencies, close to the learning speed. The effect of tuning the amplitude- phase tables is minimal. The effect of the changing frequency content in the repetitive disturbance as a function of speed is dominating. This problem will be reduced in Implementation B.

Implementation B

As mentioned in Table 7, ILC implementation B compensates for the Coulomb- and viscous friction as a function of position (and speed). Therefore the model based feed-forward components discussed in sections 7.2.1 and 7.2.2 are deactivated. In order to retrieve a feed forward signal with the correct frequency spectrum at each motor speed (see section 7.1.3), multiple ILC learning procedures are performed at different constant speeds. The selected speeds are -5 -4 -3 -2 -1 0 1 2 3 4 5 Hz.

At each constant speed only one learning run is executed because Figure 44 showed that more iterations do not contribute substantially. After the learning phase, interpolation is used to determine the correct feed forward signal at each speed within the performance specifications of the setup.

This implementation requires not only motor position information but also motor speed information, therefore a two-dimensional lookup table will be used as shown in Figure 49. In Figure 50 the content of the table is presented in a plot. The steep ramp at speed-row 7 is caused by the Coulomb friction that, together with the speed, changes of sign.

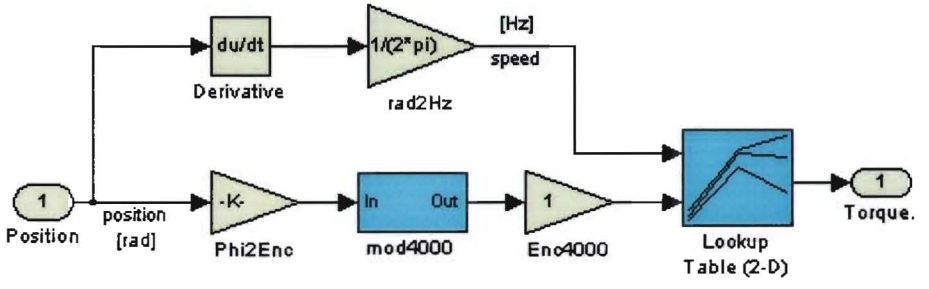

Figure 49. Disturbance compensation with two-dimensional lookup table

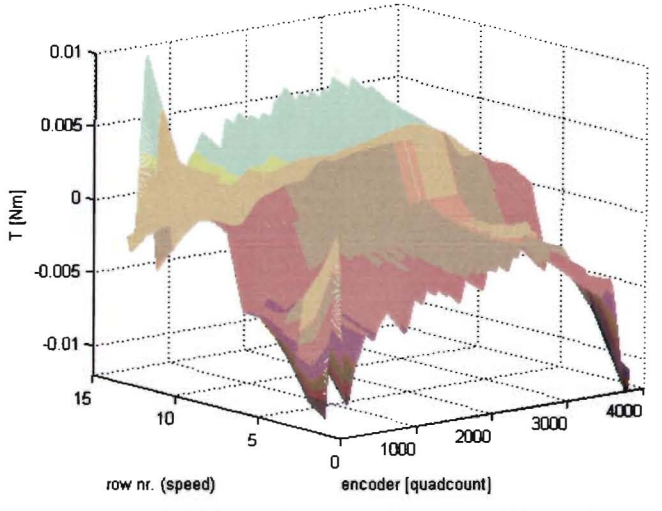

Figure 50. Two-dimensional lookup table content

Figure 51 shows the repetitive disturbance and the learned ILC feed forward signal both in one plot at a motor speed running from -5 Hz up to +5 Hz. Both signals match well and overlap at all frequencies except for very low speeds. This mismatch results in a spike in Figure 52 that shows the controller output signal when ILC implementation B is active. This behaviour at low speeds is probably related to the Stribeck effect. This can be reduced by adding more low speed learning to the ILC learning phase.

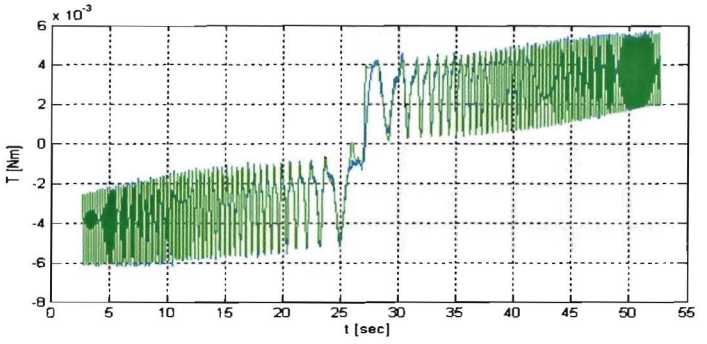

Figure 51. Repetitive disturbance (blue) and ILC feed forward (green)

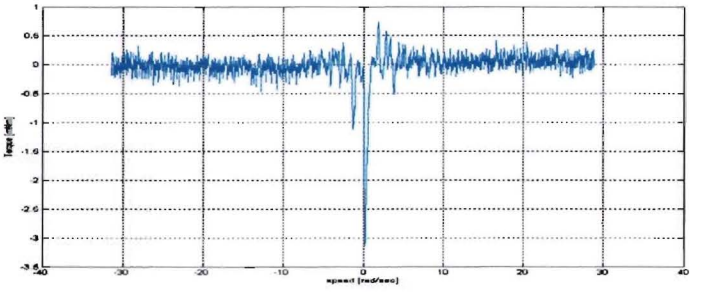

Figure 52. Implementation B, torque-speed curve

Learning at low speeds (0.1 … 0.01 Hz.) is time consuming when each run involves 20 rotations. Therefore, for these low rotation frequencies the data of the run at 1 Hz is used to generate the feed forward data for the low speeds. To do this, an amplitude table as described in implementation A, is added to the design of Figure 49. The total disturbance compensation is shown in Figure 53.

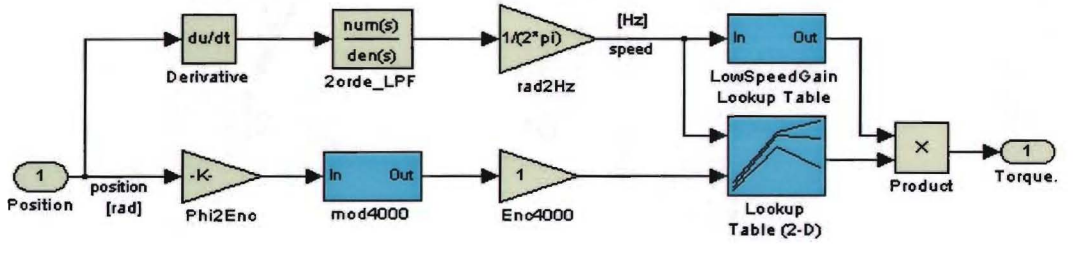

Figure 53. Two-dimensional lookup table and an Amplitude Lookup Table

As can be seen in Figure 54 (x-axis: time [sec], y-axis: torque [mNm], speed range from –5 Hz to 5 Hz) the disturbance reduction at low frequencies is improved drastically compared to Figure 52. The signal in green is the feed-forward signal and the blue signal is the controller output.

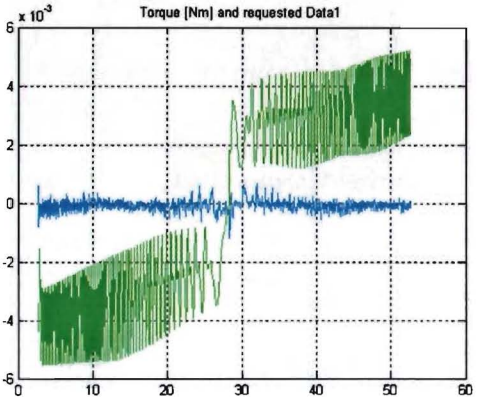

Figure 54. Impl. B with ampl. lookup table, torque-speed curve

Repetitive disturbance compensation on a limited rotation angle

Since the pitch of the forceps can rotate over a limited angle of approximately 180 degrees only, ILC implementation B must be adapted. The disturbance compensation shown in Figure 53 remains unchanged but in stead of averaging the learned data of twenty motor rotations at different constant speeds, the data will be averaged of twenty moves over an angle of 180 degrees, also with different constant speeds in both directions. Per value of speed one learning run of 20 moves is executed.
Only friction is analyzed and not the instrument dynamics. Therefore, in order to reduce dynamic effects, the 45 degrees at the beginning of the trajectory and the 45 degrees at the end will not be included in the measurement results. These parts will be used for acceleration and deceleration during learning. ILC is used to reduce repetitive disturbances.

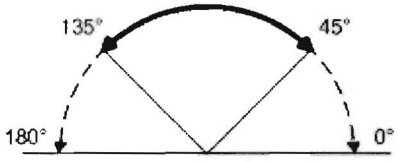

Figure 55. Limited forceps pitch rotation angle

During measurements in this section the position setpoint of the setup is a triangle providing a constant speed alternating in both directions. Measurement results for speeds at 1 and 2 Hz are shown in Figure 56.

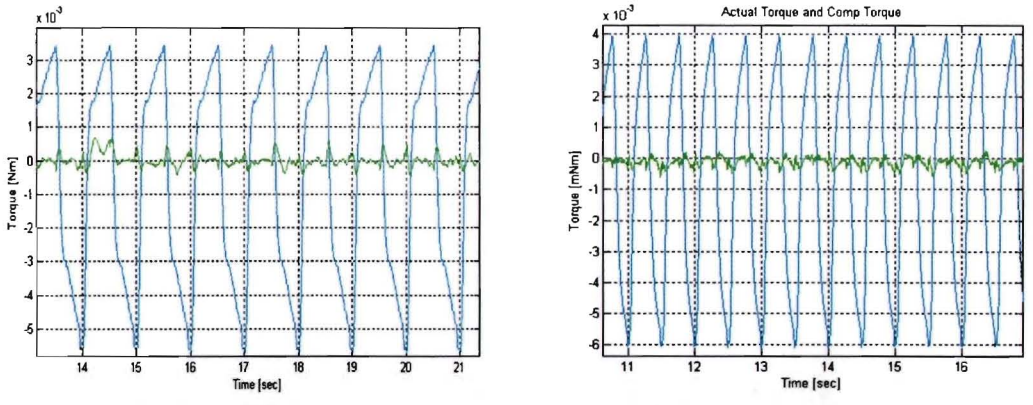

Figure 56. Remaining disturbance (green) and ILC feed forward signal (blue)

For all learned speeds, 0.2, 1, 2, 3, 4, and 5 Hz, the disturbance that remains after compensation is below ±1 mNm. As in implementation B, interpolation is used to determine the feed forward signal for other speeds in this range and below 0.2 Hz an amplitude table is used with data of speed 0.2 Hz.
This ILC implementation will be referred to as implementation C. It will be used in the next chapter in measurements on the Da Vinci instrument.

8 Measurements on the Da Vinci instrument

In this chapter we will measure and compensate the friction of the pitch joint of the Da Vinci forceps using ILC implementation C discussed in the previous section.

8.1 Measurement method

In order to rotate the pitch of the forceps over an angle of 180 degrees, the motor rotates over an angle of approximately $0.85 \cdot 180 = 153$ degrees. So the transmission from the instrument driving wheel to the forceps pitch is 0.85:1. For measurement of forces working on the forceps this means that the torque determined by the motor current must be multiplied by the reciprocal of 0.85 which is about 1.18.

The friction of the pitch axis depends on the positions of the other DOF's of the instrument therefore the other axes of the instrument are fixed. Due to the mechanical construction of the instrument, the positions of the pitch axes of the instrument are coupled with the position of the jaw axis. This means that a position change of the jaw axis results in a position change of the pitch without rotation of the pitch motor. Such a change in pitch position would not mean that the lookup table of the pitch can be shifted because the friction in the instrument house and in the instrument shaft has not changed since the motor position has not changed. The position dependent friction in the forceps itself though is shifted. This means that for each pitch axis a lookup table must be generated for each (infinite) position of the jaw. Since we will concentrate on the pitch axis only, and the jaw axis is fixed, this topic is not discussed any further in this work.

During force measurement a force is applied to the forceps by hanging a mass at the tip of the vertically moving grasper. The position trajectory of the pitch axis results in a constant speed with alternating direction running over an angle between 0 and 180 degrees. See Figure 57 for a schematic overview of the measurement setup.

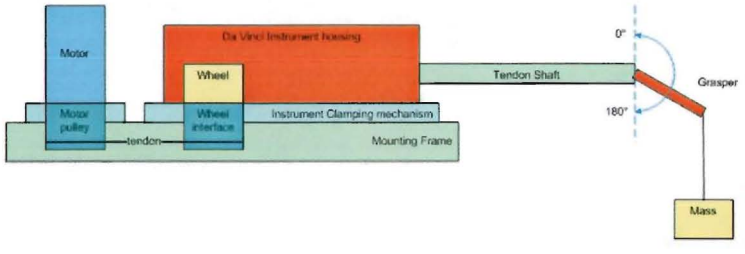

Figure 57. Force measurement

The torque applied by the motor during the rising and falling part of the trajectory is a function of the grasper position and has the shape of a half sine. At a grasper position of 90° the applied torque has its maximum. Because the measurements described in this section include low frequent motion only, the maximum torque required for the acceleration of the mass is in the order of micro Newton-meters. At a 90° grasper position

where the torque measurements are performed, the acceleration of the mass is zero. For these reasons the mass acceleration torque is not taken into account.
Before a measurement with a mass is performed, first an ILC learning procedure is executed without that mass in order to suppress the repetitive disturbances in the total setup. After a force measurement we will analyze the amplitude of the motor current signal at a grasper position of 90 degrees during the rising part of the trajectory. The motor torque measurement results are corrected for the gear-ratio of the Da Vinci instrument discussed earlier. The x-axes of the plots show the motor encoder position in quad counts. A grasper position of 0° corresponds with a motor encoder value of 0 qc and a grasper position of 180° corresponds with (180/360)·4000·0.85=1700 qc (encoder = 4000 cq and the gear-ratio = 0.85). In quad counts the angle range of interest (45° till 135°) is between 425 qc and 1275 qc. Plots with an x-axis running from 0 qc up till 3400 qc must be interpreted as a total cycle of the grasper move, starting at position 0° (0qc) going up till 180° (1700 qc) and back to 0° (3400 qc) again.

Measurements will concentrate on low torques / forces because here the accuracy of the measurements will suffer the most from remaining disturbances. Four different forces are applied to the forceps: 60 mN (minimum required resolution according to section 6.1), 250 mN, 1 N and 2 N. The measurements are performed at a grasper rotation speed of $0.2 \cdot 2 \cdot \pi$ rad/sec. The measured signals are low-pass filtered at 5 Hz.

8.2 Measurements results

As mentioned above, first we will compensate the repetitive disturbances of the setup including the Da Vinci forceps instrument without applying any forces. The ILC feed forward signal shown in Figure 58 shows that, now the entire instrument is attached to the setup, the disturbance forces are increased by more than 10 mNm compared to the measurements where only the setup plus the instrument wheel were involved.

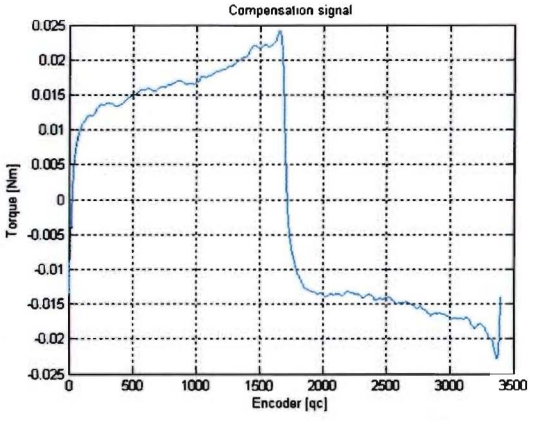

Figure 58. ILC feed forward signal at speed 0.2Hz

Instrument friction changes in time. Because the ILC signal does not adapt to these changes this results in a changing remainder of the disturbance. This inconstant friction introduces an inaccuracy for our force measurement as we will see later in this section.

Where Figure 58 showed the average disturbance over forty cycles, Figure 59 shows all forty cycles of the disturbance in one plot showing the variations of the disturbance.

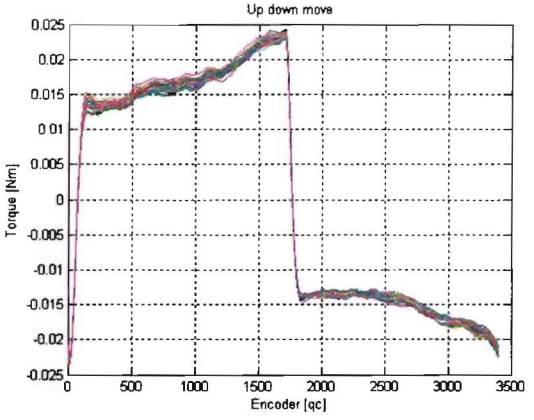

Figure 59. Variation in forty cycles

Force measurement is analyzed at a grasper angle of 90° therefore the variations of the measurement data at this position is analyzed. The normal probability plot in Figure 60 shows that the disturbance torque of the forty measurements at position 90° shows a normal distribution.

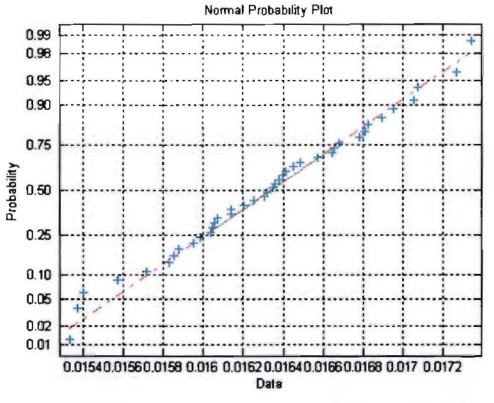

Figure 60. Normal probability plot

The standard deviation S of the data at this position is S = 0.5 mNm. This means 99.7% of the data points have a distance of less than 3·S = 1.5 mNm from the average value. So if the ILC feed forward signal compensates all repetitive disturbances, we can expect a measurement inaccuracy due to the non-repetitive disturbances equal to approximately ±1.5 mNm.

Unfortunately the ILC feed forward signal is not perfect since it is based on a finite number of measurements. Further, the friction of the instrument changes in time due to wear and temperature changes. Therefore the spread in measurement values and so the standard variation will vary slightly with each measurement.

In Figure 61 the ILC feed forward signal (blue) and the remaining disturbance (green) are plotted as function of time.

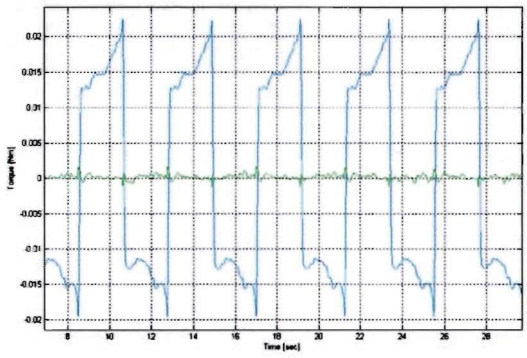

Figure 61. ILC feed forward signal and remaining disturbance

The first torque/force measurement is performed with a force of 60 mN applied to the tip of the grasper. Since the length of the grasper is 20 mm, at a position of 90° the mass applies a torque of 0.06·0.02 = 1.2 mNm.
Due to the remaining disturbance of approximately ±1.5 mNm, we know that force measurement is only possible by averaging the measured motor torque over a number of cycles. The number of cycles used is 40.
At the position of 90° during the rising part of the trajectory, the mean torque applied by the motor (corrected for the instrument gear-ratio) is 1.3 mNm (S = 0.33 mNm).
This means a measuring error of 8%. The results of the measurements with forces of 60mN, 250 mN, 1 N, 2 N and 2.5 N are presented in Table 8.

Applied force [mN]	Applied torque [mNm]	Mean measured torque [mNm]	Standard dev S [mNm]	Error	
				[mNm]	[%]
60	1.2	1.3	0.33	0.1	+8
250	5	5.35	0.24	0.35	+7
1000	20	22.4	0.98	2.4	+12
2000	40	44.7	0.87	4.7	+12
2500	50	55	0.6	5	+10

Table 8. Torque/force measurement results with the Da Vinci instrument

The same forces are used to perform the measurements directly on the motor pulley with an effective radius of 14 mm. The results are presented in Table 9. The standard deviations of the direct drive measurement are much lower than those of the

measurements performed with the DaVinci instrument. This increase of spread in the measurement data indicates that the instrument introduces non-repetitive disturbances that cannot be compensated by ILC.

Applied force [mN]	Applied torque [mNm]	Mean measured torque [mNm]	Standard dev S [mNm]	Error	
				[mNm]	[%]
60	0.84	0.90	0.08	0.06	+7
250	3.5	3.42	0.09	-0.08	-2
1000	14	14.5	0.09	0.5	+4
2000	28	26.8	0.11	-1.2	-4
2500	35	34	0.11	-1	-3

Table 9. Torque/force measurement results with the motor direct drive

Further, the errors of the instrument measurements all show a positive value so a higher torque is measured than the torque that was applied to the forceps. The cause of this is discussed below.

Measurement of (high) torques at the tip of the forceps suffers from several problems. First, due to the limited stiffness of the tendons in the Da Vinci instrument a position shift is introduced between the instrument wheel and the position of the grasper. This also introduces a position shift between the grasper and the motor encoder and therefore makes the ILC feed forward signal incorrect. Figure 62 shows the position shift between the motor encoder and the grasper at a load of 5 N. As mentioned before, the maximum force takes place at a grasper angle of 90° which corresponds with an encoder value of 850 quad counts. In Figure 62 can be seen that the maximum torque occurs at an encoder value of about 1200 quad counts which means a shift of 350 qc, corresponding to 31.5°. In this situation the ILC feed forward data is not applicable.

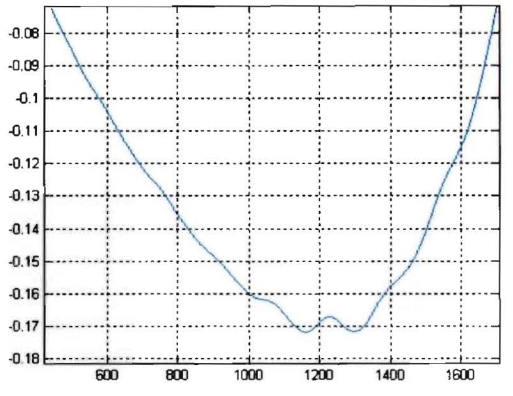

Figure 62. High torque measurement

The second problem with (high) torque measurement is also illustrated by Figure 62. As mentioned before the torque is expected to have the shape of a half sine wave when the grasper moves with a constant velocity lifting a mass. In Figure 62 though, we see that the shape of the applied torque is asymmetric. This is because the stiffness of the Da Vinci instrument works as a spring. Also this effect makes the ILC feed forward data not applicable.

The third problem with torque measurement is that the friction of the Da Vinci instrument increases with increasing torque. This is clearly illustrated by comparing the torque applied when lifting a mass and when lowering that same mass. See Figure 63. The torque applied by the motor equals:

$$T_{motor} = T_{load} + T_{ef}$$

where T_{ef} is the extra friction due to the applied torque which is not compensated by ILC feed forward and T_{load} is the torque due to the gravitation of the mass. As discussed before the acceleration torque may be neglected. During the trajectory the mass is being lifted, the maximum torque is approximately 65 mNm. During the lowering trajectory the maximum torque is approximately 55 mNm. Neglecting the fact that due to the effects discussed above the ILC feed forward does not properly compensate the repetitive disturbances, extra friction T_{fe} is equal to (65 – 55) / 2 = 5 mNm.

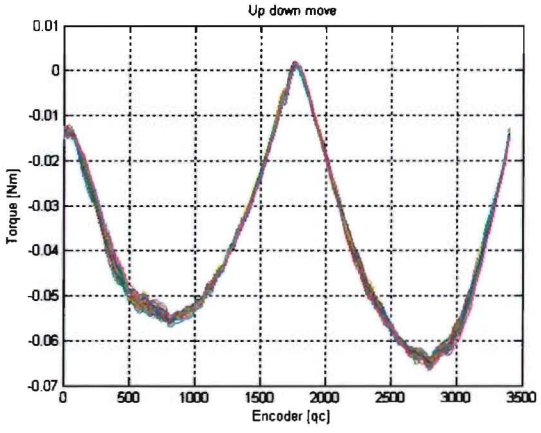

Figure 63. Lowering and lifting of a mass

Due to the limited stiffness of the instrument tendons the grasper does not reach the upright position at the end of the lifting trajectory. Because of this, the motor torque does equal zero at encoder position zero (see Figure 63). At encoder position 1700 the grasper is fully down so here the motor torque does equal zero.

Fourth problem with torque measurement is that due to the low stiffness of the instrument a resonance may occur as shown in Figure 61 at position 1200 qc and in Figure 63 at position 2800 qc. The frequency of the oscillation shown is about 5 Hz. Since this

frequency lies within the bandwidth of the system specifications, this resonance is not filtered out and it affects the accuracy of the force measurement.

9 Conclusions and recommendations

In Chapter 7 an ILC method is described that suppresses friction and disturbances that are function of the motor encoder position without including acceleration disturbances. Acceleration is compensated using model based feed forward. In this way a trajectory independent, repetitive disturbance suppression is achieved.
The ILC method is used in Chapter 8 for constant speeds only and it is shown that torque applied on the Da Vinci forceps can be derived from the current of the motor that drives the forceps.
Due to non-repetitive disturbances and the limited stiffness of the instrument the accuracy of the torque determination does not meet the specifications described in section 6.1. Another reason why the specifications cannot be met is because the instrument friction is a function of the applied torque. This variation of friction is not compensated for by ILC. It may be possible to determine a more accurate torque value if a calibrated or learned correction method is introduced in order to suppress this torque dependant friction.

As we saw in section 7.1.3 the repetitive disturbances caused by the motor and the current amplifier are also a function of the magnitude of the motor current. These disturbances may be suppressed more effectively when the ILC method is extended to a three dimensional lookup table where not only position setpoint and speed are inputs but also (an approximation of) the current magnitude is an input.
Adding torque as a third input of the ILC lookup table may also mean an improvement with respect to the problem described in Chapter 8 where we saw that due to the limited stiffness of the instrument, the learned ILC feed forward data gets inadequate with increasing torque.

Resonance due to the limited stiffness of the instrument in combination with the applied force is not necessarily a problem for accurate force measurement as long as the resonance frequency is higher than the bandwidth of the force measurement system. The stiffness of the Da Vinci instrument is too low for accurate force measurements as specified in section 6.1. For future instrument design higher stiffness is recommended.

Also future low-friction instrument designs will suffer from disturbances and some level of friction. The ILC approach described in this work can be used to compensate these disturbances and friction when they are a function of position and speed (and if extended, a function of applied torque).

For future designs of laparoscopic instruments it is recommended not to couple the positions of different DOF's like is done with the pitch and the jaw axis in the Da Vinci tool. Such a coupling is a complicating factor if ILC is used for friction compensation and it can lead to longer calibration (learning) procedures and possibly lower accuracy of the friction compensation.

For future haptic feedback development it is important that clear specifications are formulated with respect to force measurement specifications. Some surgeons state that haptic feedback in robotic laparoscopic surgery would not contribute any useful information because they never missed it up till now since the deformation of the tissue on which the force is appied, gives enough visual force feedback information. On the other hand it is imaginable that a new unexplored information source is opened up if magnifications of normally insensible small forces are fed back to the hands of the surgeon. For such a development the requirements of force measurement are higher than used in this work.

10 References

[1] Kitagawa M., Dokko D., Okamura A.M., Yuh D.
EFFECT OF SENSORY SUBSTITUTION ON SUTURE-MANIPULATION FORCES FOR ROBOTIC SURGICAL SYSTEMS.
In: Journal of Thoracic and Cardiovascular Surgery, vol. 129. Jan 2005, pages 151-158.

[2] Kitagawa M., Okamura A.M., Bethea B.T., Gott V.L., Baumgarten W.A.
ANALYSIS OF SUTURE MANIPULATION FORCES FOR TELEOPERATION WITH FORCE FEEDBACK.
In: Lecture Notes in Computer Science, vol. 2488. Proceedings of the Fifth International Conference on Medical Image Computing and Computer Assisted Intervention-MICCAI 2002 September 26-29; Tokyo, Japan. Heidelberg, Springer-Verlag; p. 155-62. Edited by Dohi T., Kikinis R.

[3] Niemeyer G., Kuchenbecker K.J, Bonneau R., Mitra P., Reid A.M., Fiene J., Weldon G. THUMP: AN IMMERSIVE HAPTIC CONSOLE FOR SURGICAL SIMULATION AND TRAINING
In: Studies In Health Technology And Informatics, Volume 98, 2004, Pages 272-274

[4] Mayer H., Nagy I., Knoll A., Schirmbeck E., Bauernschmitt R.
ROBOTIC SYSTEM TO EVALUATE FORCE FEEDBACK IN MINIMALLY INVASIVE COMPUTER AIDED SURGERY
In: Proceedings of the ASME Design Engineering Technical Conference and Computers and Information in Engineering Conference 2004: Volume 2: 28th Biennial Mechanisms and Robotics Conference; Proceedings of the ASME Design Engineering Technical Conference, Volume 2 A, 2004, Pages 141-146

[5] Mayer H., Nagy I., Knoll A.
INVERSE KINEMATICS OF A MANIPULATOR FOR MINIMALLY INVASIVE SURGERY
Technical Report, Technische Universitaet Muenchen. January 2004.

[6] HAPTIC FEEDBACK DEVICES
Wichita State Univ. Summer 2004.
Website: http://imfge.wichita.edu/slvr/papers/vr2005/HenryTP.pdf

[7] Khoudja M, Hafez M, Alexandre J, Kheddar A.
TACTILE INTERFACES: A STATE-OF –THE-ART SURVEY
35TH International Symposium on Robotics, 23-26 March, Paris, France, 2004.

[8] Fast K, Gifford T, Yancey
VIRTUAL TRAINING FOR WELDING
Third IEEE and ACM International Symposium on Mixed and Augmented Reality (ISMAR'04). November 02 - 05, 2004. Arlington, VA, USA

[9] Fokker Control Systems (FCS). Oude Meer, Holland.
Website: www.fcs.com

[10] Penn State Hershey Medical Center, College of Medicine. Hershey, Pennsylvania, USA. Website: http://www.hmc.psu.edu

[11] Schijven M., Jakimowicz J.
FACE-, EXPERT, AND REFERENT VALIDITY OF THE XITACT LS500 LAPAROSCOPY SIMULATOR.
Surg. Endosc, 2002 16: 1764-1770.

[12] Hirzinger G, Landzettel K, Brunner B, Fischer M, Preusche C, Reintsema D, Albu-Schaffer A, Schreiber G, Steinmetz B.
DLR's ROBOTICS TECHNOLOGIES FOR ON-ORBIT SERVICING
Advanced Robotics, Vol. 18, No. 2, pp. 139-174 (2004)

[13] Diftler M, Culbert C, Ambrose R, Platt R, Bluethmann W.
EVOLUTION OF THE NASA/DARPA ROBONAUT CONTROL SYSTEM
Proceedings of the 2003 IEEE International Conference on Robotics & Automation. Taipei, Taiwan, September 14-19, 2003

[14] Kortschack A, Shirinov A, Trüper T, Fatikow S.
DEVELOPMENT OF MOBILE VERSATILE NANOHANDLING MICROROBOTS: DESIGN, DRIVING PRINCIPLES, HAPTIC CONTROL
Cambridge University Press, UK, 2005, in print.
Website: http://www-users.itlabs.umn.edu/classes/Spring-2004/csci8980/Papers/fatikow.Robotica.pdf

[15] Shirinov A., Fatikow S.
STABLE TELEOPERATION OF NANOHANDLING MICROROBOTS BY USING A HAPTIC-BASED HUMAN-MACHINE INTERFACE. 10th Biomedical Science and Technology Symposium BIOMED 2003. Northern Cyprus, 10-12 October 2003.

[16] Fahlbush S, Shirinov A, Fatikow S.
AFM-BASED MICRO FORCE SENSOR AND HAPTIC INTERFACE FOR A NANOHANDLING ROBOT. Proceedings of the 2002 IEEE/RSJ Int. Conference on Intelligent Robots and Systems. EPFL, Lausanne, Switzerland October 2002

[17] Schilling Robotics, Davis, California, USA.
Website: http://schilling.com/interim/company/customers/subsea.php

[18] Dennerlein J, Millan P, Howe R.
VIBROTACTILE FEEDBACK FOR INDUSTRIAL TELEMANIPULATORS
Sixth annual symposium on haptic interfaces for virtual environment and teleoperator systems, ASME IMECE, Dallas, November 15021, 1997.

[19] Çavusoğlu M.
TELESURGERY AND SURGICAL SIMULATION: DESIGN, MODELING, AND EVALUATION OF HAPTIC INTERFACES TO REAL AND VIRTUAL SURGICAL ENVIRONMENTS
Berkeley (USA), University of California.
Doctoral dissertation, 2000

[20] Gersem G.
KINAESTHETIC FEEDBACK AND ENHANCED SENSITIVITY IN ROBOTIC ENDOSCOPIC TELESURGERY
Leuven (Belgium), University of Leuven
Doctoral dissertation, 2005.

[21] Interview with surgeon I. Broeders of the Academic Hospital of Utrecht, Netherlands (2004)

[22] Interview with gynaecologist M. Vleugels, Ziekenhuis Rivierenland, Tiel. (2004)

[23] Rovers A.
DESIGN OF A ROBUST MASTER-SLAVE CONTROLLER FOR SURGERY APPLICATIONS WITH HAPTIC FEEDBACK
Master's Thesis. June 2003.
Eindhoven (Netherlands): Eindhoven University of Technology.

[24] Lazeroms M.
FORCE REFLECTION FOR TELEMANIPULATION, APPLIED TO MINIMALLY INVASIVE SURGERY
Delft (Netherlands), University of Delft
Doctoral dissertation. 1999.

[25] Merry R, Molengraft R, Steinbuch M.
DISTURBANCE AND MODEL UNCERTAINTIES IN ITERATIVE LEARNING CONTROL
Eindhoven (Netherlands): Eindhoven University of Technology
In: 4th International Workshop on Multidimensional (nD) Systems (NDS 2005), Wuppertal (2005)

[26] Steinbuch M.
REPETITIVE AND ITERATIVE LEARNING CONTROL DESIGN EXERCISE
Eindhoven (Netherlands): Eindhoven University of Technology.

[27] Broeders I, Ruurda J
ROBOTICS REVOLUTIONIZING SURGERY: THE INTUITIVE SURGICAL "DA VINCI" SYSTEM
Industrial Robot: An International Journal Volume 28, Number 5. 2001, pp. 287-391.

[28] EndoVia Medical Inc. Norwood, Massachusetts, USA.
Website: http://endovia.millersystems.com/products/laprotek_system.shtml

[29] Jaspers J, Grimbergen C.
MECHANICAL MANIPULATOR FOR INTUITIVE CONTROL OF ENDOSCOPIC INSTRUMENTS WITH SEVEN DEGREES OF FREEDOM.
2004 IEEE International Conference on Systems, Man and Cybernetics, Volume 3, 10-13 Oct. 2004 Page(s):2479 - 2485

[30] Interviews with Jaspers J. at AMC (Amsterdam), at the theme-day Precisie-technologen ontmoeten medici, and other occasions 2004.

[31] Interview with account manager Boudrez S. of Intuitive Surgical during a visit of a Da Vinci training session for surgeons at the University Hospital of Maastricht. Further the author of this report experienced the intuitive control of the Da Vinci. 2004

[32] Salisbury K, Guthart G.
THE INTUITIVE TELESURGERY SYSTEM: OVERVIEW AND APPLICATION
Proceedings of the 2000 IEEE International Conference on Robotics & Automation. San Francisco, California, April 2000.

[33] University of Tokyo, Tokyo, Japan.
Website: http://www.nml.t.u-tokyo.ac.jp/research/research-e.html

[34] Immersion Corporation, San Jose, California, USA.
Website: www.immersion.com

[35] HAPTIC RADIO
Northwestern University, Evanston, USA.
Website article:
www.mech.northwestern.edu/courses/433/2002/Projects/HapticKnob/index.html

[36] Rogers G, Cao C.
Chapter 10. COMPUTER-ENHANCED INSTRUMENTS: THE NEXT GENERATION OF SURGICAL ROBOTS
March 2004. Website:
http://ase.tufts.edu/mechanical/EREL/web/Next%20Generation%20of%20Surgical%20Robots.pdf

[37] Casula R, Athanasiou T.
TOTALLY ENDOSCOPIC CORONARY ARTERY BYPASS ON THE BEATING HEART IN JEHOVAH'S WITNESS AND HIV PATIENTS: CASE REPORT.
Heart Surg. Forum. 2004 April 1; 7(2):E174-6.

[38] Niemeyer G.
ROBOTS CREEP INTO BIOMED LANDSCAPE
Article by Merritt R. in EE Times. Website: www.eetimes.com.

[39] Salisbury K,
REMOTE CONTROL. TRADE YOUR SCALPEL FOR A JOYSTICK AND GAIN A SURGICAL TEAM MEMBER WITH AN INCREDIBLE SET OF HANDS
Article by Conger K. in Stanford Medicine Magazine. Spring 2004.

[40] University of Nebraska Medical Center
Website: www.unmc.edu/mis/robot.htm

[41] E-mail exchange with the University of Nebraska Medical Center. 2004

[42] Dokko D., Kitagawa M., Okamura M.
UNDERGRADUATE HELPS GIVE MEDICAL ROBOTS A SENSE OF TOUCH
In Johns Hopkins University News Releases. March 2003.
Website: www.jhu.edu/news/home03/apr03/dokko.html

[43] E-mail exchange with M. Okamura, Johns Hopkins University. 2005.

[44] Dong-Soo Kwon, I Young Woo, Se Kyong Song, Wan Soo Kim, Hyung Suck Cho. MICROSURGICAL TELEROBOT SYSTEM
Proceedings of the 1998 IEEE/RSJ International Conference on Intelligent Robots and Systems, Victoria,B.C., Canada. October 1998

[45] Jones, Lynette A.
KINESTHETIC SENSING
HMH'97, Workshop on Human and Machine Haptics, in 'Human and machine haptics', MIT Press.

[46] Tavakoli M, Patel R, Moallem M.
DESIGN ISSUES IN A HAPTIC-BASED MASTER-SLAVE SYSTEM FOR MINIMALLY INVASIVE SURGERY
Proceedings of the 2004 IEEE International Conference on Robotics & Automation, New Orleans, LA, April 2004.

[47] Çavusoğlu M, Cohn C, Tendick F, Sastry S.
LAPAROSCOPIC TELESURGICAL WORKSTATION
Proceedings of the SPIE International Symposium on Biological Optics (BIO'98), San Jose, CA, January 24-30, 1998.

[48] Verner L, Jeung K, Okamura M.
EFFECTS OF GRIPPING AND TRANSLATIONAL FORCES ON TELEOPERATION
Website: http://www.haptics.me.jhu.edu/publications/icra04-verner.pdf

[49] Jinno M, Matsuhira N, Sunaoshi T, Hato T,
Miyagawa T, Morikawa Y, Furukawa T, Ozawa S, Kitajima M, Nakazawa K.
DEVELOPMENT OF A MASTER SLAVE COMBINED MANIPULATOR FOR LAPAROSCOPIC SURGERY
Medical Image Computing and Computer-Assisted Intervention - MICCAI 2002: 5th International Conference, Tokyo, Japan, September 25-28, 2002, Proceedings, Part I, Editors: T. Dohi, R. Kikinis (Eds.):
pp. 52 – 59, June 2003

[50] Cohn B, Crowford L, Wendlandt J, Sastry S.
SURGICAL APPLICATIONS OF MILLI-ROBOTS
Journal-of-Robotic-Systems. June 1995; 12(6): 401-16

[51] University of Tokyo, Nakamura & Yamane Laboratory. 2004
Website: www.ynl.t.u-tokyo.ac.jp/research/medical_b/medical_b.html

[52] School of Mechanical & Production Engineering
Nanyang Technological University. Singapore.
Website: http://mrcas.mpe.ntu.edu.sg/research/urobot/index.htm

[53] Website: http://ranier.oact.hq.nasa.gov/telerobotics_page/Technologies/0903.html
and Website: http://robotics.jpl.nasa.gov/tasks/rams/homepage.html

[54] Intuitive Surgical Inc., Sunnyvale, California.
Website: www.intuitivesurgical.com

[55] Integrated Surgical Systems (ISS), Davis, California.
Website: www.robodoc.com/eng/

[56] MicroDexterity Systems, San Mateo, Albuquerque, Mexico.
Website: www.microdexsys.com/page3.html

[57] Rosen J, Hannaford B, MacFarlane M, Sinanan M.
FORCE CONTROLLED AND TELEOPERATED ENDOSCOPIC GRASPER FOR MINIMALLY INVASIVE SURGERY – EXPERIMENTAL PERFORMANCE EVALUATION
IEEE transactions on biomedical engineering, Vol. 46, no. 10, October 1999

[58] Hannaford B, Trujillo J, Sinanan M, Moreyra M, Rosen J, Brown J, Leuschke R, MacFarlane M
COMPUTERIZED ENDOSCOPIC SURGICAL GRASPER
Proceedings, Medicine Meets Virtual Reality, San Diego, California. January, 1998.

[59] Çavusoğlu M, Williams W, Tendick F, Sastry S.
ROBOTICS FOR TELESURGERY: SECOND GENERATION BERKELEY/UCSF LAPAROSCOPIC TELESURGICAL WORKSTATION AND LOOKING TOWARDS THE FUTURE APPLICATIONS
In Industrial Robot, Special Issue on Medical Robotics, Vol. 30, No.1, January 2003, pp. 22-29.

[60] Madhani A, Niemeyer G, Salisbury K.
THE BLACK FALCON: A TELEOPERATED SURGICAL INSTRUMENT FOR MINIMALLY INVASIVE SURGERY
Proceedings of the 1998 IEEE/RSJ International Conference on Intelligent Robots and Systems. Victoria, B.C. Canada, October 1998.

[61] Franken M.
SMART MEMORY ALLOY ACTUATED SLAVE SYSTEM FOR MEDICAL ROBOTICS, WITH HAPTIC FEEDBACK
Eindhoven (Netherlands): Eindhoven University of Technology
Master's Thesis. June 2003.

[62] Taylor R., Kumar R, Berkelman P, Gupta P, Barnes A, Jensen P, Whitcomb L, Stoianovici D, Wang Z, deJuan E, Kavoussi L.
A STEADY-HAND ROBOTIC SYSTEM FOR MICROSURGICAL AUGMENTATION
International Journal of Robotic research, 18(12): 1201-1210 December 1999.

[63] Charles S, Das H, Ohm T, Boswell C, Rodriguez G, Steele R, Istrate D.
DEXTERITY-ENHANCED TELEROBOTIC MICROSURGERY
Presented at NASA University Centers Conference, February, 1997, Albuquerque, NM and 8th International Conference on Advanced Robotics (ICAR `97), July 1997, Monterey, CA.

[64] Stoianovici D, Cadeddu J, Demaree R, Basile H, Taylor R, Whitcomb L, Sharpe W, Kavoussi L,
AN EFFECTIVE NEEDLE INJECTION TECHNIQUE AND RADIOLOGICAL GUIDANCE METHOD FOR PERCUTANEOUS PROCEDURES
Lecture Notes in Computer Science, 1997 CVRMed-MRCAS, Sringer-Verlag, Vol. 1205, pp. 295-298, 1997.

[65] Deutsches Zentrum fur Luft- und raumfahrt
Website: www.dlr.de/rm/en/
Article: Actuated and sensorized surgical instruments
Article: Telemanipulation in minimally invasive surgery
Article: Universal robot for surgical interventions

[66] Hu T, Castellanos A, tholey G, Desai J.
REAL-TIME HAPTIC FEEDBACK IN LAPAROSCOPIC TOOLS FOR USE IN GASTRO-INTESTINAL SURGERY
Medical Image Computing and Computer Assisted Intervention MICCAI 2002. 5th International Conference. Proceedings, Part I Lecture Notes in Computer Science Vol.2488. 2002: 66-74

[67] Kwon D, Woo K, Cho H.
HAPTIC CONTROL OF THE MASTER HAND CONTROLLER FOR A MIRCOSURGICAL TELEROBOT SYSTEM
Proceedings of the 1999 IEEE International Conference on Robotics & Automation. Detroit, Michigan, May 1999.

[68] Prasad S, Kitagawa M, Fisher G, Zand J, Talamini M, Taylor R, Okamura A.
A MODULAR 2-DOF FORCE SENSING INSTRUMENT FOR LAPAROSCOPIC SURGERY
Sixth International Conference on Medical Image Computing and Computer-Assisted Intervention - MICCAI 2003, Montreal, Canada, Lecture Notes on Computer Science, Vol 2878, pp 279-286, Springer, 2003

[69] Tholey G, Pillarisetti A, Green W, Desai J.
DESIGN, DEVELOPMENT, AND TESTING OF AN AUTOMATED LAPAROSCOPIC GRASPER WITH 3-DOF FORCE MEASUREMENT CAPACITY
Medical Simulation: International Symposium, ISMS 2004: 38-48, ISMS 2004, Cambridge, MA, USA.

[70] Tholey G, Chanthasopeephan T, Hu T, Desai J,Lau A.
MEASURING GRASPING AND CUTTING FORCES FOR REALITY-BASED HAPTIC MODELING
Computer Assisted Radiology and Surgery - 1st International Workshop on Haptic Devices in Medical Applications, pp. 794-800, London, UK, 2003.

Appendix A *Interface wheels of the Da Vinci forceps*

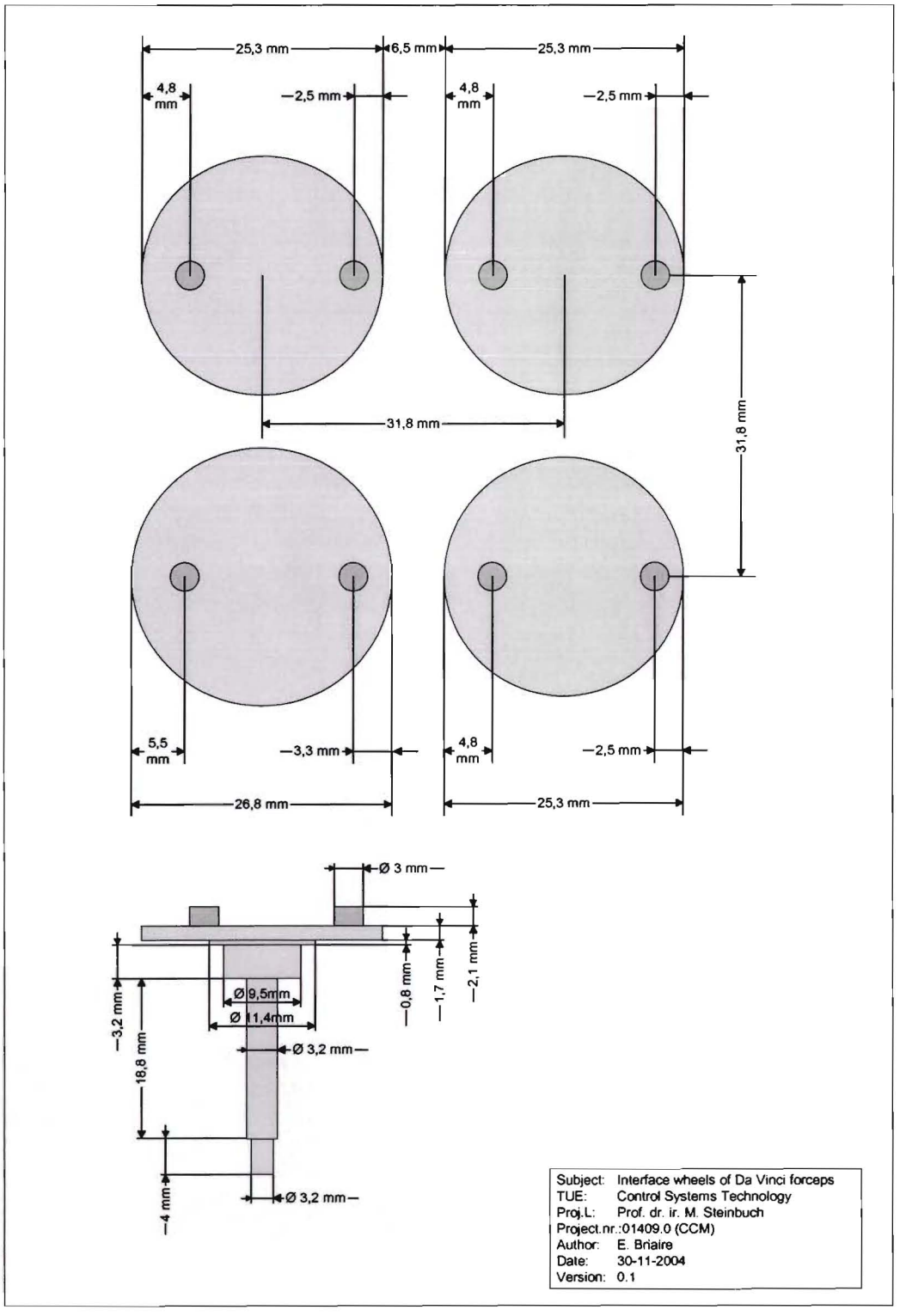

Appendix B *Alternative concepts for the setup*

For driving the four instrument wheels and for measurement (or determination) of the torques applied by the actuators to the instrument wheels, among several alternatives, mainly the following three different concepts were considered and compared:

- direct-drive, torque measurements using a load cell,
- tendon driven, torque measurement using a load cell or tendon tension,
- direct-drive, torque measurement using motor current.

The first two concepts do not use motor current for the determination of the motor torque and are therefore beyond the scope of this research. In spite of this, these concepts are analyzed briefly because they provide alternative methods of torque measurement without using sensors in the Da Vinci instrument.
All three concepts are described below. A description of the selected concept, which is a combination of the concepts mentioned above, can be found in Chapter 6.

Concept 1:
Direct-drive, torque measurement using a load cell

In this concept the stator of the motor that drives an instrument wheel is mounted in such a way that all degrees of freedom are fixed except for rotation. So X, Y, Z, Rx, Ry are fixed and Rz is not fixed. This Rz direction is blocked only by a load cell or metal arm with a strain gauge. In Figure 64 the motor suspension is drawn schematically. The two leaf springs fix the motor in the desired degrees of freedom.
Torque applied by the motor shaft on the instrument wheel will result in reaction torque of the motor stator on the load cell in the opposite direction. The force measured by the loadcell is proportional to the torque applied on the instrument wheel.

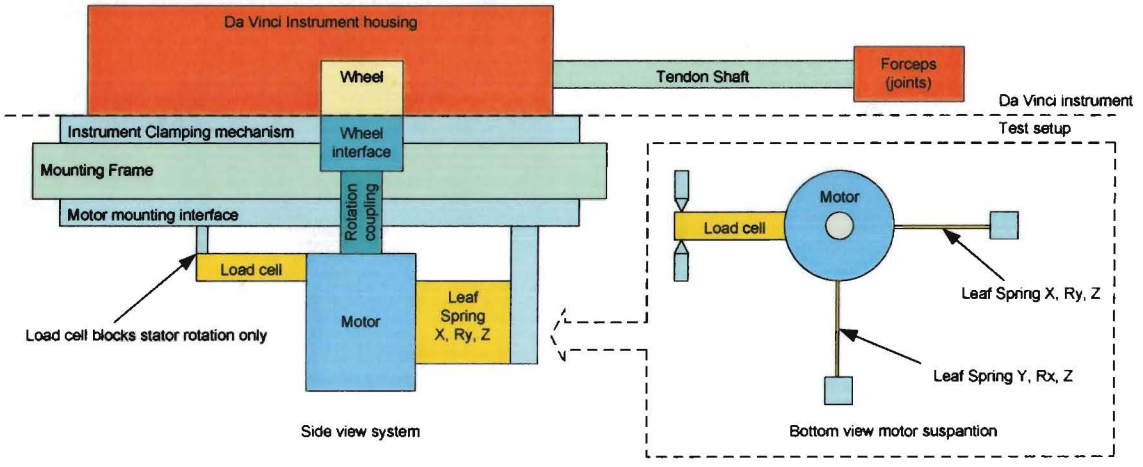

Figure 64. Motor suspension with load cell

Advantage of this concept is that friction of the motor is not measured by the load cell. With respect to friction also a gear head could be used without serious disturbance of the torque measurement. The load cell or metal arm can be chosen stiff enough not to have a negative effect on the bandwidth of the system.

There are also a few disadvantage of this concept. First, additional electronics should be designed, build and tested to amplify the weak signals of the load cell. Second, a complicated motor mounting mechanism should be used. Third, temperature changes of the motor and its mounting mechanism would influence the strain gauge measurement. This effect may be difficult to predict and calibrate. Forth, external forces (disturbances) working on the setup will excitate the mass of the motor housing and mounting construction resulting in measurement errors. For the stand-alone setup these external forces may be minor but in case the setup will be mounted on a 6-DOF robot arm in the future, the disturbance forces of the movements will make force measurement impossible.

Concept 2:
Tendon driven, torque measurement using a load cell or wire tension

In this concept the motor drives the instrument wheel using a tendon similar to the concept Intuitive Surgical implemented in the DaVinci robot. In this way the motor can be mounted far from the instrument, e.g. in the base frame of the robot. In Figure 65 this is illustrated for one DOF. Different methods of force measurement are possible. For instance measuring the tension in the tendon, or the method described above.

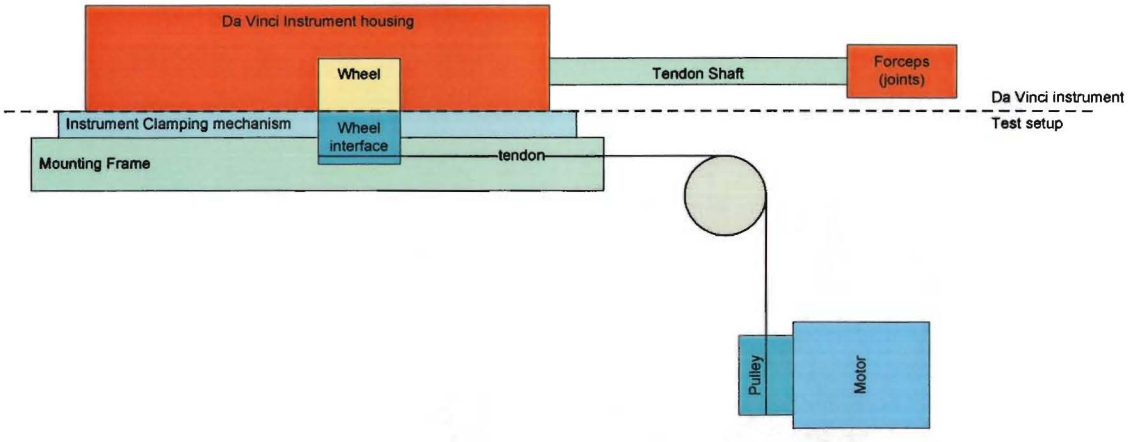

Figure 65. Tendon driven

Disadvantage of driving the instrument using tendons are the following. First, it would introduce more friction in the setup if extra pulleys and ball bearings would be used. Second, the limited stiffness of the tendons and the inertia's of the applied pulleys potentially influence the dynamic behavior of the setup of which the primary function is to analyze the isolated DaVinci instrument, not the setup plus instrument as a complete system.

Concept 3:
Direct-drive, torque measurement using motor current

In this concept the motors are mounted on the frame on which the DaVinci instrument is mounted on and they drive the instrument wheels directly, resulting is a simple construction as shown in Figure 66.

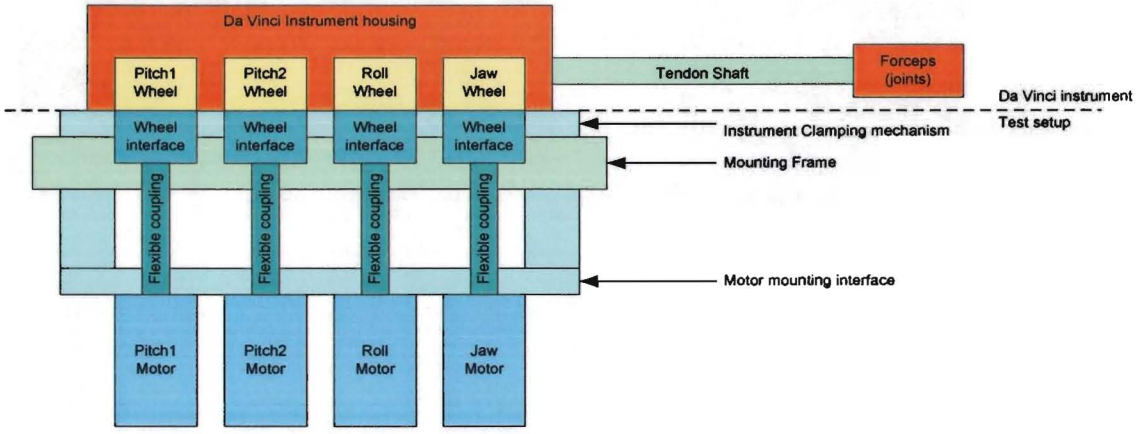

Figure 66. Direct drive

When an EC-motor is selected, friction will be limited to the friction of the ball bearings of the motor. The motor current is a direct measure for the applied torque so the motor can be used as a torque sensor. The rotor inertia of an EC-motor is low, therefore if the setup would be mounted on a 6-DOF robot the force measurement error caused by this inertia will be neglectable compared to those described in concept 1. Since the torque measurement depends fully on the characteristics of the motor constant some calibrations must be done in order to determine this characteristic precisely.
If the motor diameter does not exceed 32 mm (see Appendix A), the direct drive configuration of Figure 66 can be implemented as shown (upside down) in Figure 67.

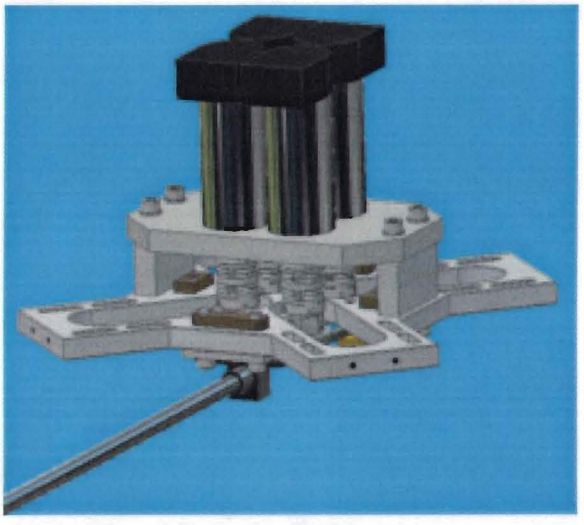

Figure 67. Direct drive configuration

In a direct drive configuration, the motor is coupled with an instrument wheel via a compliant coupling since the motor shaft and the instrument wheel may not be perfectly in line. This will avoid an over constrained construction. The coupling must be tolerant for angular as well as radial misalignment. The type of coupling that is suitable for this application must meet the following requirements:

- no backlash,
- low friction,
- low inertia,
- no preferred rotational positions,
- high rotational stiffness,
- minimum applied force on (motor)bearings.

Appendix C *Stribeck curve with MC IDM640*

The IDM640 of Technosoft seemed not to function correctly in current control mode when an unloaded (or low loaded) EC-motor is controlled. This gets very clear when looking at the Stribeck curve of the unloaded motor measured with this controller.

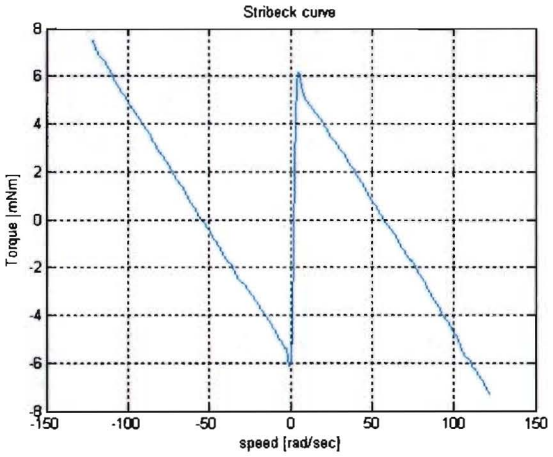

Figure 68. Stribeck curve with motion controller IDM640.

Since we are highly interested in measuring low torques, the IDM640 seemed not suitable for the setup and was not used any further.

Appendix D *Maxon motor data sheet*

maxon *EC*-max

***EC*-max 40** ∅40 mm, brushless, 120 Watt

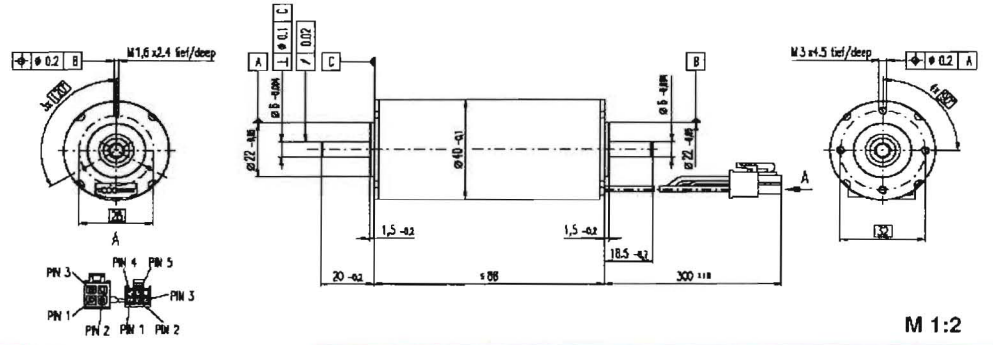

M 1:2

Stock program
Standard program
Special program (on request)

Order Number		283870	283871	283872	283873
Motor Data					
1	Assigned power rating	W	120	120	120	120
2	Nominal voltage	Volt	48.0	48.0	48.0	48.0
3	No load speed ¹⁾	rpm	10100	7240	4720	3610
4	Stall torque ¹⁾	mNm	2090	1490	1050	838
5	Speed / torque gradient ¹⁾	rpm / mNm	4.89	4.90	4.55	4.35
6	No load current ¹⁾	mA	348	202	105	71.4
7	Terminal resistance phase to phase	Ohm	1.03	2.02	4.40	7.19
8	Max. permissible speed	rpm	12000	12000	12000	12000
9	Max. continuous current at 5000 rpm ¹⁾	mA	4450	3170	2150	1680
10	Max. continuous torque at 5000 rpm	mNm	168	167	174	178
11	Max. efficiency ¹⁾	%	84	83	82	81
12	Torque constant	mNm / A	44.8	62.8	96.1	126
13	Speed constant	rpm / V	213	152	99.4	76.1
14	Mechanical time constant	ms	5.2	5.2	4.8	4.6
15	Rotor inertia	gcm²	101	101	101	101
16	Terminal inductance phase to phase	mH	0.204	0.400	0.937	1.60
17	Thermal resistance housing-ambient	K / W	3.5	3.5	3.5	3.5
18	Thermal resistance winding-housing	K / W	0.3	0.3	0.3	0.3
19	Thermal time constant winding	s	3.9	3.9	4.2	4.3
20	Thermal time constant stator	s	1140	1140	1140	1140

1) Values determined with block commutation

Specifications

- Axial play at axial load < 10 N — 0 mm
- Preloaded **ball bearing** — Preload strength min. — 10 N
- Max. **ball bearing** loads — axial (dynamic) — 9 N; radial (5 mm from flange) — 80 N; Force for press fits (static, shaft supported) — 4000 N
- Ambient temperature range — -40 ... +100°C
- Max. permissible winding temperature — +155°C
- Weight of motor — 660 g
- 2 pole permanent magnet
- Values listed in the table are nominal.
- **Connection** (Cable AWG 20)

red	Motor winding 1	Pin 1
black	Motor winding 2	Pin 2
white	Motor winding 3	Pin 3
	N.C.	Pin 4

Connector	Article number
Molex	39-01-2040

Connection (Cable AWG 26)

yellow	Hall sensor 1	Pin 1
brown	Hall sensor 2	Pin 2
grey	Hall sensor 3	Pin 3
blue	GND	Pin 4
green	V_{Hall} 4.5 ... 24 VDC	Pin 5
	N.C.	Pin 6

Connector	Article number
Molex	430-25-0600

- For wiring diagram for Hall sensors see p. 26

Operating Range

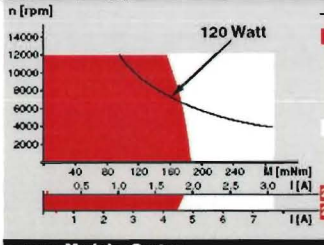

283873 Motor with high resistance winding
283870 Motor with low resistance winding

Comments

Curve of constant assigned power rating

Continuous operation
In observation of above listed thermal resistances (lines 17 and 18) the maximum permissible winding temperature will be reached during continuous operation at 25°C ambient.
= Thermal limit.

Short term operation
The motor may be briefly overloaded (recurring).

Details on page 149

maxon Modular System

Overview on page 17 - 21

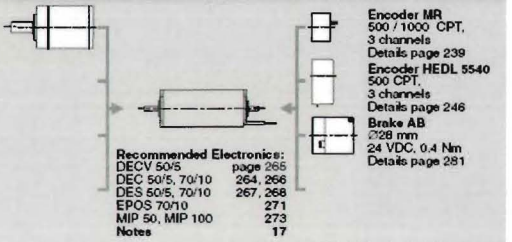

Planetary Gearhead
∅52 mm
4 - 30 Nm
Details page 228

Encoder MR
500 / 1000 CPT,
3 channels
Details page 239

Encoder HEDL 5540
500 CPT,
3 channels
Details page 246

Brake AB
∅28 mm
24 VDC, 0.4 Nm
Details page 281

Recommended Electronics:

DECV 50/5	page 265
DEC 50/5, 70/10	264, 266
DES 50/5, 70/10	267, 268
EPOS 70/10	271
MIP 50, MIP 100	273
Notes	17

April 2005 edition / subject to change

Appendix E *Spring constant of the motor assembly*

As discussed in section 6.2.1 the motor is mounted by means of two leaf springs. These leaf springs allow some compliance for unroundness and eccentricity of the instrument wheels and motor pulleys but on the other hand they make the drive train less stiff. Compared to the stiffness of the tendon, the relatively low stiffness of the leaf spring construction will be of major influence on the overall stiffness of the total setup. Since the first goal of the setup is creating a low friction, backlash free drive platform for a DaVinci instrument, this reduced stiffness is accepted. (Later stiffer leaf springs may be used).

The construction consists of two leaf springs mounted parallel. The spring constant of this construction in direction x (see Figure 69) is given by:

$$k = \frac{2 \cdot E \cdot b \cdot t^3}{a^3}$$

where E is the elasticity modulus, t is the thickness of the leaf springs and the other dimensions are shown in Figure 69.
With E = 2.1e5 [Nmm-2], a = 50 [mm], b = 40 [mm], t = 0.5 [mm] the calculated spring constant is 16.9 kN/m.

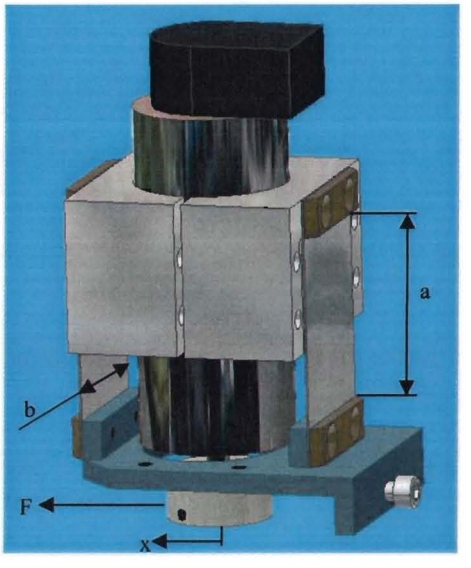

Figure 69. Dimensions of the leaf springs

From measurements, performed with a micrometer and a digital force sensor the following spring constant curve was determined.

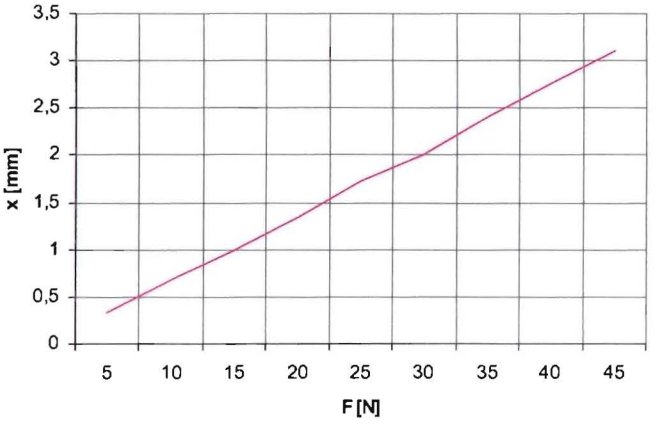

Figure 70. Spring constant of Motor construction

The measured spring constant is 14.5 kN/m which means an error of 14% compared to the calculated value. This may be caused by measurement errors and inaccuracies in the spring leaf dimensions (error of the spring thickness [to the third power] has major influence on the spring constant).

Appendix F *Magnetic alignment of the MC*

The torque ripple of a servo motor is neglectable when it is commutated sinusoidal electronically in stead of block-shaped commutation, triggered by Hall-sensors or mechanical commutator segments (see Figure 71).

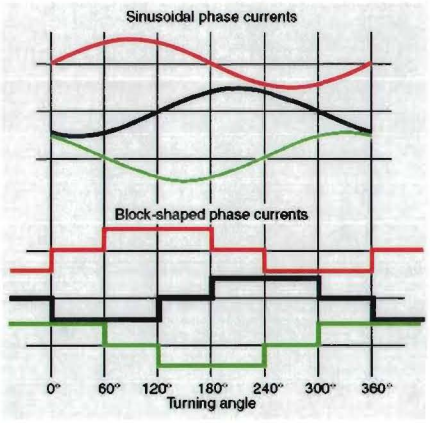

Figure 71. Sinusoidal vs. block commutation

Before a motion controller switches from Hall commutation to sinusoidal commutation it will perform a magnetic alignment in order to find the relation between the Hall sensor positions, coil positions and digital encoder index position of the motor. After this alignment the rotating magnetic field of the motor is based on the (higher resolution) value of the digital encoder.
The magnetic alignment procedure takes place during the first full revolution of the motor. Since the driving wheels of the DaVinci tool have a limited rotation angle that is less than one revolution this means the motors must be initialized before they are connected to the DaVinci tool.

Appendix G *Control Unit Details*

The sampling time of the code running on the Target PC is 125 microseconds corresponding with a frequency of 8000 Hz. For the Pentium II that is used, this is the minimum sampling time for the loaded project. A Pentium III or higher would result in a shorter sample time since XPC is designed for this processor.

The Target PC contains an Ethernet board and two data acquisition boards of National Instruments that are supported by XPC. These boards provide sufficient digital and analog I/O to control the setup (DAC, ADC, DIO and Encoder inputs).

The control unit is not yet fully wired, though it is prepared for future expansion. This means there are electrical interfaces for six motors: four motors to drive the Da Vinci tool and two to drive the two DOF joystick (see Figure 19) which is also developed during this project but will be discussed no further in this report.
On the front panel of the control unit, for each motor a connector is available for:

- motor current,
- hall signals,
- encoder signals,
- homing sensor.

The power supply of each motion controller is individually fused and can be switched off/on by a switch on the front panel.
Two (switchable) connectors are available for RS232 communication with the motion controllers. These communication ports are used for test purposes and configuration of the motion controllers only. All motion controllers, home sensors and the loadcell amplifier are directly wired to the National Instruments interface boards.

Motor temperature may be monitored by means of a sensor that can be physically attached to the motor cool body and electrically to the National Instrument interface board (not implemented, see section 7.1.1).
A proximity switch [Peperl and Fuggs] is used as homing sensor. This sensor detects the high-low transition that is implemented on the Tendon Wheel that is mounted on the instrument wheel (Figure 16).

Appendix H *Location of applied torque*

When measuring torques during grasping, the exact location of the spot where the object is grasped inside the forceps is not measured. This exact location determines the force applied on the object. The applied torque though, is measurable.

For the following reason it is assumed that it is not essential to measure the exact location of the object inside the jaws of the forceps:
When the surgeon is grasping an object with the forceps, not a force but a torque is measured. The measured torque is fed back to the hands of the surgeon. Since the surgeon also receives visual feedback via the stereo optical system he sees where the tissue or object is located inside the jaws of the forceps.

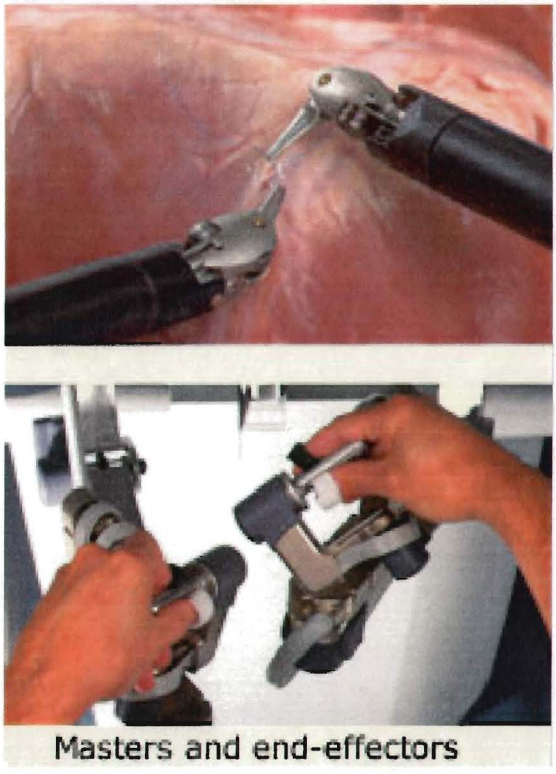

Figure 72. Da Vinci forceps and joysticks

The forceps-like joystick the surgeon is handling with his fingers has a 'similar' geometry as the forceps interfacing with the tissue. If the surgeon places his fingers at the same relative place as where the force is working on the instrument, he will feel the same force as is working on the forceps in the body if the joystick is physically similar to the forceps that is in contact with the tissue.
So in order to realize haptic feedback, torque measurement and visual feedback are combined.

Appendix I *Mechanical drawings*

Appendix J *Torque disturbance due to eccentricities in pullies*

In this section the motor is coupled with a wheel of the instrument that is internally disconnected from the forceps. In this way the following components are added compared to the measurements of the previous sections:

- the motor suspension (leaf spring construction),
- instrument wheel friction,
- tendon stiffness and friction.

Only the effect of the motor suspension will be analyzed with respect to the disturbance forces it introduces due to unroundness and eccentricity of the pullies.

Displacement

During friction measurements the pre-tension applied by the leaf springs of the motor assembly is 5 N as described in section 6.2.1.

In Appendix E *Spring constant of the motor assembly*, the spring constant of the motor assembly is calculated and also measurement results are presented.

With a spring constant of 14.5 kN/m, a pre-tension of 5 Newton corresponds with a leaf spring deflection of $d_s = 0.345$ mm (it is assumed that tendon stiffness is infinite and that the motor axis and the tool axis are mounted to resp. the motor stator and the instrument housing infinitely stiff for the all degrees of freedom except for rotation).

The eccentricity of the motor axis plus the motor pulley is measured with a Tesa sensor while slowly rotating the motor. The error is

$$e_m = \frac{|r2 - r1|}{2} = \pm 10 \mu m .$$

The eccentricity of the tool wheel pulley is measured in the same way. An eccentricity of this pulley can be reduced by adjusting the pulley w.r.t. the clamping block that is mounted on the tool wheel. Depending on the adjustment an eccentricity of

$$e_t = \frac{|r4 - r3|}{2} = \pm 50 \mu m$$

may remain. Depending on the rotational orientation of both eccentricities, worst case the leaf springs are deflected over a distance of ±60 µm during rotation. The maximum changing deflection during rotation (see Figure 73) is described by

$$\Delta d_{max} = (e_m + e_t) \cdot \sin(\theta) .$$

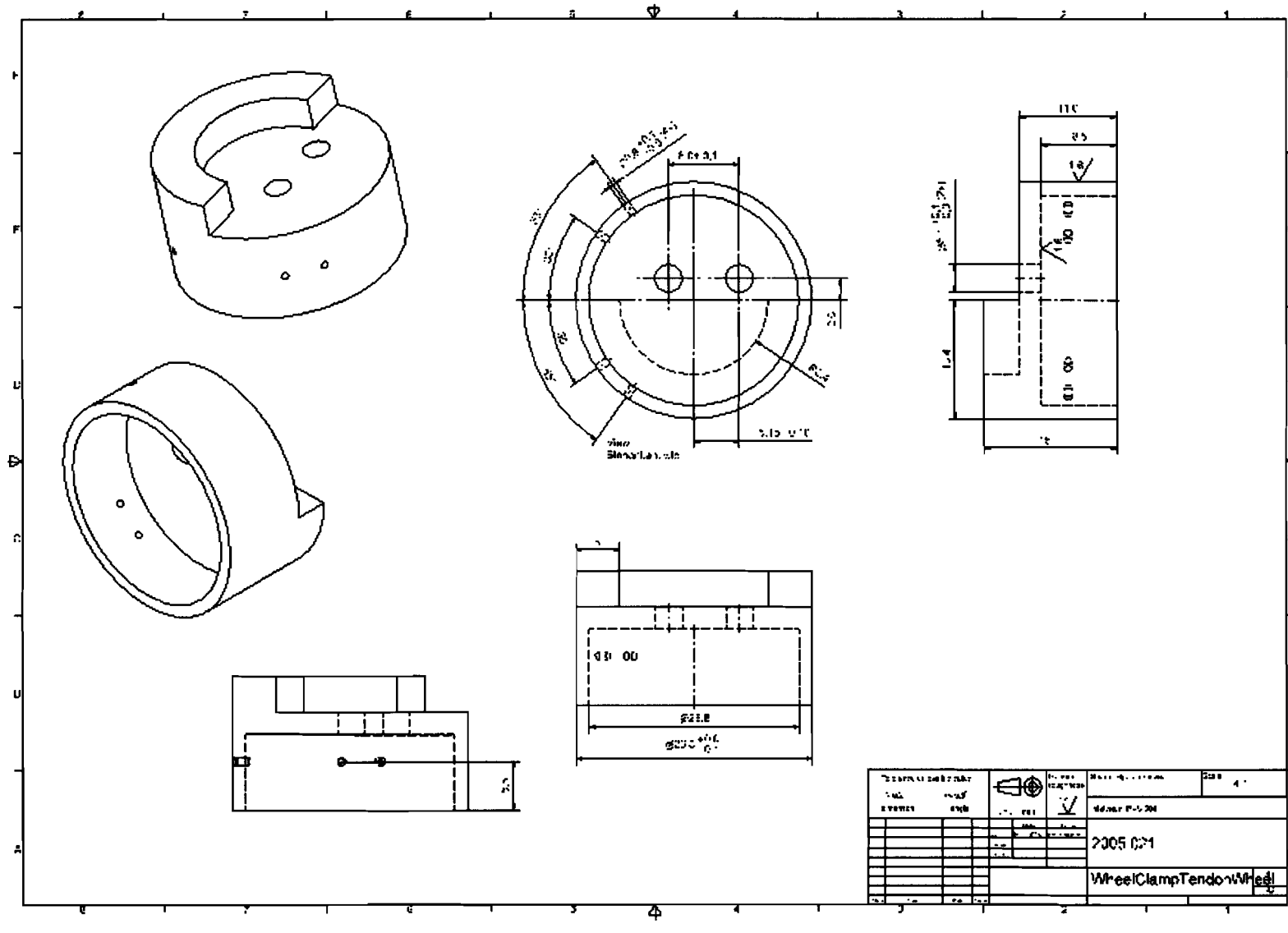
2005 021
WheelClampTendonWheel

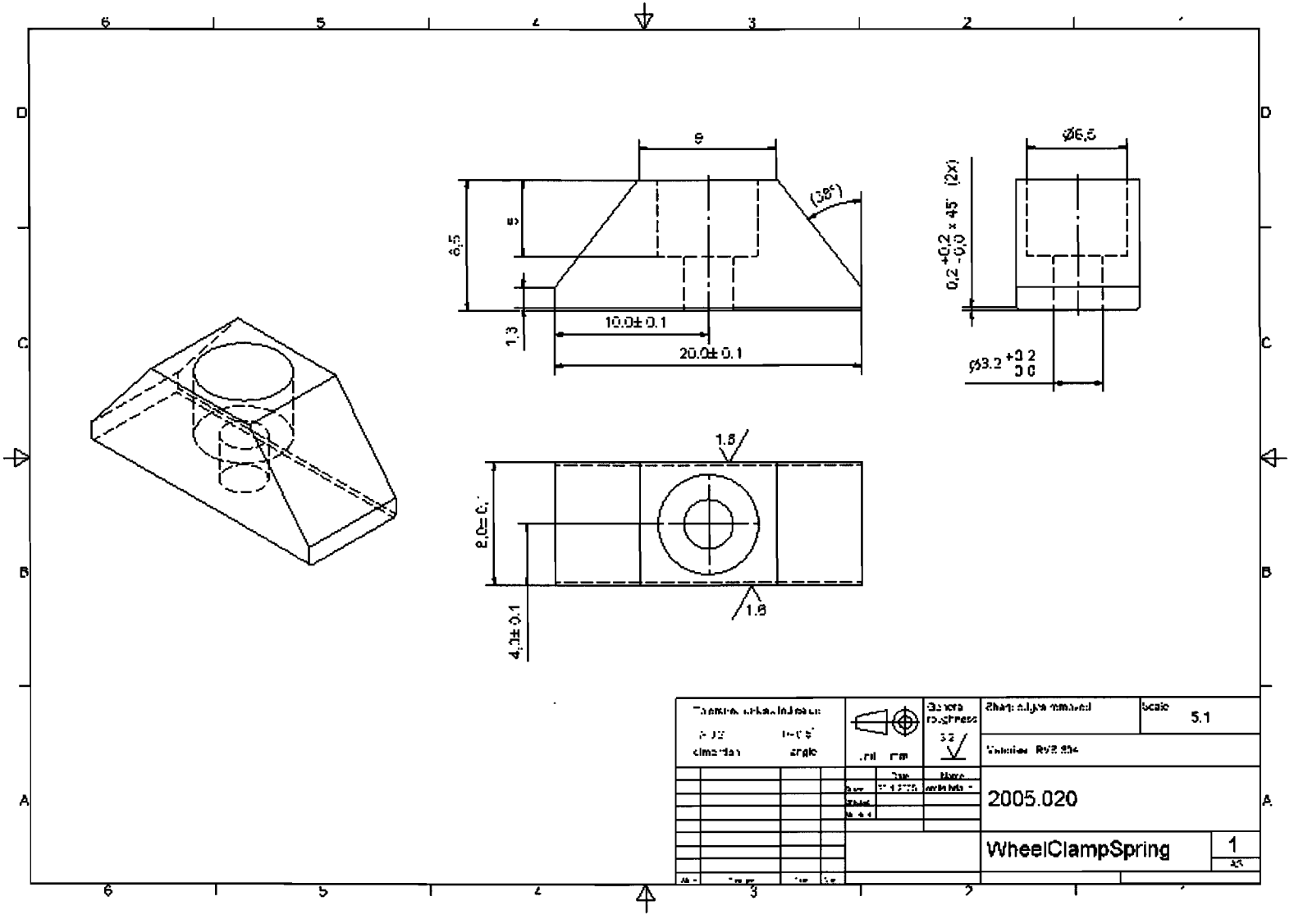
6
5
4
3
2
1
D
C
B
A
8
5
(38°)
8,5
1,3
10,0± 0,1
20,0± 0,1
Ø6,5
0,2 +0,2 -0,0 x 45° (2x)
Ø3,2 +0,2 0
1,6
8,0± 0,1
4,2± 0,1
1,6
Scale
5,1
2005.020
WheelClampSpring
1

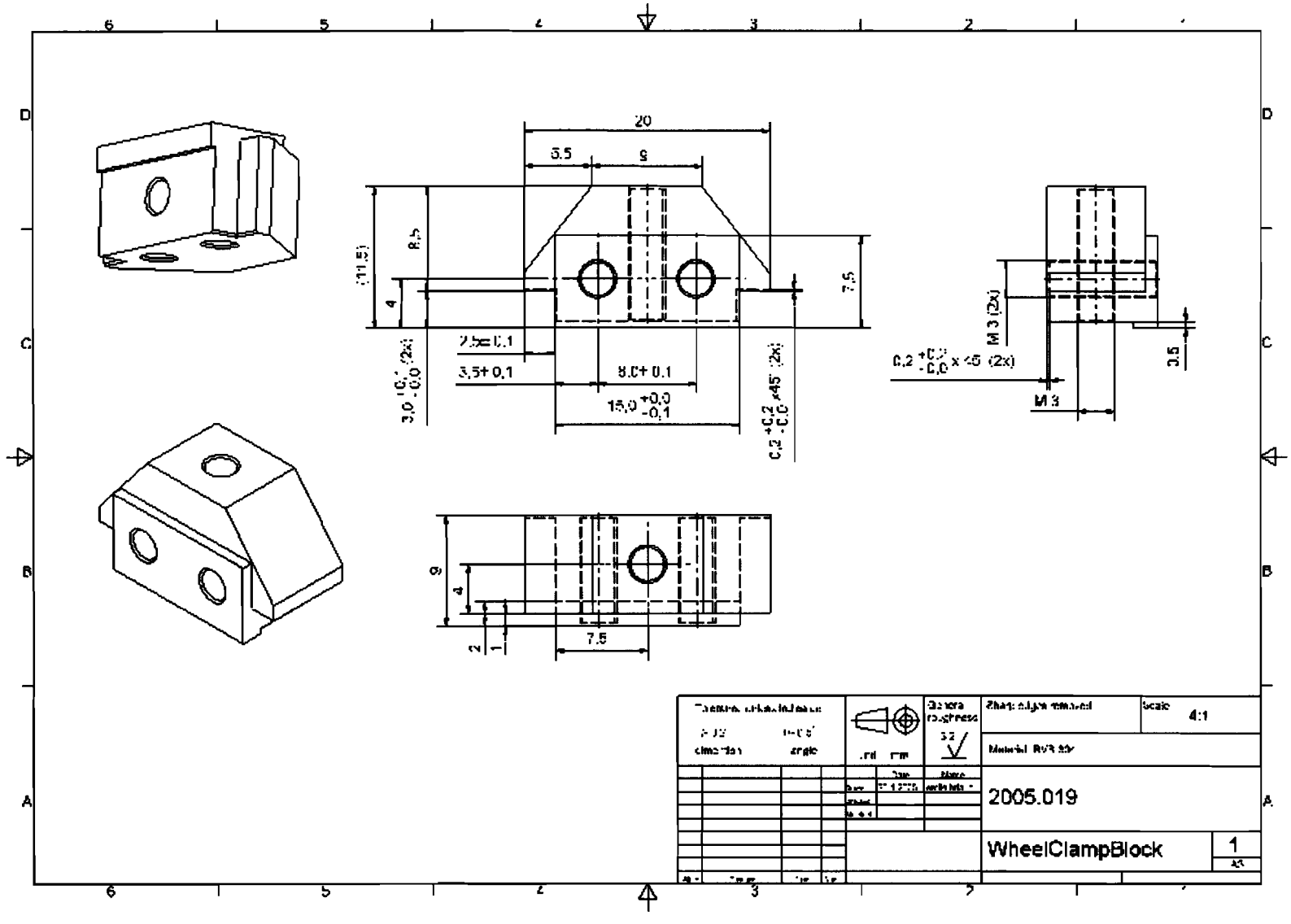
20
5.5
9
11.5
8.5
4
7.5
2.5±0.1
3.5±0.1
8.0±0.1
15.0 +0.0 -0.1
3.0 +0.1 -0.0 (2x)
0.2 +0.2 -0.0 x45° (2x)
M3 (2x)
0.2 +0.2 -0.0 x 45° (2x)
M3
3.5
9
4
2
1
7.5
Scale 4:1
2005.019
WheelClampBlock
1

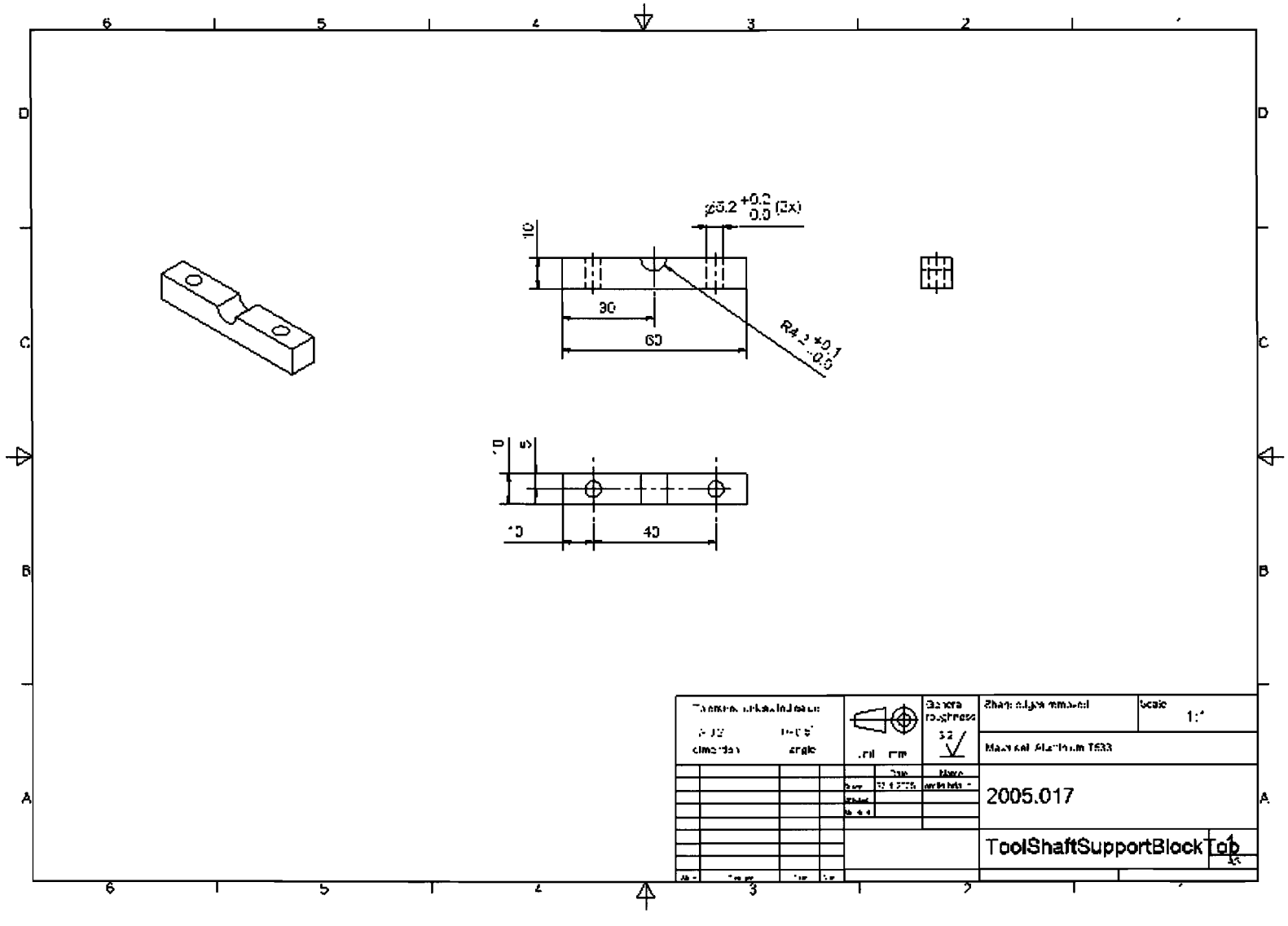
6
5
4
3
2
D
C
B
A
ø5.2 +0.2 0.0 (2x)
10
30
60
R4.2 +0.1 -0.5
10
40
Scale 1:1
Material Aluminium T651
2005.017
ToolShaftSupportBlockTop

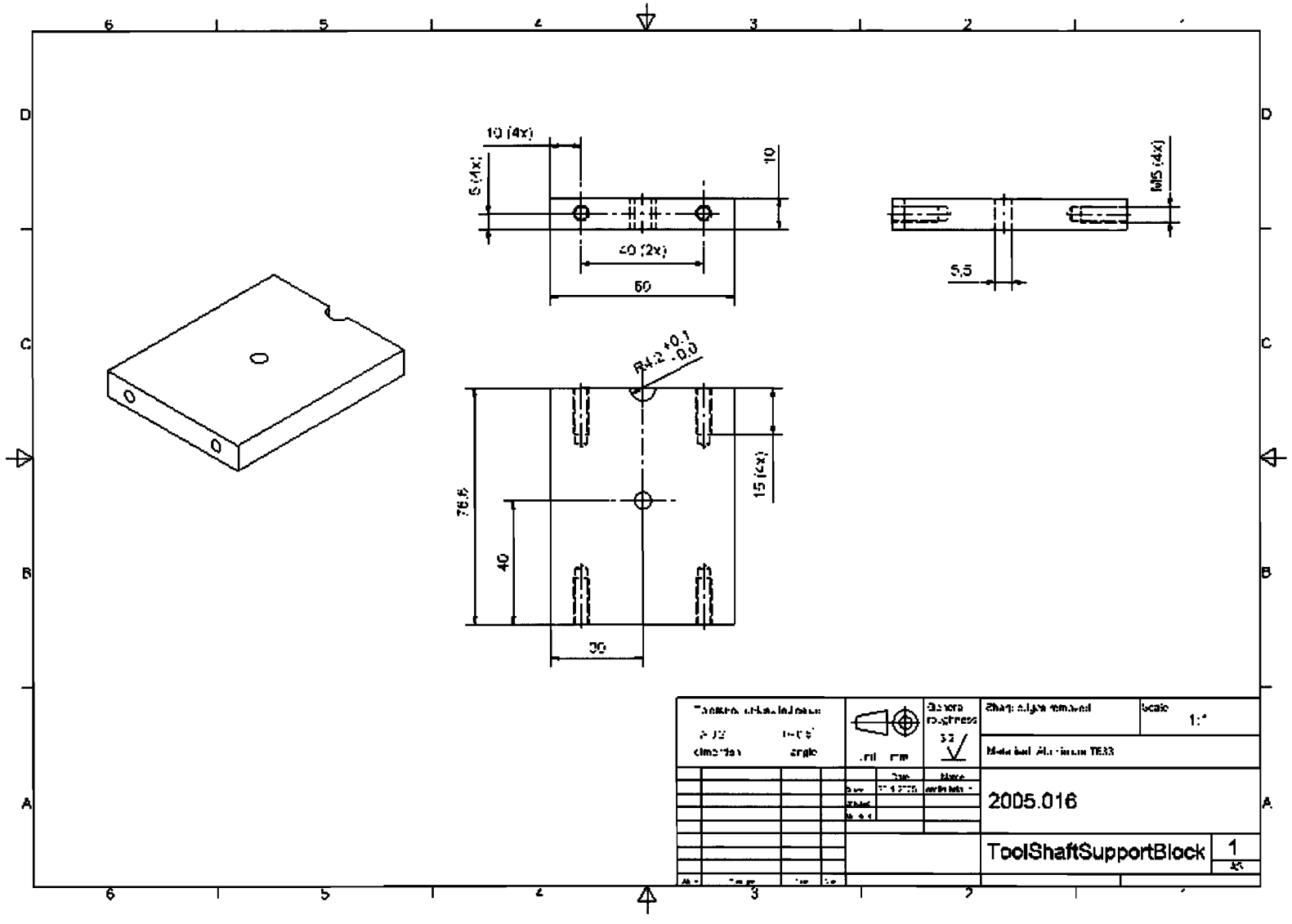
10 (4x)
5 (4x)
10
50 (2x)
60
M5 (4x)
5,5
R4,2 +0,1 -0,0
15 (4x)
76,6
40
30
2005.016
ToolShaftSupportBlock
1

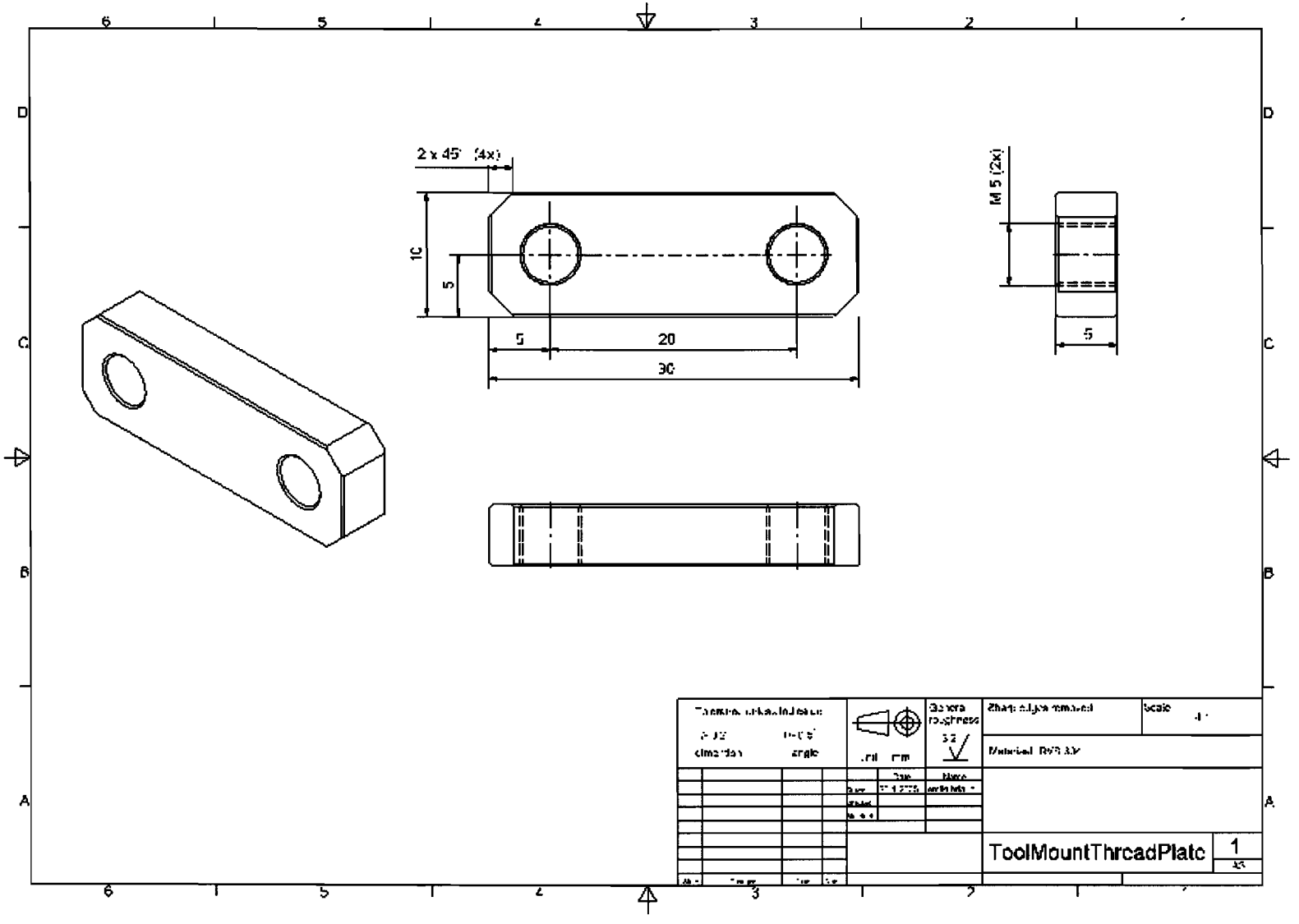
2 x 45° (4x)
10
5
5
20
30
M 5 (2x)
5
ToolMountThreadPlate
1

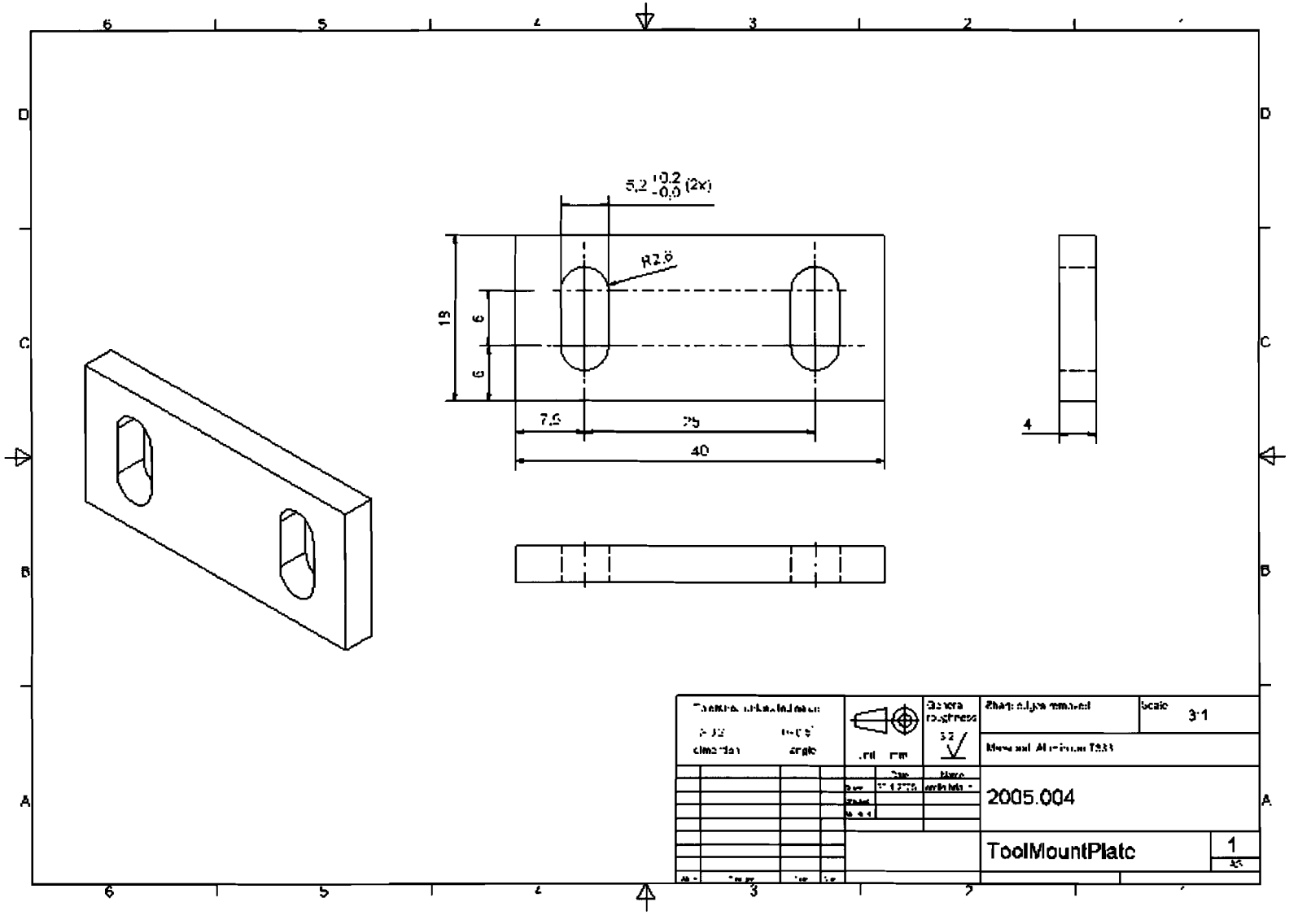
5,2 +0,2 -0,0 (2x)
R2,6
18
6
6
7,5
25
40
4
2005.004
ToolMountPlate
1
Scale 3:1

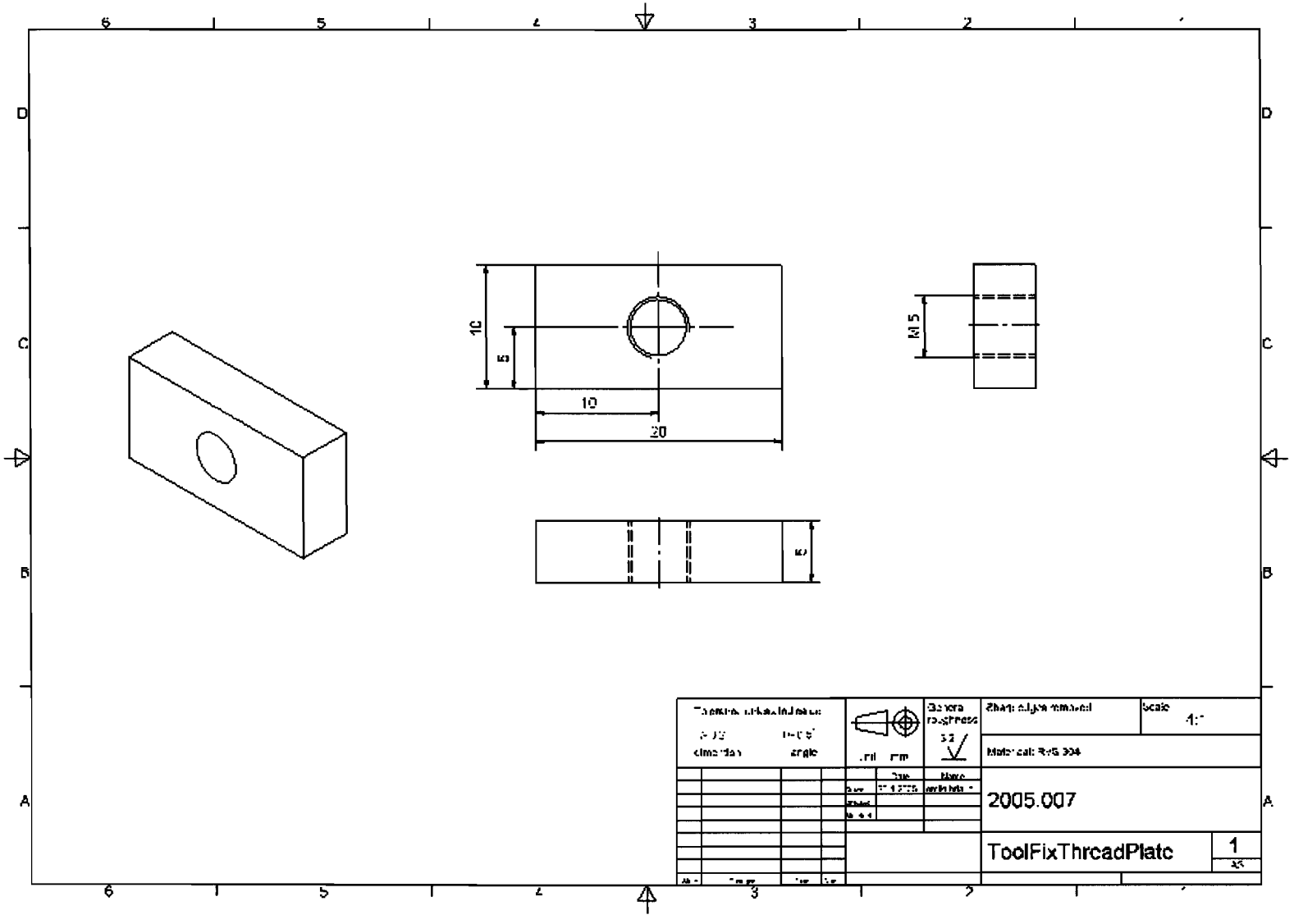
10
5
10
20
M5
5
2005.007
ToolFixThreadPlate
1

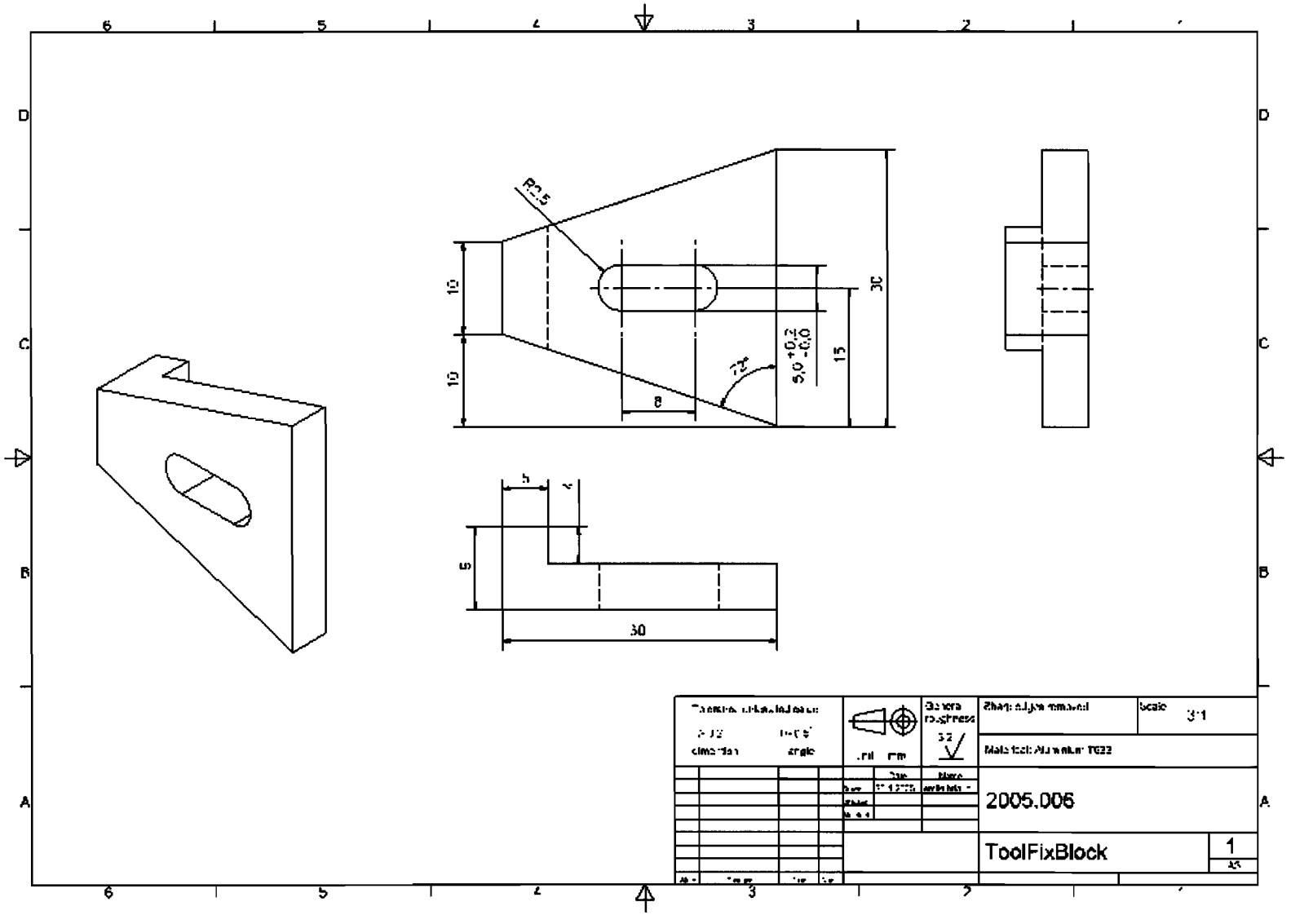
R2.5
10
10
30
15
8
22°
5,0 +0,2 -0,0
5
4
5
30
2005.006
ToolFixBlock
1
Scale 3:1

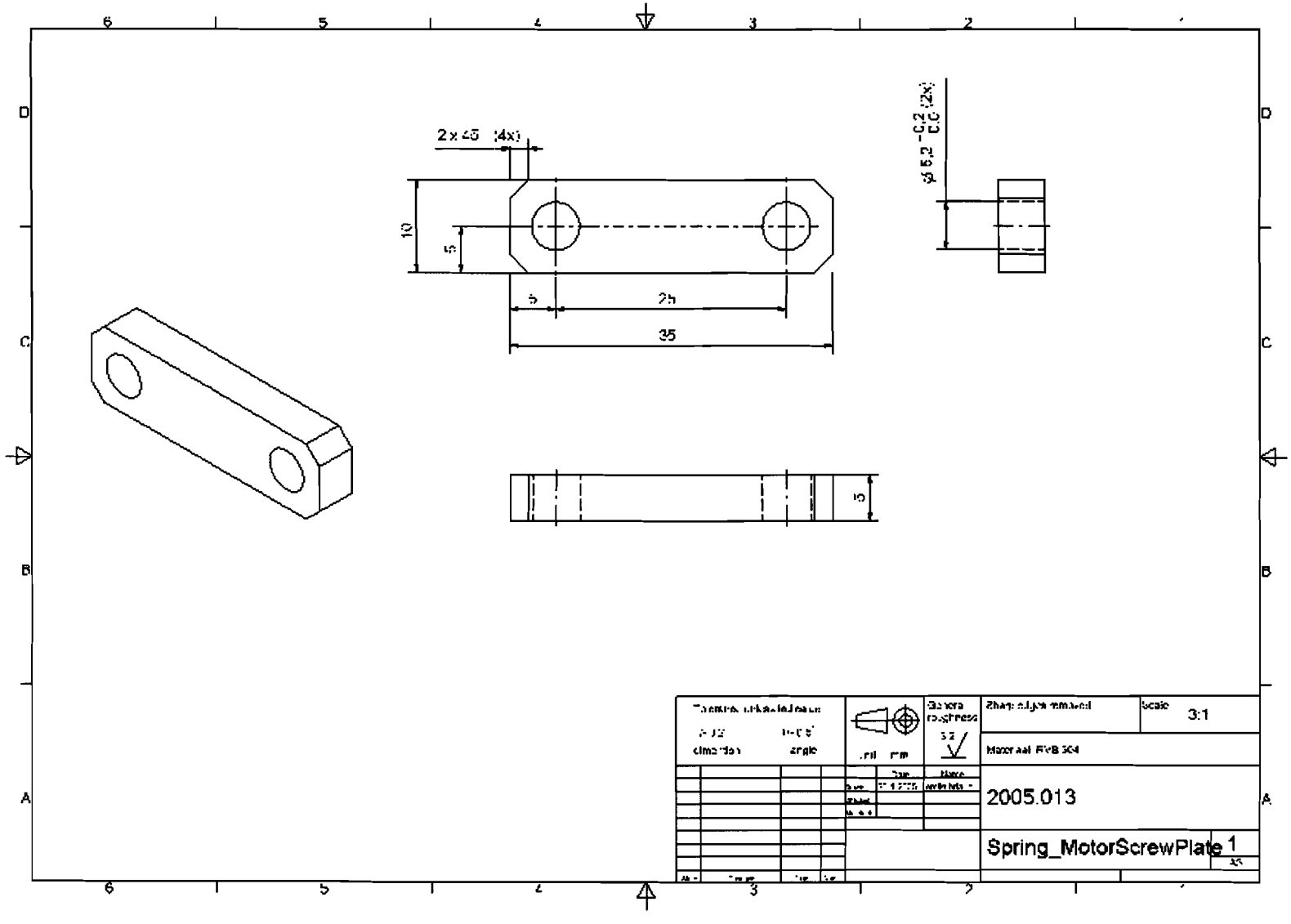
2x 45° (4x)
10
5
5
25
35
5
Scale 3:1
2005.013
Spring_MotorScrewPlate 1

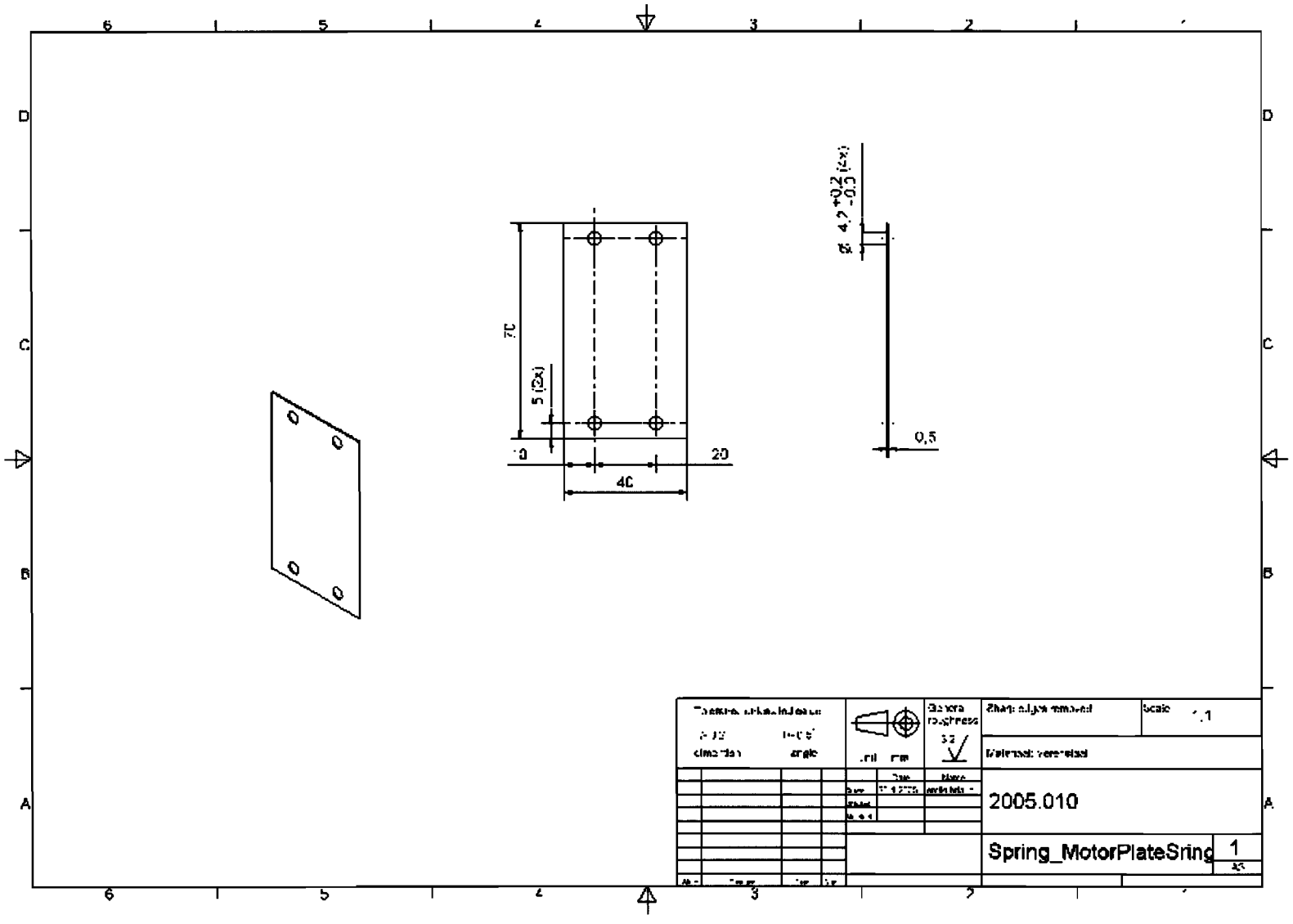
70
5 (2x)
0
20
40
0,5
2005.010
Spring_MotorPlateSring
1

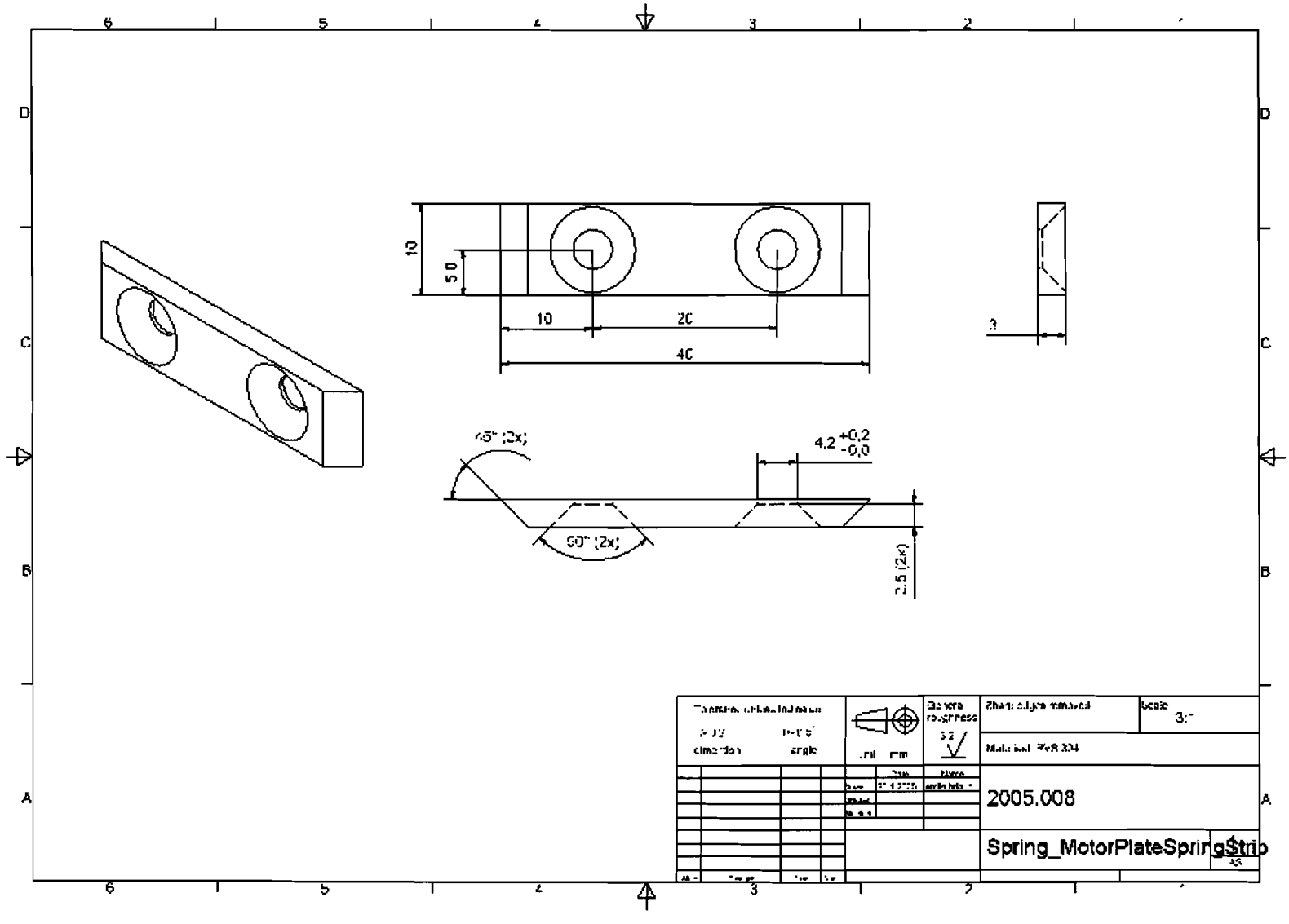
10
5.0
10
20
40
3
45° (2x)
4,2 +0,2 -0,0
60° (2x)
2005.008
Spring_MotorPlateSpringStrip

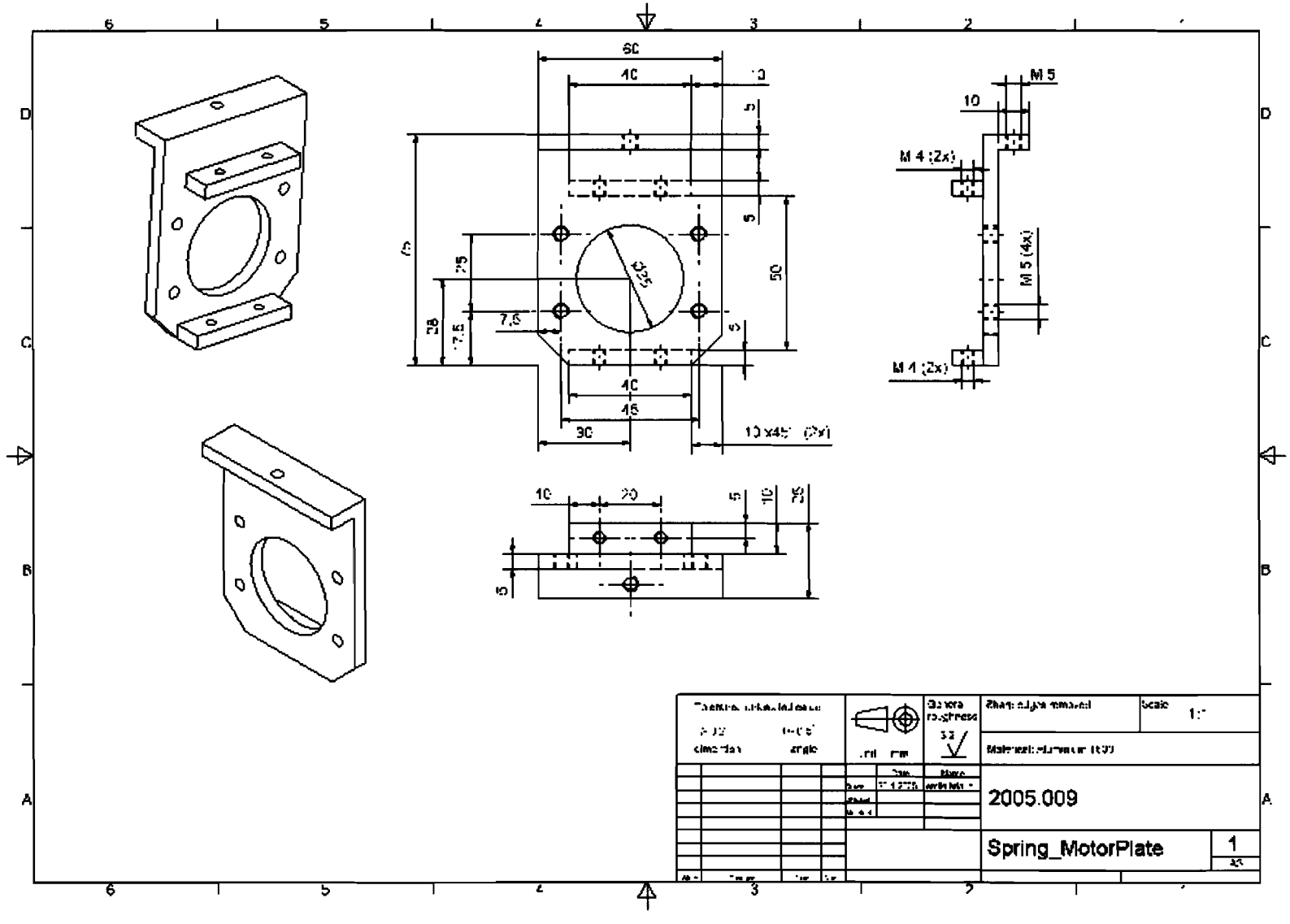
80
10
10
5
5
50
28
7.5
25
7.5
Ø25
40
45
30
10x45° (2x)
M 5
10
M 4 (2x)
M 5 (4x)
M 4 (2x)
10
20
5
10
25
5
2005.009
Spring_MotorPlate
1

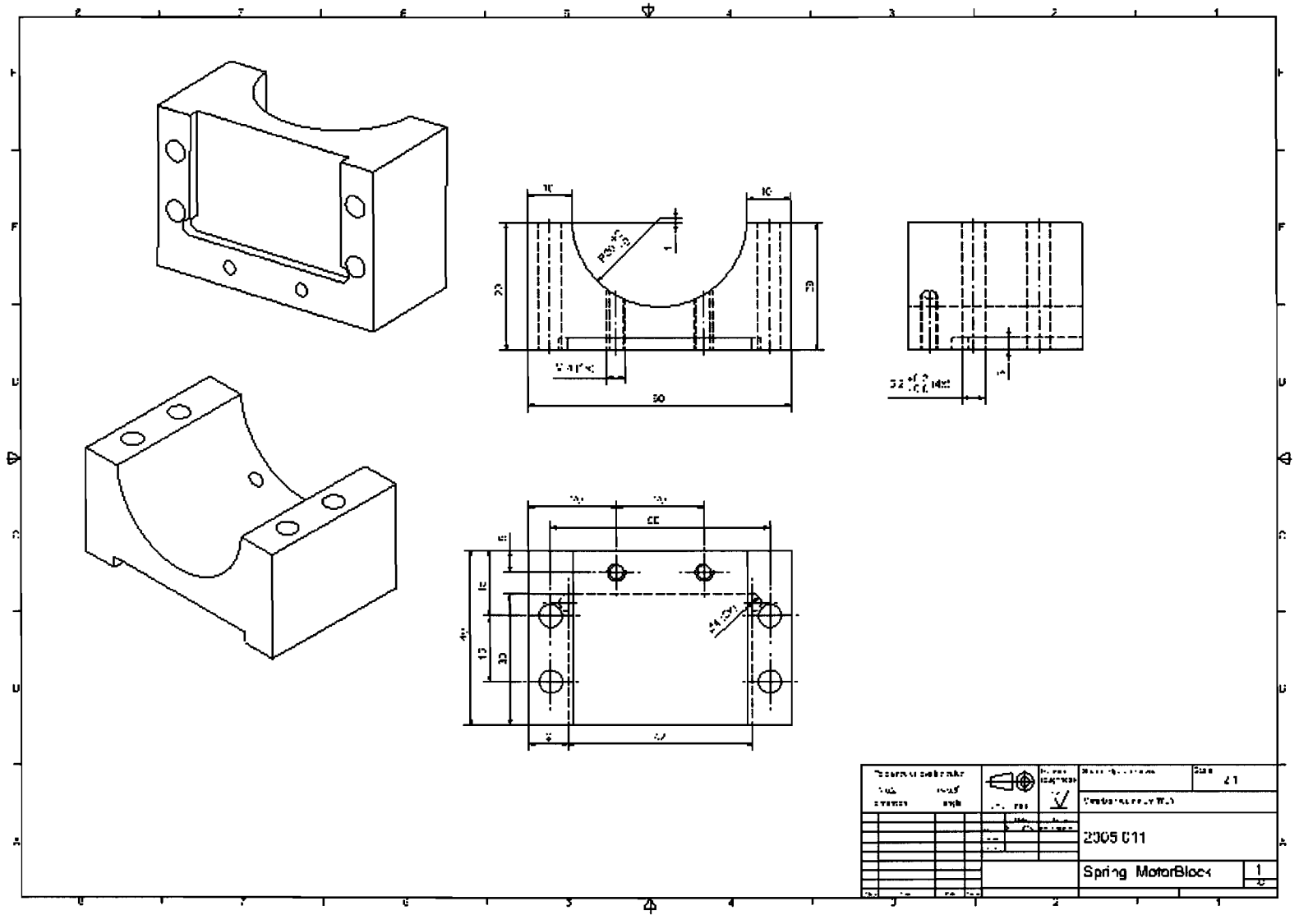
2005 011
Spring MotorBlock
1

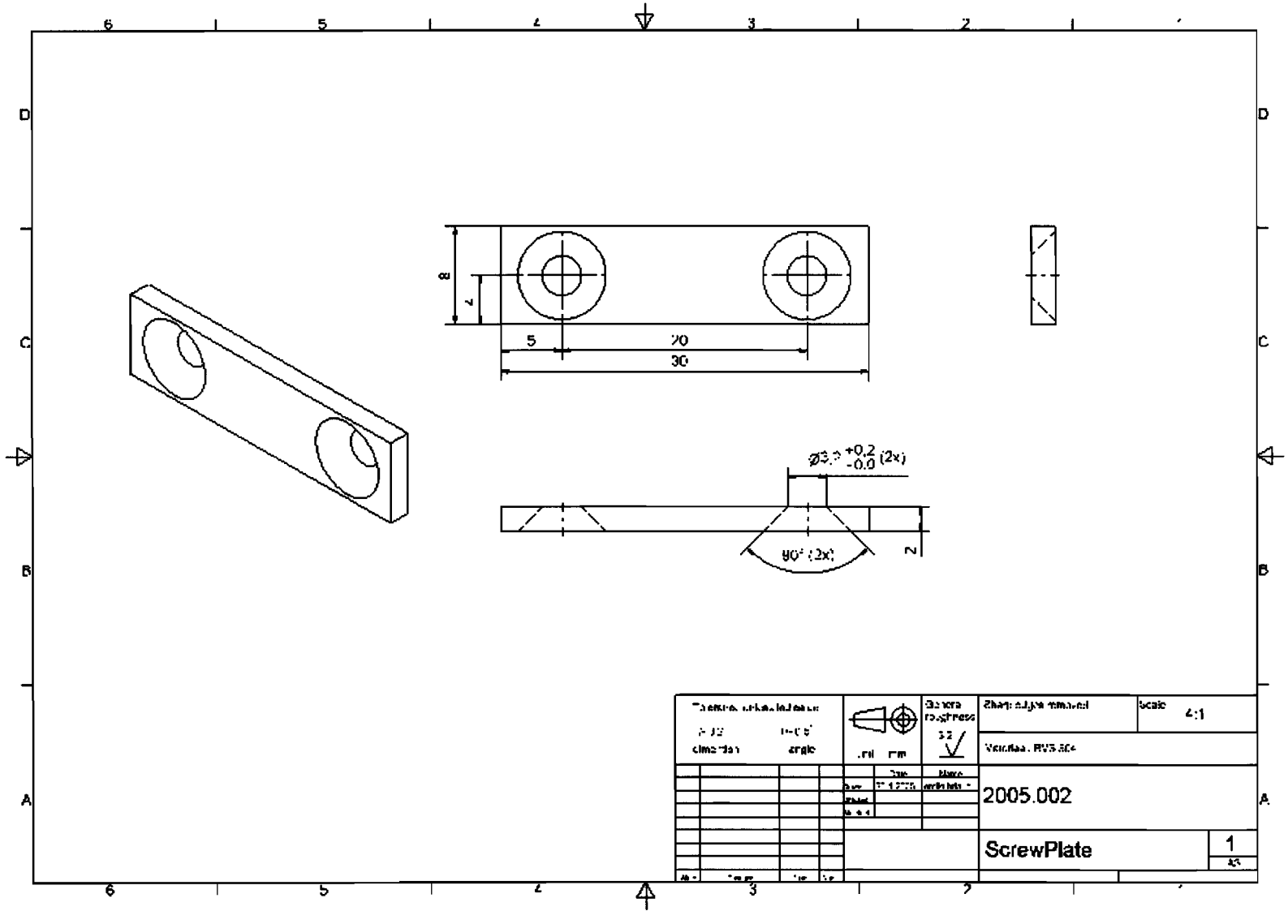
8
4
5
20
30
2
2005.002
ScrewPlate
1
4:1

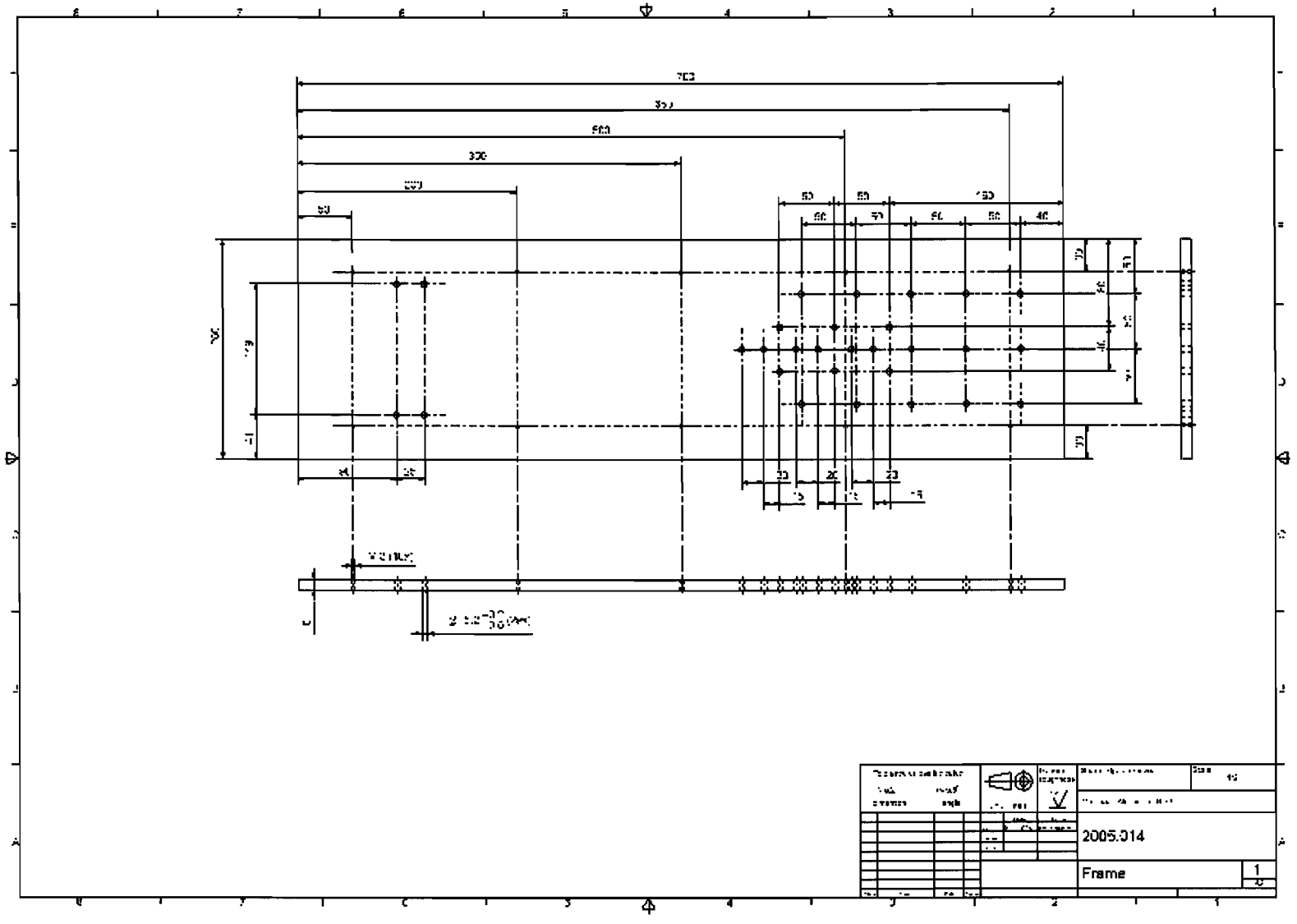
2005.014
Frame

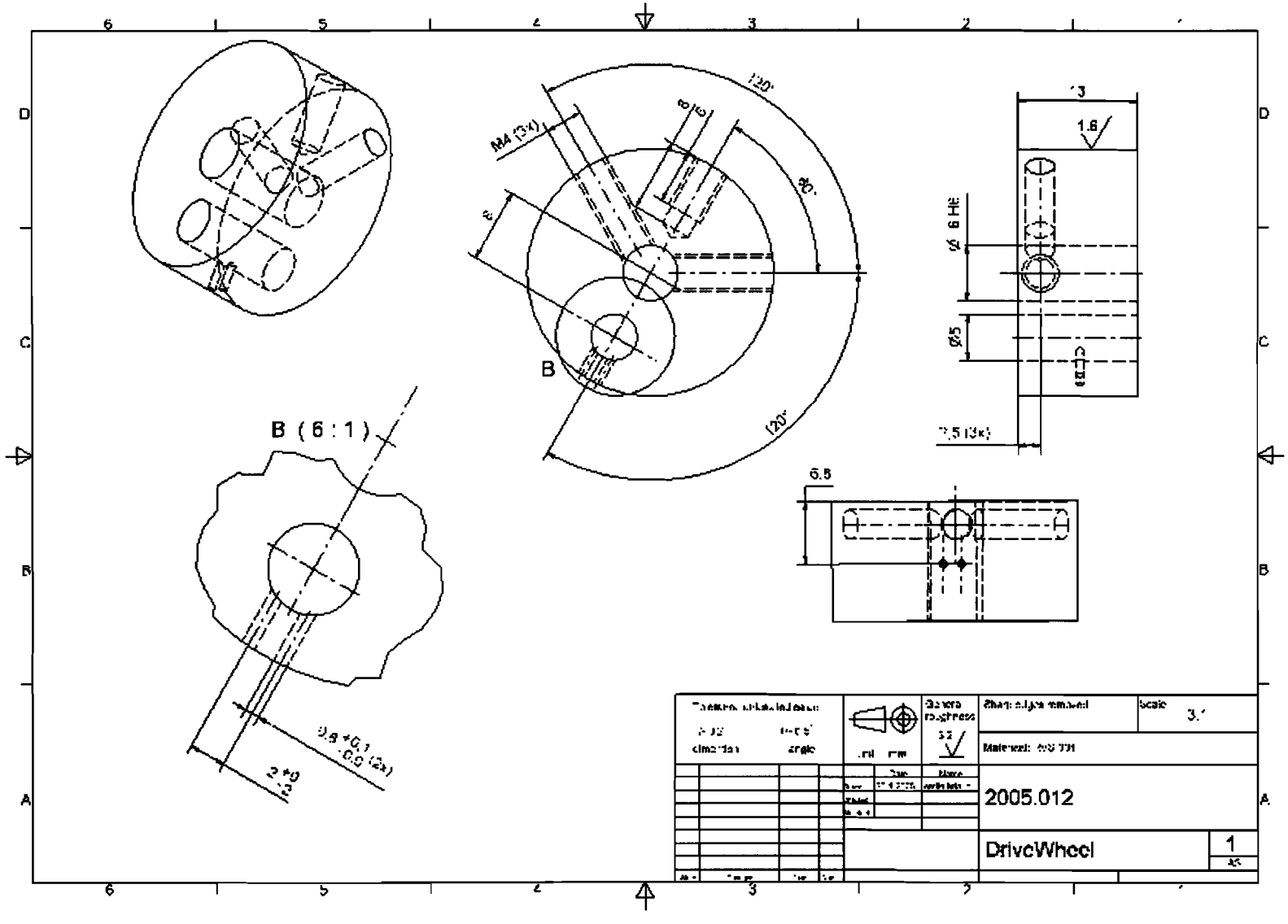
B
B (6 : 1)
M4 (3x)
120°
90°
120°
Ø5
1.6
6.8
2.5 (3x)
DriveWheel
2005.012

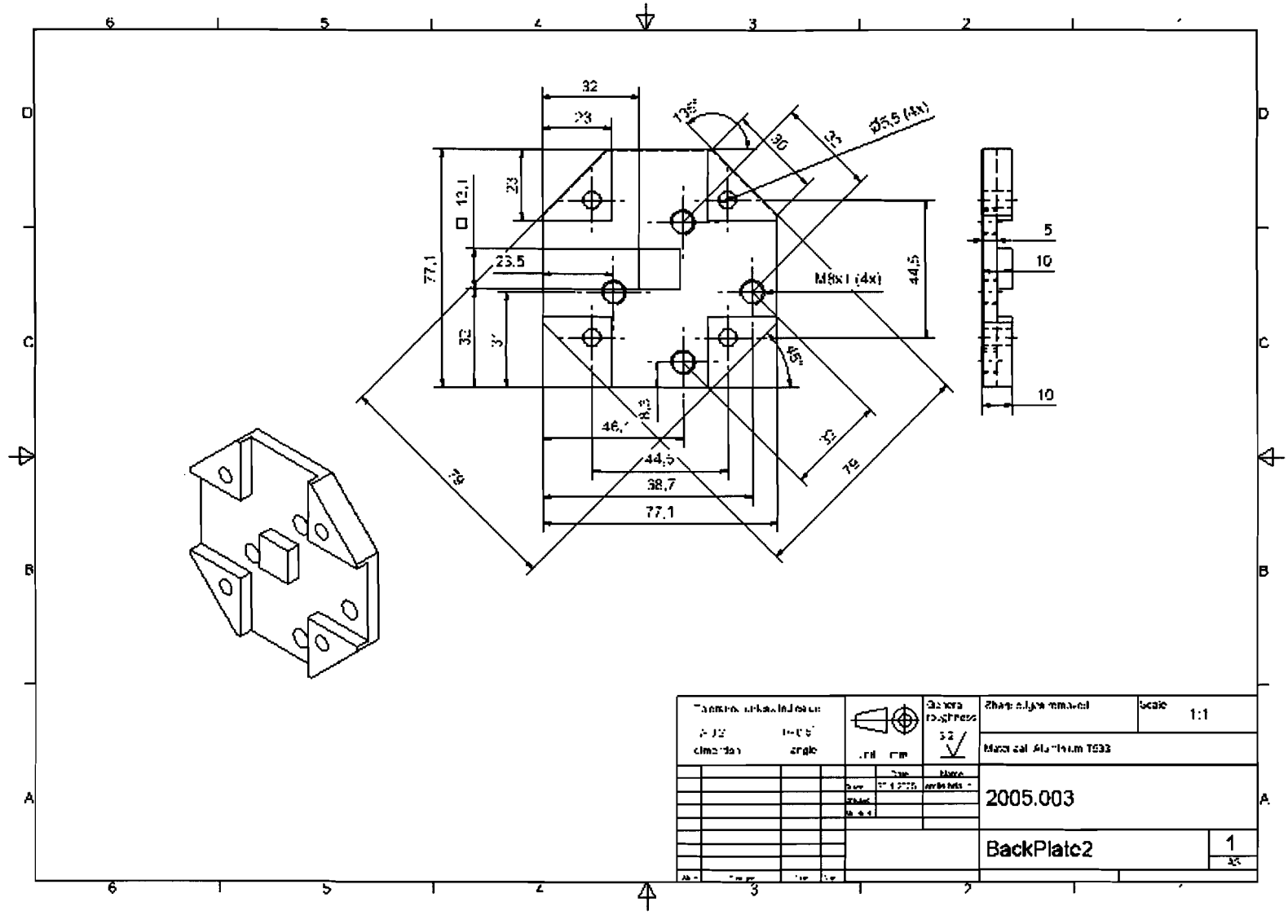
32
23
135°
30
13
Ø5.5 (4x)
12.1
23
77.1
23.5
M8x1 (4x)
44.5
32
3
45°
8.3
46.
44.5
38.7
77.1
32
75
5
10
10
2005.003
BackPlate2
1
1:1

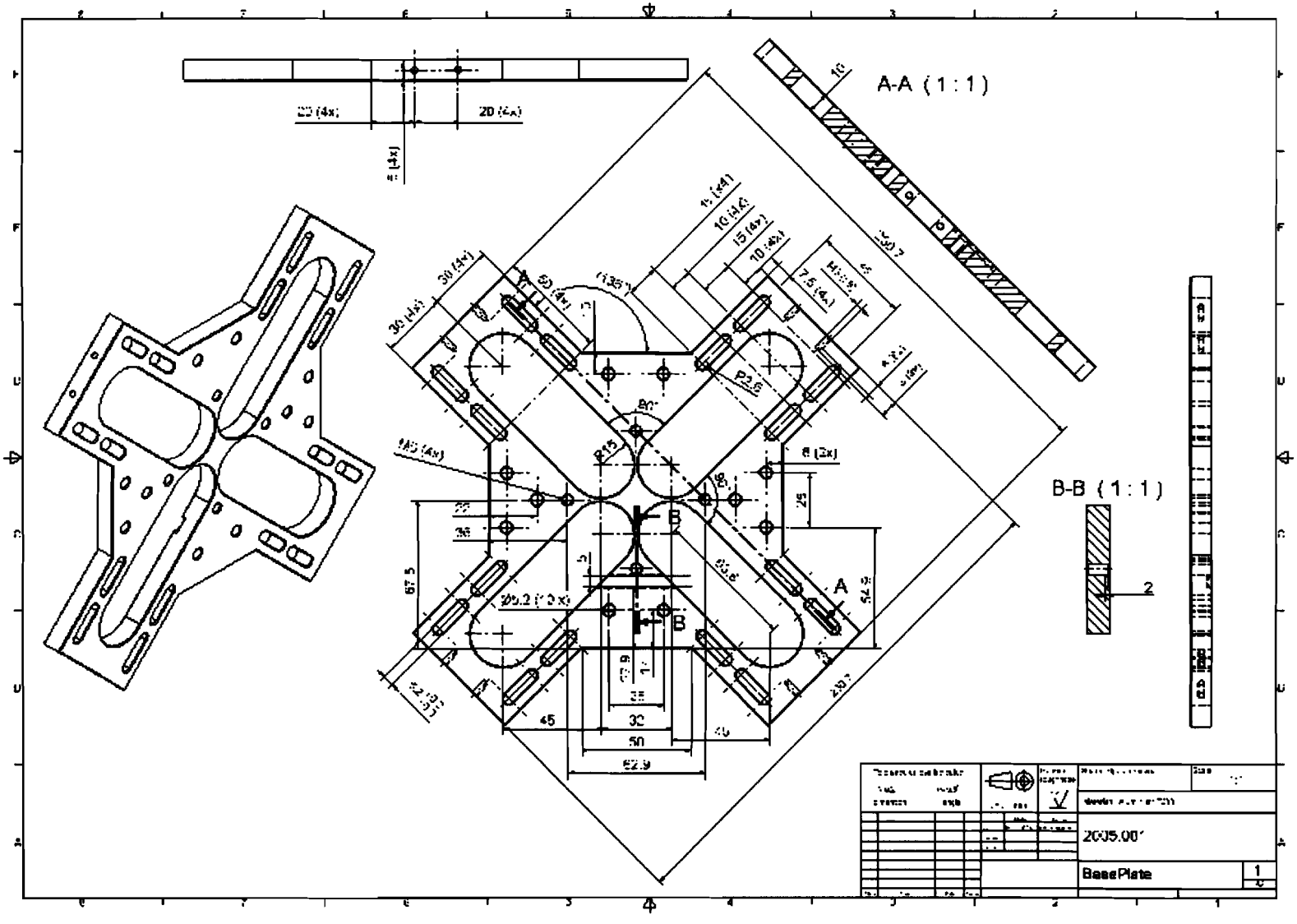
A-A (1 : 1)
B-B (1 : 1)
2005.00
BasePlate

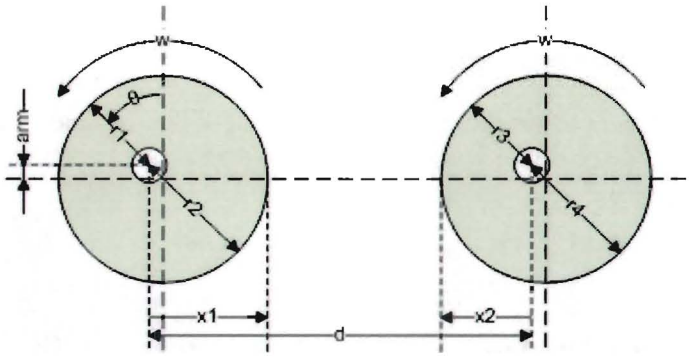

Figure 73. Pulley eccentricity, θ = 45 deg.

The maximum effective arm length (Figure 73) also depends on the rotational orientation of both eccentricities

$$arm_{\max} = (e_m + e_t) \cdot \cos(\theta) .$$

With a spring constant of k = 14.5 kN/m, the maximum disturbance torque due to the eccentricities and position θ of the pullies is

$$T_{p\_\max} = \Delta d_{\max} \cdot k \cdot arm_{\max} \Rightarrow$$

$$T_{p\_\max} = (e_m + e_t) \cdot \sin(\theta) \cdot k \cdot (e_m + e_t) \cdot \cos(\theta) \Rightarrow$$

$$T_{p\_\max} = k \cdot (e_m + e_t)^2 \cdot \sin(\theta) \cdot \cos(\theta) \Rightarrow$$

$$T_{p\_\max} = \frac{1}{2} \cdot k \cdot (e_m + e_t)^2 \cdot \sin(2 \cdot \theta) .$$

The maximum value of torque T_{p_max} occurs where $\sin(2 \cdot \theta) = 1$. The maximum magnitude of T_{p_max} is

$$\frac{1}{2} \cdot 14.5 \cdot 10^3 \cdot (60 \cdot 10^{-6})^2 = 2.61 \cdot 10^{-5} Nm .$$

Since the magnitude of this disturbance torque is very small, it will be of no influence on the measurements. Nevertheless, this disturbance torque is automatically compensated for by the ILC implementation B discussed earlier.

Acceleration

During friction measurements motor rotation is low frequent, e.g. $0.2 \cdot 2 \cdot \pi$ rad/sec. For these measurements the disturbance forces caused by the motor assy inertia moving due to the eccentricity of the pullies have a magnitude that is determined as follows.
In Figure 73, d is the distance between the two axes and ω is a constant rotation speed in rad/sec. Due to the eccentricity in the pullies, d changes according to

$$d_{delta\_x} = (e_m + e_t) \cdot \sin(\omega \cdot t).$$

The speed d_{delta_x} changes with is

$$d_{delta\_v} = \frac{d}{dt}(d_{delta\_x}) = \omega \cdot (e_m + e_t) \cdot \cos(\omega \cdot t).$$

The acceleration of d_{delta_a} is

$$d_{delta\_a} = \frac{d}{dt}(d_{delta\_v}) = -\omega^2 \cdot (e_m + e_t) \cdot \sin(\omega \cdot t).$$

The disturbance force at a constant rotation frequency ω due to eccentricity equals

$$F = m \cdot d_{delta\_a} = m \cdot (-\omega^2 \cdot (e_m + e_t) \cdot \sin(\omega \cdot t)).$$

The maximum effective arm length during rotation is

$$arm_{\max} = (e_m + e_t) \cdot \cos(\omega \cdot t).$$

The maximum disturbance torque at a constant rotation frequency ω due to eccentricity equals

$$T_{a\_\max} = F \cdot arm_{\max} \Rightarrow$$

$$T_{a\_\max} = -m \cdot \omega^2 \cdot (e_m + e_t) \cdot \sin(\omega \cdot t) \cdot (e_m + e_t) \cdot \cos(\omega \cdot t) \Rightarrow$$

$$T_{a\_\max} = -\frac{1}{2} \cdot m \cdot \omega^2 \cdot (e_m + e_t)^2 \cdot \sin(2 \cdot \omega \cdot t).$$

The maximum value of torque T_{a_max} occurs when $\sin(2 \cdot \omega \cdot t) = 1$. The mass of the motor plus mounting parts is $m = 1.025\ kg$. The sum of e_m and e_t is $\pm 60\ \mu m$. The maximum disturbance torque at a constant rotation frequency of $0.2 \cdot 2 \cdot \pi$ *rad/sec* due to the moving motor assy inertia, caused by the eccentricities, is

$$\left|T_{a\_\max}\right| = \frac{1}{2} \cdot 1.025 \cdot (0.2 \cdot 2 \cdot \pi)^2 \cdot (60 \cdot 10^{-6}) = 2.9 \cdot 10^{-9}\ Nm.$$

This is a neglectable disturbance occurring during torque measurement at low speeds. Also at the maximum speed of 5 Hz (system specifications), the magnitude of this disturbance is only 1.8 µNm which is also neglectable. Nevertheless, this disturbance torque is automatically compensated for by the ILC implementation B discussed earlier. The calculations have been simulated in 20-Sim shown in Figure 73 and Figure 74.

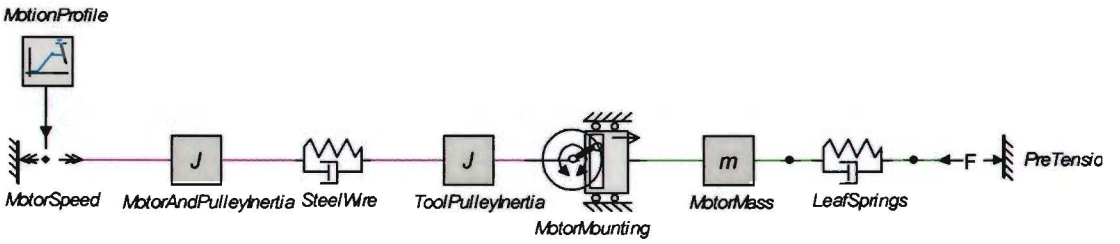

Figure 74. Motor suspension simulation

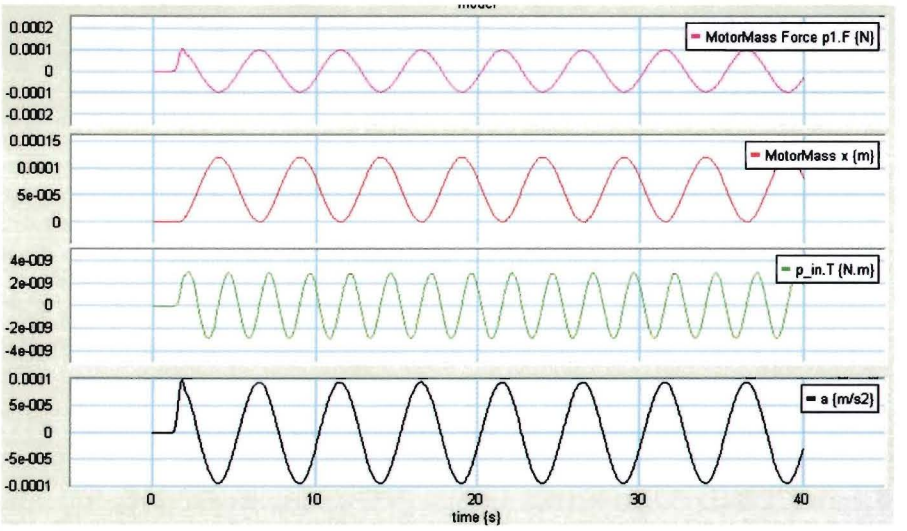

Figure 75. Disturbance torque due to motor assy inertia and pulley eccentricity

During friction measurements the thinnest set of leaf springs is selected since a low pre-tension is required as described in section 6.2. This results in a motor assy with a low bandwidth which is not a problem since motor movements will be < 1 Hz.
The mass of the motor plus mounting parts is m = 1.025 kg. The spring constant of the leaf spring construction is k = 14.5 kN/m. The eigen-frequency of the motor assy plus leaf springs is

$$f_{eigen} = \frac{1}{2 * \pi}\sqrt{\frac{k}{m}} = 18.9 \text{ Hz}.$$

Figure 76 shows the open loop gain of the setup including the instrument pulley driven by the tendon. The figure shows no anti-resonance-resonance at 18.9 Hz indicating that the

eigen-frequency of the motor assy is not exitated. This is because the tensile forces in the tendon are much lower than the applied pre-tension and therefore these forces do not deflect the motor assy leaf springs. Also the disturbance forces caused by eccentricities are too small and low frequent to exitate the eigen-frequency of 18.9 Hz.

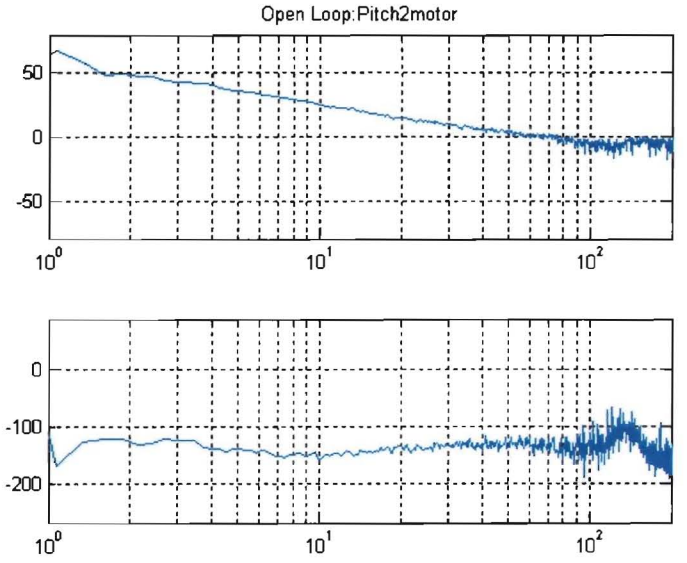

Figure 76. FRF of the setup incl. instrument pulley